

Summer 8-12-2022

The Development and In Vivo Immunologic Assessment of Biodegradable Microparticles Incorporating CPDI-02 and Mucosal Protein Vaccine

Jacob E. Parriott
University of Nebraska Medical Center

Tell us how you used this information in this [short survey](#).

Follow this and additional works at: <https://digitalcommons.unmc.edu/etd>

 Part of the [Pharmaceutics and Drug Design Commons](#)

Recommended Citation

Parriott, Jacob E., "The Development and In Vivo Immunologic Assessment of Biodegradable Microparticles Incorporating CPDI-02 and Mucosal Protein Vaccine" (2022). *Theses & Dissertations*. 679.
<https://digitalcommons.unmc.edu/etd/679>

This Dissertation is brought to you for free and open access by the Graduate Studies at DigitalCommons@UNMC. It has been accepted for inclusion in Theses & Dissertations by an authorized administrator of DigitalCommons@UNMC. For more information, please contact digitalcommons@unmc.edu.

**THE DEVELOPMENT AND IN VIVO IMMUNOLOGIC
ASSESSMENT OF BIODEGRADABLE MICROPARTICLES
INCORPORATING CPDI-02 AND MUCOSAL PROTEIN VACCINE**

By

JACOB E. PARRIOTT

A DISSERTATION

Presented to the Faculty of
the University of Nebraska Graduate College
in Partial Fulfillment of the Requirements
for the Degree of Doctor of Philosophy

Pharmaceutical Sciences Graduate Program

Under the Supervision of Professor Joseph A. Vetro

University of Nebraska Medical Center
Omaha, Nebraska

August 2022

Supervisory Committee:

Joseph A. Vetro, Ph.D.

Thomas L. McDonald, Ph.D.

Joyce Solheim, Ph.D.

Geoffrey M. Thiele, Ph.D.

ACKNOWLEDGMENTS

The completion of my dissertation would not be possible without the longstanding and unwavering support of my family, friends and coworkers. First, I would like to give special thanks to my advisor, Dr. Joseph Vetro. Dr. Vetro has been instrumental in my growth and development on both as a pharmaceutical scientist and on a personal level during my tenure in his lab. His mentorship, guidance, and technical training have been invaluable, and has helped provide me with knowledge and expertise that will serve me throughout my future career. Next, I would like to thank the late Dr. Sam Sanderson. He, along with Dr. Vetro, took a chance on welcoming a former medical student into their lab, and enabled me to pursue a career path of which I am passionate about. He is greatly missed, but his advice and leadership have made a lasting impact on me. I would also like to sincerely thank the other members of my PhD supervisory committee—Dr. Tom McDonald, Dr. Joyce Solheim, and Dr. Geoffrey Thiele—for their important input and advice on my research the last 6 years.

In addition to my advisors, I would also like to thank all the past and present members of the Vetro lab group. Of this group, there are several individuals of whom I would like to give special thanks. Firstly, I would like to thank Steve Curran. Steve has been fundamental towards my training in nanoscale formulation development. He has always been readily available to provide instruction, technical assistance, and troubleshooting insights related to all of my projects throughout my graduate school career. Secondly, I would like to thank our collaborator Dr. D. David Smith of Creighton University. Dr. Smith taught me everything I know about peptide synthesis, lyophilization, and HPLC/UPLC purification methodologies, and has been a great mentor and friend. Last, but not least, from the Vetro lab, I would like to thank my fellow graduate student Jason Stewart. Jason has provided critical assistance on running many of my experiments

(specifically, serum sample collection and running ELISAs, amongst other things). He has been a steadfast friend and scientific resource as we both navigate through our graduate school careers.

I would like to thank Chris Bauer of the Wyatt Lab at UNMC. His flexibility and willingness to help with BALF and NLF sample collection were invaluable for many of my humoral immunity assessments. He has been a great friend and provided levity during stressful days when experiments were particular lengthy.

Most of all, I would like to thank my family. My wife Macey and son Jett have provided me with unconditional love and support throughout my education. They have been with me in good times and bad, remained patient and understanding, and have been a constant source of motivation and joy. I would also like to thank my parents Joel and Lori, as well as my sister Sydney and brother-in-law Philip, for their everlasting support, love and personal advice.

THE DEVELOPMENT AND IN VIVO IMMUNOLOGIC ASSESSMENT OF BIODEGRADABLE MICROPARTICLES INCORPORATING CPDI-02 AND MUCOSAL PROTEIN VACCINE

Jacob E. Parriott, Ph.D.

University of Nebraska Medical Center, 2022

Supervisor: Joseph A. Vetro, Ph.D.

Encapsulation in biodegradable microparticles (MPs) is a promising approach to increase the efficacy of intranasally administered protein vaccines. The generation of long-lived adaptive immune responses against encapsulated protein vaccines, however, requires the incorporation of a suitable mucosal adjuvant. CPDI-02—a complement peptide-derived immunostimulant that selectively activates dendritic cells and macrophages over neutrophils while minimizing the inflammatory side effects of parent C5a—has previously been incorporated into both systemic and mucosal vaccine formulations via direct conjugation to chemical moieties, peptides, proteins, inactivated pathogens, and the surface of biodegradable particles, to enhance Th1-biased cellular immune responses. The effect of CPDI-02 surface conjugation to MPs encapsulating protein vaccine on short- and long-term mucosal and systemic humoral immune responses, however, has not previously been assessed. Further, alternative strategies for incorporating CPDI-02 into PLGA particles encapsulating protein vaccine (such as co-encapsulation of CPDI-02 with protein vaccine; or separately encapsulating protein vaccine and CPDI-02 and co-administering) have not been explored. In this dissertation, we report that respiratory immunization of naive mice with the model antigen ovalbumin (OVA) encapsulated in PLGA MP surface-conjugated with CPDI-02 generated: (i) increased numbers of OVA-specific IgA, IgM, and IgG antibody secreting cells (ASCs) in the lungs and spleen, (ii) increased short- and long-lived mucosal IgA and IgG antibody titers, and (iii) increased

short- and long-lived OVA-specific serum titers of IgG subclasses relative to encapsulation in particles modified with scrambled, inactivated CPDI-02 and PBS vehicle control. We further report that co-administration of CPDI-02 and OVA separately encapsulated in PLGA MPs via the intranasal route increases the generation of: (i) short-term OVA-specific IgA ASCs in the lungs, (ii) mucosal IgA and IgG antibody titers, (iii) OVA-specific IgG ASCs in the spleen, (iv) OVA-specific serum titers of IgG subclasses, and (v) OVA-specific CD4+ and CD8+ T cells in the spleen, compared to other strategies for incorporating CPDI-02 into MPs encapsulating protein vaccine. Thus, the strategy by which CPDI-02 is incorporated into MPs affects the generation of mucosal and systemic cellular and humoral immune responses by encapsulated protein vaccines after respiratory immunization.

Table of Contents

ACKNOWLEDGMENTS	i
ABSTRACT	iii
TABLE OF CONTENTS	v
LIST OF FIGURES AND TABLES	xiii
LIST OF ABBREVIATIONS	xvii
CHAPTER 1 – GENERAL INTRODUCTION	1
Section 1.1: Introduction	2
Section 1.2: Nasal and respiratory anatomy, physiology, and immunity	3
Section 1.2.1: Anatomy of the nasal cavity and respiratory tract	3
Section 1.2.2: Nasal-associated lymphoid tissue (NALT)	4
Section 1.3: Delivery strategies for nasal vaccination	5
Section 1.3.1: Lipid-based particles for intranasal administration	6
Section 1.3.1.1: Liposomes	6
Section 1.3.1.2: Solid lipid nanoparticles	7
Section 1.3.1.3: ISCOMs	7
Section 1.3.2: Polymer-based particles for intranasal vaccination	7
Section 1.3.2.1: Chitosan-based particles	7
Section 1.3.2.2: Biodegradable-polyester-based particles	8
Section 1.4: PLGA particle characteristics affecting immunogenicity of encapsulated antigen after intranasal administration	9

Section 1.4.1: Polymer composition and surface characteristics	9
Section 1.4.2: Particle size	10
Section 1.5: Effect of adjuvants on the generation of mucosal and systemic immunity by intranasally administered vaccines.....	12
Section 1.5.1: Bacteria-derived toxins	12
Section 1.5.2: CpG ODNs	13
Section 1.5.3: Cytokines and chemokines.....	13
Section 1.5.4: Complement Peptide-Derived Immunostimulants (CPDIs)	14
CHAPTER 2 – HYPOTHESES & SPECIFIC AIMS	17
Section 2.1: Hypotheses	18
Section 2.2: Specific Aims	20
Section 2.2.1: Part I (Chapter 4) Specific Aims	20
Section 2.2.2: Part II (Chapter 5) Specific Aims	20
Section 2.2.3: Part III (Chapter 6) Specific Aims	21
CHAPTER 3 – MATERIALS & METHODS	22
Section 3.1: LPS removal from Ovalbumin.....	23
Section 3.2: Synthesis of CPDI-02, scCPDI-02, Cys-CPDI-02 and Cys-scCPDI-02 Peptides	23
Section 3.3: Development of CPDI-02-based biodegradable PLGA microparticle formulations.....	23
Section 3.3.1: Encapsulation of OVA into biodegradable PLGA microparticles ("OVA Only MPs").....	24

Section 3.3.2: Encapsulation of OVA into CPDI-02 or scCPDI-02 surface-modified PLGA microparticles	24
Section 3.3.3: Development of PLGA microparticles co-encapsulating OVA and CPDI-02 or scCPDI-02.....	25
Section 3.3.4: Development of PLGA microparticles encapsulating CPDI-02 or scCPDI-02	26
Section 3.4: Diameter, polydispersity index (PDI), and zeta potential of PLGA microparticles	27
Section 3.5: Quantitation of CPDI-02, scCPDI-02 and OVA loading and burst release in MPs using ultra performance liquid chromatography (UPLC)	27
Section 3.5.1: CPDI-02, scCPDI-02 and OVA loading in MPs	27
Section 3.5.2: OVA burst release from microparticle formulations	30
Section 3.6: Animals used in experimental procedures	30
Section 3.7: Respiratory immunization with CPDI-02- or sc-CPDI-02-based OVA MPs	31
Section 3.8: Isolation of murine lung lymphocytes and splenocytes	31
Section 3.9: Collection of serum, BALF, and NLF from immunized mice.....	33
Section 3.10: IgA, IgG, IgM, and IFN- γ ELISpots (General)	34
Section 3.10.1: OVA-specific IgA, IgG, and IgM ELISpots (Special Considerations).....	34
Section 3.10.2: OVA-specific CD4+ and CD8+ IFN- γ ELISpots (Specific Considerations).....	34

Section 3.11: FACS analysis of OVA-specific CD4+ and CD8+ T-cells.....	35
Section 3.12: OVA-specific antibody titers of serum, BALF, and NLF	36
Section 3.13: Lung histology of immunized mice	37
Section 3.14: Statistics	38
CHAPTER 4 – Surface conjugation of the host-derived immunostimulant CPDI-02 to biodegradable microparticles increases short-term and long-term mucosal and systemic antibodies against encapsulated protein immunogen after IN administration to naïve mice	39
Section 4.1: Introduction	40
Section 4.2: Results.....	41
Section 4.2.1: Encapsulation of LPS-free OVA in biodegradable microparticles surface-conjugated with CPDI-02 or inactive, scrambled CPDI-02.....	41
Section 4.2.2: Effect of surface conjugating CPDI-02 to biodegradable microparticles and IAV on the generation of short-term IgA, IgM, and IgG ASCs against encapsulated protein immunogen in the lungs of young, naïve mice	41
Section 4.2.3: Effect of surface conjugating CPDI-02 to biodegradable microparticles and IAV on generation of short-term and long-term mucosal antibodies against encapsulated protein immunogen in the nasal cavity and lungs of young, naïve mice.....	43
Section 4.2.4: Effect of surface conjugating CPDI-02 to biodegradable microparticles and IAV on the generation of short-term IgA, IgM, and IgG ASCs against encapsulated protein immunogen in the spleens of young, naïve mice.....	44

Section 4.2.5: Effect of CPDI-02 surface conjugation to biodegradable microparticles and IAV on the generation of short-term and long-term systemic antibodies against encapsulated protein immunogen in the serum of young, naïve mice	46
Section 4.2.6: Longitudinal analysis of Th1-Th2 profile of systemic antibodies in mice treated with CPDI-02-SM MPs in 50 µL IAV	48
Section 4.2.7: Effect of surface-conjugating CPDI-02 to biodegradable microparticles and intranasal administration volume on long-term inflammatory changes in the lungs in naïve female C57BL/6 mice after respiratory immunization with encapsulated LPS-free OVA.....	49
CHAPTER 5 – The effect of intranasal administration volume on short- and long-term memory T-cells generated in naïve mice by intranasal immunization with protein vaccine encapsulated in CPDI-02-surface-modified biodegradable microparticles.....	66
Section 5.1: Introduction	67
Section 5.2: Results.....	69
Section 5.2.1: Effect of IAV on the magnitude of early-memory CD127/KLRG1 subsets and late-memory CD127/CD62L subsets of mucosal CD4+ T cells in the lungs generated by protein vaccine encapsulated in CPDI-02-SM MPs	69
Section 5.2.2: Effect of IAV on the magnitude of early-memory CD127/KLRG1 subsets and late memory CD127/CD62L subsets of mucosal CD8+ T cells in the lungs generated by protein vaccine encapsulated in CPDI-02-SM MPs	71

Section 5.2.3: Effect of IAV on the magnitude of mucosal OVA-specific CD4+ and CD8+ T cells generated in the lungs by protein vaccine encapsulated in CPDI-02-SM MPs, as measured by IFN- γ ELISpot.....	73
Section 5.2.4: Effect of IAV on the magnitude of late-memory CD127/CD62L subsets of systemic CD4+ T cells in the spleen generated by protein vaccine encapsulated in CPDI-02-SM MPs.....	75
Section 5.2.5: Effect of IAV on the magnitude of early-memory CD127/KLRG1/CD62L subsets and late-memory CD127/CD62L subsets of systemic CD8+ T cells in the spleen generated by protein vaccine encapsulated in CPDI-02-SM MPs	78
Section 5.2.6: Effect of IAV on the magnitude of systemic OVA-specific CD4+ and CD8+ T cells generated in the spleen by protein vaccine encapsulated in CPDI-02-SM MPs, as measured by IFN- γ ELISpot.....	80
CHAPTER 6 – The effect of CPDI-02 adjuvant incorporation strategy on humoral and cellular immune responses generated by biodegradable microparticles encapsulating mucosal protein vaccine	94
Section 6.1: Introduction	95
Section 6.2: Results.....	96
Section 6.2.1: Development and characterization of biodegradable microparticles incorporating CPDI-02 and mucosal protein vaccine (OVA)	96
Section 6.2.1.1: CPDI-02-ECA and scCPDI-02-ECA MPs.....	96
Section 6.2.1.2: CPDI-02-CE and scCPDI-02-CE MPs.....	97
Section 6.2.1.3: CPDI-02-SM and scCPDI-02-SM MPs.....	98

Section 6.2.1.4: Dosing of OVA and CPDI-02 or scCPDI-02 in developed ECA, CE, and SM microparticle formulations	98
Section 6.2.2: CPDI-02-ECA MP strategy generates greater magnitudes of OVA-specific IgA ASCs in the lungs of naïve mice compared to CPDI-02-CE and CPDI-02-SM MP strategies	99
Section 6.2.3: CPDI-02-ECA MP strategy generates greater magnitudes of short-term mucosal antibodies against encapsulated protein immunogen in the nasal cavity and lungs of young, naïve mice compared to the CPDI-02-CE MP strategy.	101
Section 6.2.4: CPDI-02-ECA MP strategy generates greater magnitudes of OVA-specific IgG ASCs in the spleens of naïve mice compared to CPDI-02-CE and CPDI-02-SM MP strategies	102
Section 6.2.5: CPDI-02-ECA MP strategy generates higher short-term systemic OVA-specific antibody titers in the serum of young, naïve mice compared to CPDI-02-CE and CPDI-02-SM MP strategies	104
Section 6.2.6: The effect of CPDI-02 incorporation strategy into biodegradable microparticles encapsulating OVA on the magnitudes of OVA-specific CD4+ and CD8+ T cells in the lungs of young, naïve mice.....	105
Section 6.2.7: CPDI-02-ECA MP and CPDI-02-SM MP strategies generate greater magnitudes of OVA-specific CD4+ and CD8+ T cells in the spleens of young, naïve mice compared to the CPDI-02-CE MP strategy	107
CHAPTER 7 – DISCUSSION, CONCLUSIONS, AND FUTURE DIRECTIONS	124
Section 7.1: Discussion – Chapter 4	125

Section 7.2: Discussion – Chapter 5	127
Section 7.3: Discussion – Chapter 6	129
Section 7.4: Conclusions	132
Section 7.5: Future Directions.....	133
CHAPTER 8 – REFERENCES	136

List of Figures and Tables

Figure 1.1: The respiratory tract and nasal cavity of humans	15
Figure 1.2: Mechanisms of immune induction in nasal-associated lymphoid tissues.....	16
Figure 4.1: Synthetic strategy for conjugating CPDI-02 to the surface of biodegradable microparticles	51
Table 4.1: Representative characteristics of OVA-encapsulated PLGA 50:50 microparticles (MP).....	52
Figure 4.2: Effect of surface-conjugating CPDI-02 to biodegradable microparticles and intranasal administration volume on magnitudes of short-term OVA-specific antibody-secreting cells (ASCs) in the lungs of naïve female C57BL/6 mice after respiratory immunization with encapsulated LPS-free OVA.....	54
Figure 4.3: Effect of surface-conjugating CPDI-02 to biodegradable microparticles and intranasal administration volume on titers of short-term and long-term OVA-specific antibodies in the nasal cavities and lungs of naïve female C57BL/6 mice after respiratory immunization with encapsulated LPS-free OVA.....	56
Figure 4.4: Effect of surface-conjugating CPDI-02 to biodegradable microparticles and intranasal administration volume on magnitudes of short-term systemic OVA-specific antibody-secreting cells (ASCs) in the spleens of naïve female C57BL/6 mice after respiratory immunization with encapsulated LPS-free OVA	58
Figure 4.5: Effect of surface-conjugating CPDI-02 to biodegradable microparticles and intranasal administration volume on the titers of short-term and long-term systemic OVA-specific Th1 and Th2 subclasses of IgG in the serum of naïve female C57BL/6 mice after respiratory immunization with encapsulated LPS-free OVA.....	60

Figure 4.6: Effect of conjugating CPDI-02 to the surface of biodegradable microparticles on the Th1/Th2 ratios of short-term and long-term systemic OVA-specific antibody titers generated in naïve female C57BL/6 mice after respiratory immunization with encapsulated LPS-free OVA.....	62
Figure 4.7: Effect of surface-conjugating CPDI-02 to biodegradable microparticles and intranasal administration volume (IAV) on long-term inflammatory changes in the lungs of naïve female C57BL/6 mice after respiratory immunization with encapsulated LPS-free OVA	64
Figure 5.1: Short- and long-term effects of IAV on generation of CD4+ memory T cell subsets in the lungs of C57BL/6 mice.....	82
Figure 5.2: Short- and long-term effects of IAV on generation of CD8+ memory T cell subsets in the lungs of C57BL/6 mice.....	84
Figure 5.3: Effect of surface-conjugating CPDI-02 to biodegradable microparticles and intranasal administration volume on the magnitude of IFN- γ secretion of mucosal OVA-specific CD4+ and CD8+ T cells in the lungs generated in naïve female C57BL/6 mice after respiratory immunization with encapsulated LPS-free OVA.....	86
Figure 5.4: Short- and long-term effects of IAV on generation of systemic CD4+ memory T cell subsets in the spleens of C57BL/6 mice.....	88
Figure 5.5: Short- and long-term effects of IAV on generation of systemic CD8+ memory T cell subsets in the spleens of C57BL/6 mice.....	90
Figure 5.6: Effect of surface-conjugating CPDI-02 to biodegradable microparticles and intranasal administration volume on the magnitude of IFN- γ secretion of systemic OVA-specific CD4+ and CD8+ T cells in the spleen generated in naïve female C57BL/6 mice after respiratory immunization with encapsulated LPS-free OVA.....	92

Figure 6.1: Conventional adjuvant incorporation strategies for biodegradable PLGA microparticles	109
Table 6.1: Representative characteristics of CPDI-02 and scCPDI-02 incorporation strategies into biodegradable PLGA 50:50 microparticles (MP) encapsulating OVA....	110
Figure 6.2: Effect of CPDI-02 incorporation strategy into biodegradable microparticles on the magnitudes of short-term mucosal OVA-specific antibody-secreting cells (ASCs) generated in the lungs of naïve female C57BL/6 mice after respiratory immunization with encapsulated LPS-free OVA.....	112
Figure 6.3: Effect of CPDI-02 incorporation strategy into biodegradable microparticles on the short-term OVA-specific antibody titers in the nasal cavities and lungs of naïve female C57BL/6 mice after respiratory immunization with encapsulated LPS-free OVA.....	114
Figure 6.4: Effect of CPDI-02 incorporation strategy into biodegradable microparticles on the magnitudes of short-term systemic OVA-specific antibody-secreting cells (ASCs) generated in the spleens of naïve female C57BL/6 mice after respiratory immunization with encapsulated LPS-free OVA	116
Figure 6.5: Effect of CPDI-02 incorporation strategy into biodegradable microparticles on the short-term OVA-specific antibody titers in the serum of naïve female C57BL/6 mice after respiratory immunization with encapsulated LPS-free OVA.....	118
Figure 6.6: Effect of CPDI-02 incorporation strategy into biodegradable microparticles on the magnitude of IFN- γ secretion of mucosal OVA-specific CD4 ⁺ and CD8 ⁺ T cells in the lungs generated in naïve female C57BL/6 mice after respiratory immunization with encapsulated LPS-free OVA.....	120

Figure 6.7: Effect of CPDI-02 incorporation strategy into biodegradable microparticles on the magnitude of IFN- γ secretion of systemic OVA-specific CD4⁺ and CD8⁺ T cells in the spleen generated in naïve female C57BL/6 mice after respiratory immunization with encapsulated LPS-free OVA..... **122**

List of Abbreviations

- APCs: Antigen-presenting cells
- 4PL: 4-parameter logistic
- ANOVA: Analysis of variance
- ASC: Antibody secreting cell
- AUC: Area under curve
- BAL: Bronchoalveolar lavage
- BALF: Bronchoalveolar lavage fluid
- C5a: Complement component 5a
- C5aR: Complement component 5a receptor
- CD62L: L-selectin
- CE: Co-Encapsulated
- CPDI-02: Complement peptide-derived immunostimulant 02
- cRPMI: Complete RPMI 1640 cell culture media
- CT: Cholera toxin
- CTL: Cytotoxic T lymphocytes
- DC: Dendritic cell
- DMSO: Dimethyl sulfoxide
- ECA: Encapsulated, Co-Administered
- EEC: Early effector cell
- ELISA: Enzyme-linked immunoassay
- ELISpot: Enzyme-linked immune absorbent spot
- ESE: Emulsion solvent evaporation
- FACS: Fluorescence-Activated Cell Sorting
- FITC: Fluorescein isothiocyanate
- HI-FBS: Heat-inactivated fetal bovine serum

IAASF: Interfacial activity-assisted surface functionalization

IAV: Intranasal Administration Volume

ID: Intradermal

IM: Intramuscular

IN: Intranasal

IP: Intraperitoneal

IV: Intravenous

IFN- γ : Interferon gamma

IgA: Immunoglobulin A

IgG: Immunoglobulin G

IgG1: Immunoglobulin G1

IgG2b: Immunoglobulin G2b

IgG2c: Immunoglobulin G2c

IgG3: Immunoglobulin G3

IgM: Immunoglobulin M

ISCOM: Immune stimulating complexes

KLRG1: Killer cell lectin-like receptor subfamily G member 1

LPS: Lipopolysaccharide

LT: *Escherichia coli* heat-labile enterotoxin

MALT: Mucosal Associated Lymphoid Tissues

MHC I: Major histocompatibility complex class I

MHC II: Major histocompatibility complex class II

MCMV: Murine cytomegalovirus

MP: Microparticle

MPEC: Memory precursor effector cell

NALT: Nasal associated lymphoid tissue

NaOH: Sodium hydroxide

NK: Natural killer

NLF: Nasal lavage fluid

NP: Nanoparticle

OD: Optical density

OVA: Ovalbumin

PEG: Polyethylene glycol

PBS: Phosphate buffered saline

PBST: Phosphate buffered saline with 0.05% Tween 20

PDI: Polydispersity index

PLGA: Poly(D,L-lactic-co-glycolic acid)

PVA: Poly(vinyl) alcohol

RCF: Relative centrifugal force

RPM: Revolutions per minute

RPMI 1640: Roswell Park Memorial Institute 1640 media

scCPDI-02: Scrambled, inactivated CPDI-02

SDS: Sodium dodecyl sulfate

SLEC: Short-lived effector cell

SLN: Solid lipid nanoparticle

SM: Surface-modified

TCM: Central memory T cells

TCR: T-cell receptor

TEM: Effector memory T cells

TEFF: Effector T cells

TFA: Trifluoroacetic acid

Th1: T helper 1

Th2: T helper 2

Treg: Regulatory T cell

TET: Tetramer

TLR: Toll-like receptor

TRM: Tissue-resident memory T-cells

UPLC: Ultra performance liquid chromatography

W₁/O/W₂: water-in-oil-in-water double emulsion

CHAPTER 1

GENERAL INTRODUCTION

1.1 Introduction

Mucosal vaccination has emerged as a promising approach towards disease prevention. Mucosal routes of administration are noninvasive and have the ability to generate protection through induction of both mucosal and systemic immune responses.¹ While mucosal vaccines can in principle be delivered to any mucosal surface, they are typically delivered via the oral or intranasal route. Of these two routes, intranasal administration is particularly advantageous, as it avoids the potential degradation of therapeutic agents through first pass metabolism, as seen in oral administration. Further, the nasal mucosa is highly vascularized and, due to abundant microvilli, has a large surface area for absorption.² The nasal route of administration can also facilitate deposition of vaccines into the lower airways in the lungs. Given that respiratory mucosal surfaces are the main point of entry for most infectious pathogens,³ developing mucosal immunity in the nasopharynx and lower airway sites is essential for providing a primary line of host defense.

Despite numerous opportunities for the intranasal route of administration for vaccines, it is not without obstacles. Firstly, due to mucocilliary clearance, administered vaccines often face rapid elimination from the nasal cavity and respiratory tract.⁴ Efficacy of vaccines is further limited by inefficient uptake of soluble antigens by immune cells within the nasal epithelial layer.⁵ As a result, intranasal vaccines require novel drug delivery strategies and/or the incorporation of suitable adjuvants to enhance uptake and immunogenicity.⁶ In the following sections, an overview of the nasal and respiratory immune system is provided, followed by a discussion of the current strategies and techniques employed by pharmaceutical scientists towards improving intranasal vaccine delivery.

1.2 Nasal and respiratory anatomy, physiology, and immunity

1.2.1 Anatomy of the nasal cavity and respiratory tract

The respiratory tract of humans and other mammals is comprised of two general regions, the upper respiratory tract (made up of the nasal cavity, pharynx, and larynx) and the lower respiratory tract (made up of the trachea, primary bronchi, bronchioles and alveoli) (**Fig.1.1**). The nasal cavity is the primary entry point for air into the body and serves to warm, moisturize, and filter the air entering the lungs. The anterior portions of the nasal cavity are made up of the vestibule and the atrium, and are lined by stratified squamous and transitional non-ciliated epithelial cells.⁷ The relatively poor vasculature and low absorptive surface area in this anterior region makes it a limited target for novel vaccine delivery strategies.

The central and posterior regions of the nasal cavity house anatomical structures including the turbinates and pharyngeal tonsils. These structures have a relatively larger surface area and vascularization than their anterior counterparts. The respiratory mucosa (**Fig.1.1B**, blue region) is lined by columnar and ciliated respiratory epithelium. The pharyngeal tonsils in the posterior region (**Fig.1.1B**, red region) are made up of nasal-associated lymphoid tissue (NALT). The pharyngeal tonsils are one component of a ringed arrangement of lymphoid tissue (“Waldeyer’s lymphatic ring”) within the upper respiratory tract in humans, which also includes the tubal tonsils, palatine tonsils, and the lingual tonsil.⁸ Lympho-epithelium covers the pharyngeal tonsillar NALT, and is comprised of cells such as M cells, goblet cells, and many other intraepithelial lymphoid cells.⁹ With their relatively higher levels of vascularity and permeability, as well as their greater presence of immune cells, these posterior regions of the nasal cavity are of

particular importance for intranasal vaccine delivery, as they serve as target areas for nanoparticulate deposition.¹⁰

Nasal mucus covers the majority of the posterior region of the nasal cavity. It is produced and secreted by both goblet cells and seromucous glands beneath the respiratory epithelium.¹¹ Mucus provides a protective barrier to exogenous materials introduced into the nasal cavity. The cilia of respiratory epithelial cells constantly drive the mucus forward in the nasal cavity to be expelled; this provides an effective means of expelling pathogenic particulates trapped in mucus that were inhaled by the host. This physiologic mechanism thus inherently also poses a barrier towards mucosal vaccine delivery, and is an important factor to consider during vaccine formulation.

1.2.2 Nasal-associated lymphoid tissue (NALT)

As mentioned in **Section 1.2.1**, the posterior region of the nasal cavity is home to the pharyngeal tonsils, which are made of NALT. In mice, the NALT is localized on the floor of the nasal cavity, whereas in humans, it is on the posterior-superior aspect of the nasopharynx. NALT serves as the primary mucosal inductive site of antigen-specific immune responses within the nasal cavity, and contains a wide-array of immunocompetent cell types.

Within the NALT and underlying cellular framework are discrete regions of enriched T Cell and B Cell populations; populations of antigen presenting cells (APC) such as dendritic cells (DCs) and macrophages; and microfold cells (M cells). M cells in particular are unique in that they reside within the epithelium, but also sample and uptake antigen and actively transport it into the underlying stroma via endocytosis, phagocytosis, or transcytosis mechanisms (**Fig.1.2A**).¹²

Transported antigen is then processed by APCs for the generation of downstream adaptive immune responses.

The ability of M cells to actively transport antigen across the nasal epithelia is not exclusive to this cell type. Projections from DCs in the underlying stroma are able to penetrate tight junctions between cells in the nasal epithelia to sample the luminal space (**Fig.1.2B**).^{13,14} This mechanism of particulate uptake from the nasal cavity provides an additional means of immune response generation, and is particularly relevant for induction of immune responses by vaccines encapsulated in micro- and nanoparticles.

Whether antigen/vaccine is (1) transported across the epithelia by M Cells and taken up by stromal DCs or (2) directly taken up by the projections of stromal DCs in the nasal lumen, these activated DCs migrate to the lymph nodes and activate resident CD4+ T cells. These T cells subsequently can activate both humoral and cellular immune pathways. With regards to stimulation of humoral immunity, activated CD4+ cells are able to activate naïve B cells which then differentiate (**Fig.1.2C**), enter systemic circulation (**Fig.1.2D**), and ultimately migrate to mucosal or systemic effector sites.¹⁵ With regards to cellular immunity, antigen-activated stromal DCs are also able to directly induce the activation of resident CD8+ cytotoxic T cells (CTLs) in the stroma via the MHC class I complex.¹⁶ Additional stimulation of cellular immunity and recruitment of relevant immune cells is achieved via the secretion of cytokines by nasal epithelial cells upon endocytosis of luminal antigen/vaccine.¹⁷

1.3 Delivery strategies for nasal vaccination

The anatomy and physiology of the nasal cavity present many opportunities for intranasal vaccination, especially in terms of high vascularity, large absorptive capabilities,

and avoidance of first-pass metabolism. In order to overcome the obstacles inherent with the intranasal route of administration (ie, mucociliary clearance and poor immunogenicity), however, several novel particle-based drug delivery strategies have been devised to boost vaccine efficacy. The most commonly used strategies often fall into one of two broad categories: (1) lipid-based nanocarriers (including liposomes, solid lipid nanoparticles, and ISCOMs) and (2) polymer-based nanoparticles (including lectin-based particles, polysaccharide-based particles, and biodegradable polyester micro-/nanoparticles).¹⁸ Each of these strategies have intrinsic advantages and disadvantages, and are typically chosen on the basis of immunologic requirements of the disease target and overall vaccine delivery goals. The subsections within **Section 1.3** discusses a selection of the most commonly found strategies in the literature for intranasal vaccination.

1.3.1 Lipid-based particles for intranasal vaccination

1.3.1.1 Liposomes

Liposomes are spherical vesicles that contain one or more lipid bilayers made up of amphiphilic phospholipids. The aqueous core allows entrapment of hydrophilic drugs or antigens; hydrophobic cargo is frequently loaded within the bilayer itself. Liposomes are biocompatible and deliver payloads through fusion with the cell membranes of target cells; they have been reported to be preferentially internalized by APCs.¹⁹ Despite this, the use of these delivery vehicles is less common in intranasal applications, due to the fact that their ability to induce systemic immunity is markedly lower compared to other drug delivery systems.²⁰

1.3.1.2 Solid lipid nanoparticles

Solid lipid nanoparticles (SLNs) are spherical particles that contain a solid lipid core matrix stabilized by surfactants. Unlike liposomes, the outer shell is composed of a single phospholipid layer (that is, no bilayer), and the core is lipophilic. This drug delivery system is thus somewhat restricted on the type of cargo it is able to successfully load; commonly entrapped payloads are nucleic acids (RNA derivatives) and other types of lipophilic small molecule drugs.²¹ Advantages of SLNs compared to other vaccine delivery systems include controlled release, improved stability of entrapped drug, scalable production capacity, and low toxicity.²²

1.3.1.3 ISCOMs

Immunostimulating complexes (ISCOMs) are spherical, cage-like particles that spontaneously form after mixing phospholipids, cholesterol, and Quillaia saponins under specific stoichiometric conditions.²³ This delivery system is notable for its ability to activate both Th1 and Th2 immunity pathways. When intranasally administered, ISCOMs are able to generate robust systemic and mucosal immune responses, including high serum antibody titers, production of mucosal IgA, and proliferation of immunogen-specific T cells.^{24,25} Disadvantages of this delivery system are difficult preparation and relatively rapid clearance (especially after intranasal administration).²⁶

1.3.2 Polymer-based particles for intranasal vaccination

1.3.2.1 Chitosan-based particles

Chitosan is a co-polymer composed of glucosamine and N-acetylglucosamine, derived from deacetylation of chitin, a naturally occurring component of the

exoskeletons of various types of shellfish.²⁷ This linear polysaccharide is notable for its inherent mucoadhesive properties (due to its polycationic charge from its amine moieties), which make it an attractive candidate for intranasal applications. The muco-adhesion seen in chitosan-based particles enables sustained residence time in the nasal cavity and subsequent release of loaded cargo. Drawbacks of this delivery strategy include poor solubility and difficulty in controlling particle pore sizes. Further, preparation methods are not universal and must be altered according to the type of drug/vaccine to be loaded, thus making formulation relatively more difficult than other alternative delivery strategies.²⁸

1.3.2.2 Biodegradable-polyester-based particles

Biodegradable polyester particles are a common intranasal vaccine delivery strategy used to boost immune responses, due to their ability to protect encapsulated cargo (such as protein, peptide or DNA-based antigens)²⁹ and their ability to facilitate the trafficking of antigens towards inductive sites within nasal and respiratory lymphoid tissues.³⁰ Poly Lactic-co-Glycolic Acid (PLGA) and poly(lactic acid) (PLA) are the two most commonly used polymers in the formulation of biodegradable-polyester-based particles for intranasal vaccination.³¹ PLGA and PLA particles are most frequently prepared using the solvent-evaporation/emulsification method^{32,33} or the nanoprecipitation method.³⁴ These polymers offer distinct advantages, including excellent biocompatibility and FDA approval, the ability to encapsulate numerous types of biomolecules with high loading efficiencies, sustained release at the site of deposition, and customizability for types of encapsulated payloads and desired pharmacokinetic profiles. Because of these characteristics and proven prior efficacy in the context of CPDI-02-based

formulations,^{32,33} the particles developed in this dissertation utilize PLGA polymer in all microparticle formulations.

1.4 PLGA particle characteristics affecting immunogenicity of encapsulated antigen after intranasal administration

1.4.1 Polymer composition and surface characteristics

The physicochemical properties of biodegradable PLGA particles—which can directly or indirectly play a determinative role in the magnitude of generated immune responses—are influenced by a number of factors including: particle production method; the molecular weight and monomer composition of the polymer; and the inclusion of osmotic agents, stabilizers, or surfactants.³⁵ With regards to molecular weight, microparticles utilizing low molecular weight PLGA often have increased burst release and faster rates of overall degradation.³⁶ Increasing the relative amount of poly(lactic acid) relative to poly(glycolic acid) within PLGA also has an inverse relationship with burst release and degradation rate in aqueous environments (such as the nasal cavity and lungs); that is, the greater the lactic acid content, the lower the burst release and degradation rate.³⁷ Thus, the molecular weight and ratio of lactic acid to glycolic acid within PLGA can be fine-tuned during particle formulation development to achieve particles of a desired pharmacokinetic release profile.

The surface characteristics of PLGA particles are also critical to their internalization and processing by immune cells within the respiratory tract. In general, particles comprised of hydrophilic polymers tend to have greater immuno-availability following intranasal immunization.¹⁸ Particles with a cationic surface charge also have increased muco-adhesion properties, given that nasal mucus contains biomacromolecules and salts that are polyanionic in nature.

In addition to the adjustable properties of the incorporated polymers, biodegradable PLGA particles can also be surface-modified using targeting ligands, adjuvants, and other moieties. Having these types of modifications on the particle surface enables the particles to be more easily recognized and taken up by immune cells in the nasal mucosa. Specific targeting moieties that have been reportedly used with PLGA particles include mannose-derived polymers; biomolecules such as influenza virus hemagglutinin and neuraminidase, inactivated viral proteins, and complement peptide-derived immunostimulants (CPDIs).^{18,33}

1.4.2 Particle size

The size of administered biodegradable particles encapsulating antigen is a critical formulation parameter that can influence the uptake and processing by immune cells lining the respiratory tract. Whereas smaller particles are more ideal for cellular uptake and delivery using injection based methods,³⁸ the relationship between particle size and mucosal absorption is less clear for intranasally administered vaccines and drugs.

The size of administered particles has been shown to affect the anatomical site of deposition following respiratory administration. Biodistribution studies have shown that particles in the 2-10 μ m diameter range are most often deposited in the tracheobronchial region after respiratory/intranasal administration, whereas smaller particles in the size range of 0.5–2 μ m are deposited more distally in the small conducting airways and alveoli.^{39,40}

In general, biodegradable particles encapsulating antigen must have sufficient bulk/size to facilitate impaction and deposition onto tissue surfaces and into the mucous layer during delivery into the lower airways. Indeed, this embedding in mucosa and the mucous layer seen with larger particles (greater than 500nm) has been shown to facilitate sustained released of encapsulated payloads at the site of induction.³⁸

Although a larger size facilitates particle deposition, they must also be small enough to be able to penetrate mucosal surfaces and/or be taken up by resident immune cells, as well as deposit in the lowest airways. Studies have reported that alveolar macrophages within the mucosal surface can uptake particles smaller than 5 μ m. Biodegradable particles up to approximately 1 μ m have been shown to rapidly enter the bloodstream following intranasal administration^{41,42}; particles of this size administered intranasally have also been shown to translocate across nasal mucosal surfaces and potentiate systemic immune responses.^{43,44} Conversely, some sources have reported that small-sized particles (sub-micron) are generally more efficient in nasal mucosal barrier permeation and localized induction of immune responses.⁴⁵

In addition to affecting tissue deposition and penetration, the size of biodegradable particles has a direct impact on encapsulation efficiency of loaded drug/vaccine. Larger particle sizes (microscale vs nanoscale) are known to enhance encapsulation and duration of encapsulated drug/antigen release.^{46,47} When designing sustained release/delivery formulations with an overall goal of higher loading efficiencies, the strong correlation between size and loading is undoubtedly an important parameter to take into account.³⁸

Taking all these factors into consideration, nanoformulations with diameters in the “middle ground” are likely optimal for intranasal applications, in terms of the ability to become deposited in the lower airways, be taken up by relevant immune cells, and have high degrees of drug/vaccine loading. Separate studies by Gutierrez et al. and Nagamoto et al. suggest that this “middle ground” for particle diameter is around 1 μ m. In the Gutierrez study, PLGA particles of 200nm, 500nm, and 1000nm were intranasally administered and humoral immunity assessed; the 1000nm particles consistently generated higher antigen-specific IgG titers relative to the smaller particles.⁴⁸ In the Nagamoto et al. study, particles with diameters of 400nm and 1000 nm induced

significantly higher IgA responses than particles of a 3000nm diameter after intranasal administration.⁴⁹ The findings in these studies were further bolstered by a number of different groups that have shown that particles around 1µm in size provide a longer durations of release of encapsulated antigen compared to particles of other sizes, which results in enhanced antigen presentation by DCs.⁵⁰⁻⁵³

In this dissertation, we have designed our biodegradable particle formulations with all of these sizing principles in mind, to facilitate generation of immune responses by our biodegradable particles incorporating CPDI-02. Thus, all of the developed PLGA particles described herein were designed with a target diameter of 1µm.

1.5 Effect of adjuvants on the generation of mucosal and systemic immunity by intranasally administered vaccines

The types of intranasal vaccine delivery strategies described in **Section 1.3** all have inherent immunogenic qualities in and of themselves. Novel mucosal delivery strategies alone, however, are often not sufficient to generate the magnitude and quality of immune responses required for long-term protection against encapsulated immunogen. As a result, mucosal formulations frequently employ the use of adjuvants to augment and magnify cellular and humoral immune responses to antigen. What follows is a description of several of the most commonly used mucosal adjuvants in intranasal vaccine formulations.

1.5.1 Bacteria-derived toxins

Given the highly immunogenic nature of many bacterial components, bacterial-derived toxins have been exploited as mucosal adjuvants. The two most commonly used bacterial-derived toxins include cholera toxin (CT) and *Escherichia coli* heat-labile enterotoxin (LT). The adjuvant activity of CT has been shown to induce Th2-

type cytokine production, whereas LT increases both Th1- and Th2-biased immune responses, leading to the increased production of IgA in the mucosa.⁵⁴⁻⁵⁶ Given the extremely high toxicity associated with both CT and LT, both of these adjuvants are often modified via site-directed mutagenesis or chemical modification to reduce side effects.⁵⁴

1.5.2 CpG ODNs

Originally derived from bacterial sources, CpG (Cytosine-phosphate-guanosine) ODNs (oligodeoxynucleotides) are synthetic DNA sequences enriched in cytosine-phosphate-guanosine motifs that are recognized by Toll-like receptor 9 (TLR9) on DCs and B cells. When CpG ODNs activate TLR9s, they are capable of inducing both pro-inflammatory and Th1-based cytokines and chemokines.⁵⁷ These synthetic biomolecules can also enhance antigen presentation through facilitating increased expression of co-stimulatory molecules and MHC II class molecules. Using CpG ODNs as both a mucosal and systemic adjuvant in disease-specific applications has shown downstream enhancement of the generation of CTLs, systemic IgG2a antibody, and mucosal IgA secretion.⁵⁸

1.5.3 Cytokines and chemokines

Cytokines and chemokines have been used individually or in combination as mucosal adjuvants for intranasally-delivered vaccines. In general, utilizing endogenous cytokines and chemokines as mucosal adjuvants has been shown to increase antigen-specific mucosal IgA secretion, systemic IgG, and resident mucosal CTLs.⁵⁹ Specific cytokine/chemokine combinations that have been used as adjuvants include: (1) IL-1a in varying combinations with IL-18, IL-12 and GM-CSF⁶⁰; (2) CCR7 ligands, secondary lymphoid tissue chemokine (SLC) and Epstein-Barr virus-induced molecule 1 ligand chemokine (ELC)⁶¹; (3) IL-1 β ⁶²; and

(4) combinations of cytokines from the IL-1 family⁶³. As a whole, disadvantages to these types of adjuvants are non-specific activation of cells at the site of intranasal deposition, resulting in cytotoxicity or unwanted inflammation.

1.5.4 Complement Peptide-Derived Immunostimulants (CPDIs)

Complement component 5a (C5a) is a protein fragment in the complement cascade of human innate immune activation, capable of inducing inflammatory responses, formation of the Membrane Attack Complex (MAC), and recruitment of phagocytic cells and APCs to the site of infection. In 1992, research by Morgan et al first demonstrated that amino acids 70-74 of the carboxyl-terminal sequence of the human complement C5a molecule comprise an "effector region" for the induction of IL-6 synthesis via agonist activity at the C5a receptor.⁶⁴ Further analysis revealed that the biologically active region of the C5a molecule is the final 10-residue sequence of the C-terminus (ISHKDMQLGR).⁶⁵ Synthetic analogues of this 10 amino acid sequence—now termed Complement Peptide-Derived Immunostimulants (CPDIs)—have subsequently been developed which are capable of selectively activating mononuclear phagocytes over neutrophils to potentiate innate and adaptive immune responses while minimizing neutrophil-mediated inflammatory responses. CPDI-02 is a second generation CPDI adjuvant peptide that has recently been extensively studied in the context of systemic and mucosal immunization. CPDI-02 has been successfully conjugated to chemical moieties, peptides, proteins, or inactivated pathogens, as well as being conjugated to the surface of biodegradable particles encapsulating protein vaccine, to facilitate the generation of Th1-biased humoral and cellular immune responses.^{32,33,66-70}

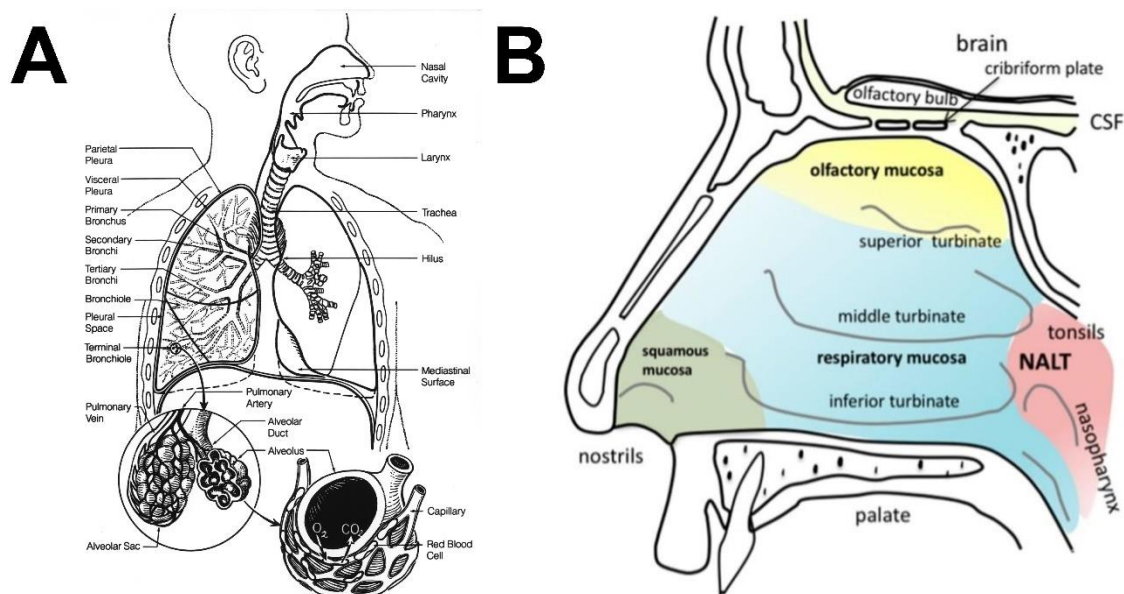


Fig.1.1. The respiratory tract and nasal cavity of humans. (A) Diagram of the entire respiratory tract. Respiratory vaccines enter the nasal cavity before proceeding through the pharynx and larynx. After passing through the trachea and primary bronchi, administered vaccines descend into the lowest airways (alveolar sacs). This is the typical site where gas exchange occurs between air and blood reservoirs within the capillaries originating from the pulmonary arteries, and is also a site of immune induction (in addition to nasal lymphoid tissues). **(B)** Diagram of the nasal cavity. The anterior portion of the nasal cavity (green) is lined by stratified squamous and transitional non-ciliated epithelial cells. The central region of the nasal cavity (blue) is lined by columnar and ciliated respiratory epithelium. The posterior region (red) is made of nasal-associated lymphoid tissue (NALT), the primary immune induction site in the nasal cavity. Lympho-epithelium covers the NALT, and is comprised of M cells, goblet cells, and many intraepithelial lymphoid cells.⁹

Fig.1.1A originally published by the National Cancer Institute (USA), currently in the public domain for free reuse. **Fig.1.1B** reproduced from "Tailoring Formulations for Intranasal Nose-to-Brain Delivery: A Review on Architecture, Physico-Chemical Characteristics and Mucociliary Clearance of the Nasal Olfactory Mucosa" by Ganger et al.⁷¹ using MDPI open-access permissions.

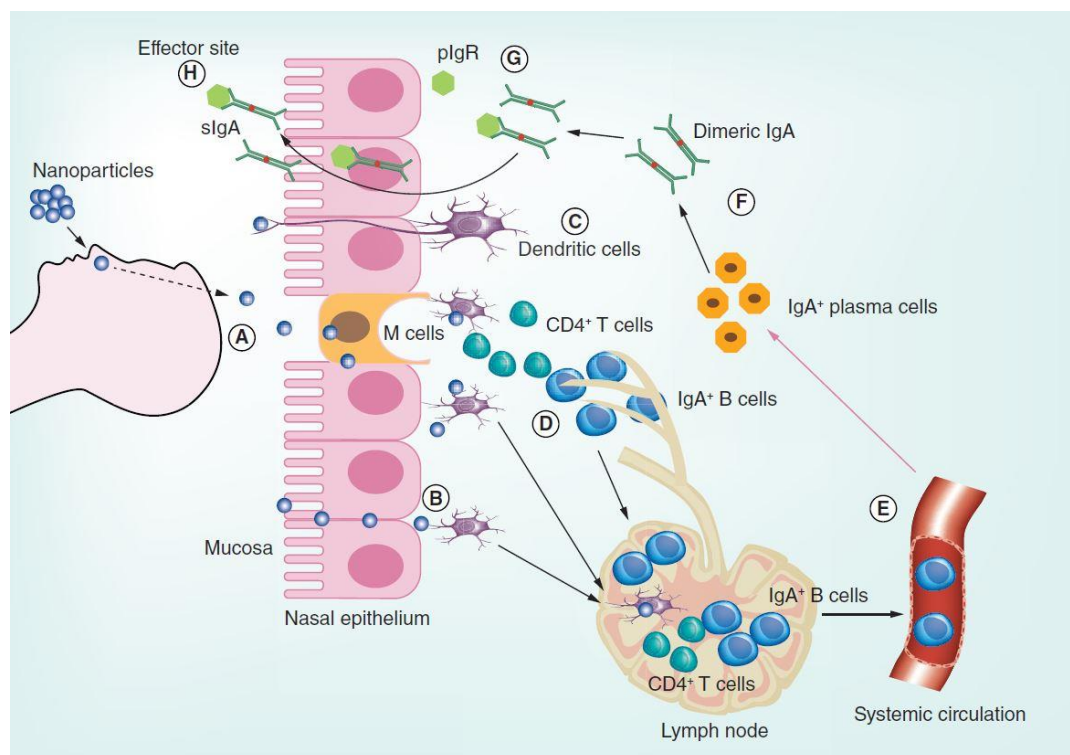


Fig.1.2. Mechanisms of immune induction in nasal-associated lymphoid tissues.

The particulate antigens are actively taken up by M cells **(A)** or permeate passively through epithelial junctions **(B)**. Alternatively, antigens are taken up by DCs extensions into the lumen **(C)**. Once antigens are captured by DCs, they migrate to nearest lymphoid follicles or lymph node to present antigens to CD4+ T cells. DCs-stimulated CD4+ T cells activate naive B cells and undergo isotype switching to form antigen-specific IgA+ committed B cells **(D)**. These IgA+ B cells migrate from lymph node to the blood circulations **(E)**. Finally, IgA+ B cells exit the blood and enter toward the effector site. They undergo final differentiation and maturation producing IgA+ plasma cells (process enhanced by IL-5 and IL-6, a subset of Th2 cells) and ultimately form dimeric or polymeric IgA **(F)**. The dimeric or polymeric IgA binds with pIgR in the basolateral region to form sIgA **(G)** and further transcytosed toward the apical side of luminal surface **(H)**.

Figure and legend reproduced with permission from the article "Intranasal delivery of nanoparticle-based vaccines," originally published by Marasini et al.⁴⁵ in the journal *Therapeutic Delivery* (a *Future Science* publication).

CHAPTER 2

HYPOTHESES & SPECIFIC AIMS

2.1 Hypothesis

Encapsulation of protein vaccines in biodegradable particles is a promising approach to mucosal immunization.^{51,72-74} The generation of long-lived adaptive immune responses against encapsulated protein, however, requires the incorporation of suitable mucosal adjuvant(s).⁷⁵ CPDI-02—previously known as “EP67”—is a novel, host-derived peptide agonist of the C5a receptor that selectively activates antigen-presenting cells (APCs) over neutrophils to drive Th1-biased humoral and cellular immune responses without the inflammatory side effects of the C5a parent molecule.^{32,33,66,68,76-78}

Previous data has shown that conjugating CPDI-02 to the surface of biodegradable nanoparticles (NPs) increases proportions of memory subsets of CD4+ and CD8+ T cells generated by encapsulated protein after respiratory immunization.³³ However, the effect of surface-conjugation of CPDI-02 to biodegradable particles encapsulating protein vaccine on the generation of mucosal and systemic *humoral* immunity has not previously been assessed. Further, neither cellular nor humoral immune responses to CPDI-02-surface-modified particles encapsulating protein vaccine after respiratory administration have been assessed at long-lived (90+ days post-final treatment) timepoints.

Mucosal vaccines are frequently delivered via intranasal administration.⁷⁹ Differing the vehicle volume for intranasal vaccines has been demonstrated to have a marked impact on the biodistribution of vaccines/nanoscale drug formulations within the respiratory tract.^{44,80-83} Results from these biodistribution studies consistently demonstrate that smaller intranasal dosage volumes in murine models (typically 10-15 μ L) are much less efficient in delivering payloads to the lungs and lower airways than their larger volume (typically 40-50 μ L) counterparts. Despite the preponderance of biodistribution data related to IAV, there remains a paucity of literature that evaluates the relationship between IAV and the generation of mucosal and systemic humoral and cellular immune responses to administered vaccines.

Similar to the variability seen with intranasal administration volumes (IAVs), there is also variability seen in literature sources in term of strategies used for incorporating adjuvants into biodegradable particles encapsulating protein vaccine. Several “conventional” strategies include: (i) encapsulating adjuvant and protein in separate particles and co-administering⁸⁴, (ii) co-encapsulation of adjuvant and protein into the same particle⁸⁵, and (iii) conjugation of adjuvant to the surface of particles encapsulating protein.⁸⁶ It is likely that the strategy for incorporating adjuvants like CPDI-02 affects the magnitude and quality of adaptive immune responses. These conventional incorporation strategies—to the best of our knowledge—have not all been directly compared in the same animal model and when assessed, often do not compare both humoral *and* cellular immune responses.

The overall long-term goal of this research is to develop efficacious biodegradable mucosal protein vaccines that incorporate the novel immunostimulant CPDI-02. The primary objectives of this dissertation, which is the next step toward our long-term goal, is to identify, develop, and immunologically assess formulation and intranasal administration strategies for incorporating CPDI-02 that are most likely to maximize the efficacy of encapsulated mucosal protein vaccines. The central hypothesis is that the strategy for incorporating CPDI-02 with biodegradable microparticles encapsulating a model mucosal protein vaccine—and the vehicle volume by which these vaccines are intranasally delivered—will affect generated mucosal/systemic humoral and cellular immune responses. The rationale for this work is that identifying an “optimal” strategy for incorporating CPDI-02 into biodegradable microparticle—and an “optimal” vehicle volume for intranasal delivery—using ovalbumin as a model protein vaccine, is an important first step towards developing and optimizing CPDI-02 based mucosal vaccines for disease-specific applications. This hypothesis will be assessed through the Specific Aims identified in **Section 2.2**.

2.2 Specific Aims

2.2.1 Chapter 4: “Surface conjugation of the novel host-derived immunostimulant CPDI-02 to biodegradable microparticles increases short-term and long-term mucosal and systemic antibodies against encapsulated protein immunogen after IN administration to naïve mice”

2.2.1.1 Specific Aim (1.1) – To develop and characterize a CPDI-02-surface-modified PLGA microparticles and scCPDI-02-surface-modified PLGA microparticles which encapsulate the model protein ovalbumin (OVA)

2.2.1.2 Specific Aim (1.2) – To intranasally administer the microparticles from **SA(1.1)** into C57BL/6 mice, and determine the effect of both CPDI-02 surface conjugation and IAV on the short- and long-term mucosal and systemic humoral immune responses generated by vaccine encapsulated within the microparticles.

2.2.2. Chapter 5: “The effect of intranasal administration volume on short- and long-term memory T-cells generated in naïve mice by intranasal immunization with protein vaccine encapsulated in CPDI-02-surface-modified biodegradable microparticles.”

2.2.2.1 Specific Aim (2.1) – To intranasally administer the microparticles from **2.2.1.1 SA(1.1)** into C57BL/6 mice, and determine the effect of CPDI-02 surface conjugation on short-term mucosal and systemic cellular immune responses generated by protein vaccine encapsulated within the microparticles.

2.2.2.2 Specific Aim (2.1) – To intranasally administer the microparticles from **2.2.1.1 SA(1.1)** into C57BL/6 mice, and determine the effect of intranasal administration volume (IAV) on the short- and long-term mucosal and systemic cellular immune responses generated by protein vaccine encapsulated within the microparticles.

2.2.3. Chapter 6: The effect of CPDI-02 adjuvant incorporation strategy on humoral and cellular immune responses generated by biodegradable microparticles encapsulating mucosal protein vaccine.

2.2.3.1 Specific Aim (3.1) – To develop and characterize a panel of PLGA microparticles encapsulating the model protein immunogen ovalbumin (OVA), which differ in the strategy by which they incorporate the adjuvant CPDI-02.

2.2.3.2 Specific Aim (3.2) – To determine the extent to which the strategy for CPDI-02 incorporation into the microparticles from **SA(3.1)** affects generated humoral and cellular immune responses in a C57BL/6 murine model after intranasal administration.

Our expectation is that the studies presented in this dissertation will identify an “optimal” strategy for incorporating CPDI-02 into a biodegradable microparticle encapsulating mucosal protein vaccine, as well as identify an “optimal” intranasal administration volume for mucosal protein vaccines in a murine model. The strengths of this dissertation include a thorough, direct comparison of MP-based mucosal protein vaccines within the same animal model, and a comprehensive characterization of humoral and cellular adaptive immune responses for all developed CPDI-02-based microparticle formulations. This dissertation will have a positive impact on the development of CPDI-02-based vaccines—as well as mucosal vaccination strategies in general—by providing a framework for the future development of mucosal vaccines against disease-specific pathogens.

CHAPTER 3

MATERIALS & METHODS

3.1 LPS removal from Ovalbumin

LPS endotoxin was removed from Grade V hen egg white ovalbumin (OVA: 385 amino acids, MW: 44,287 Da, Sigma) [40mg] using a Detoxi-Gel™ column (Thermo Scientific) according to manufacturer instructions. The resulting LPS-free ovalbumin (referred to as simply “OVA” henceforth) was utilized in all microparticle formulations, and applicable characterization assays and immunoassays herein described.

3.2 Synthesis of CPDI-02, scCPDI-02, Cys-CPDI-02 and Cys-scCPDI-02 peptides

CPDI-02 (YSFKDMP[MeL]aR, where “MeL” is N-methyl leucine and “a” is D-alanine; previously referred to as “EP67”) or inactive, scrambled CPDI-02 (“scCPDI-02”; [MeL]RMYKPaFDS) were synthesized using an AAPPTEC Apex 396 Synthesizer and purified using preparative reversed-phased HPLC as previously described.⁷⁷ CPDI-02 or scCPDI-02 were functionalized with sulfhydryl groups by introducing N-terminal cysteine during solid-phase synthesis through a cleavable glycine double arginine linker (GRR). The two resulting 14-amino acid peptides (“Cys-CPDI-02” and “Cys-scCPDI-02”) were purified and characterized as previously described.⁸⁷

3.3 Development of CPDI-02-based biodegradable PLGA microparticle formulations

Results shown in Chapter 4 and Chapter 5 of this dissertation strictly utilize a biodegradable PLGA microparticle formulation in which ovalbumin is encapsulated, and the MPs have been surface-modified with CPDI-02 or scrambled, inactivated scCPDI-02. The development of this formulation is described in Section 3.3.2. Results shown in Chapter 6 of this dissertation utilize

a panel of CPDI-02-based microparticle formulations. Each of these unique formulations are described in Sections 3.3.1 to 3.3.4.

3.3.1 Encapsulation of OVA into biodegradable PLGA microparticles (“OVA Only MPs”)

OVA was encapsulated into biodegradable PLGA 50:50 microparticles (MP) at a theoretical loading of 10 wt% (mass OVA / mass of MP-OVA) by the emulsion solvent evaporation method (ESE), with the goal of attaining particles approximately 1 μ m in diameter (see **Section 1.4.2**). We made modifications to our previously reported protocol to generate OVA-encapsulated MPs of ~1 μ m diameter.³³ Specific modifications (text in **bold**) included: using ester-terminated poly D,L-lactic-co-glycolic acid (PLGA 50:50; research grade; inherent viscosity **0.65 dL/g**; Lactel Pelham, AL) [50 mg PLGA/mL; 2 mL], utilizing a **Hielscher UP200ST ultrasonic homogenizer with an S26d14 sonotrode (Hielscher Ultrasound Technology, Teltow, Germany)**, sonicating the primary water-oil emulsion (W_1/O) for **2 minutes**, forming the crude secondary water-oil-water emulsion ($W_1/O/W_2$) by vortexing [**400RPM**] for **25 seconds**, and sonicating the secondary $W_1/O/W_2$ emulsion with a total energy applied of **60Ws (60J) at full amplitude**. The resulting microparticles encapsulating OVA alone are referred to as the “OVA Only MPs” formulation in Chapter 6 (**Table 6.1**) and are a component of the Encapsulated, Co-Administered (“ECA”) CPDI-02/scCPDI-02 incorporation strategy (later described).

3.3.2 Encapsulation of OVA into CPDI-02 or scCPDI-02 surface-modified PLGA microparticles

OVA was encapsulated into biodegradable PLGA 50:50 microparticles (MP) at a theoretical loading of 10 wt% (mass OVA / mass of MP-OVA) by the emulsion

solvent evaporation method (ESE). The MP surface was modified during encapsulation with either CGRR-CPDI-02 or an inactive scrambled CGRR-scCPDI-02 sequences through PLLA(10 kDa)-PEG(2 kDa)-maleimide linkers by interfacial activity-assisted surface functionalization (IAASF) as previously described by our lab group.³³ The same protocol parameters specified in **Section 3.3.1** were used to generate particles of approximately 1µm in diameter. The resulting microparticles encapsulating OVA and surface-modified with CPDI-02 or scCPDI-02 are the only MP formulations utilized in Chapters 4 and 5, and are referred to as the “CPDI-02 SM” MP or “scCPDI-02 SM” MP formulations in Chapter 6.

3.3.3 Development of PLGA microparticles co-encapsulating OVA and CPDI-02 or scCPDI-02

OVA and either CPDI-02 or inactive scrambled scCPDI-02 were co-encapsulated into biodegradable PLGA 50:50 microparticles (MP) at a theoretical loading of 10wt% OVA (mass OVA/mass of final MP formulation) and 5wt% CPDI-02/scCPDI-02 (mass of [CPDI-02 or scCPDI-02] / mass of final MP formulation) by the ESE method. The same protocol parameters specified in Section 3.3.1 were used to generate particles of approximately 1µm in diameter, with a single modification: during the formation of the W_1 phase, both OVA and either CPDI-02 or scCPDI-02 were dissolved in PBS at specified weight percentages (10wt.% and 5wt%, respectively) before adding to the Oil phase to form the primary emulsion. The resulting microparticles co-encapsulating OVA and either CPDI-02 or scCPDI-02 are referred to as the “CPDI-02 CE” or “scCPDI-02 CE” MP formulations, respectively, in Chapter 6.

3.3.4 Development of PLGA microparticles encapsulating CPDI-02 or scCPDI-02

CPDI-02 or scCPDI-02 was encapsulated into biodegradable PLGA 50:50 microparticles (MP) at a theoretical loading of 5wt% CPDI-02 or scCPDI-02 (mass of [CPDI-02 or scCPDI-02] / mass of final MP formulation) via an Oil-in-Oil (O_1/O_2) emulsion using a modification of previously reported ESE methods.^{88,89} The O_1/O_2 emulsion approach for microparticles encapsulating only CPDI-02 or scCPDI-02 was selected on the basis of poor loading and encapsulation efficiencies seen with $W_1/O/W_2$ techniques (<0.5wt% loading and <10% encapsulation efficiency) when attempts were made to encapsulate only CPDI-02 or scCPDI-02. Briefly, 8mg of CPDI-02 or scCPDI-02 (~5wt% loading) was dissolved in 200 μ L of methanol and added to a solution of 150mg PLGA 50:50 (research grade; inherent viscosity 0.65 dL/g; Lactel Pelham, AL) dissolved in 1.8mL of acetonitrile. The resulting co-solvent O_1 phase was then vortexed at 1000RPM for 30 seconds. The O_1 phase was then added to 4mL of O_2 phase (0.6% SPAN-80 in Cottonseed Oil [v/v%]) and vortexed at 1000RPM for 30 seconds to form a crude emulsion. Crude O_1/O_2 emulsion was then sonicated at full amplitude using a Hielscher UP200ST ultrasonic homogenizer with an S26d14 sonotrode (Hielscher Ultrasound Technology, Teltow, Germany) with a total energy limit of 400J to achieve desired particle diameter of ~1 μ m. Fully formed emulsion was then added dropwise to a beaker containing 75mL of O_2 continuous phase and stirred at 1000RPM for 16 hours to evaporate methanol and acetonitrile. CPDI-02/scCPDI-02 MPs were recovered and washed with hexane over vacuum filtration to remove residual O_2 phase components.

3.4 Diameter, polydispersity index (PDI), and zeta potential of PLGA microparticles

Average hydrodynamic diameter, PDI, and zeta-potentials \pm SD (n=3 independent samples from the same batch) of the developed microparticles were measured according to NIST standards using a ZetaSizer Nano ZS90 (Malvern Instruments, Malvern, UK) equipped with a He-Ne laser ($\lambda = 633$ nm) as the incident beam as previously reported.⁹⁰ Briefly, MPs were suspended at a concentration of 0.5mg/mL in 10mM NaCl in dH₂O at 25°C, and allowed to equilibrate within the instrument for 4 minutes before measuring.

3.5 Quantitation of CPDI-02, scCPDI-02 and OVA loading and burst release in MPs using ultra performance liquid chromatography (UPLC)

3.5.1 CPDI-02, scCPDI-02 and OVA loading in MPs

Note: The following protocol was used for all developed MP formulations (see Sections 3.3.1 through 3.3.4), with the exception of the quantitation of CPDI-02/scCPDI-02 loading on the CPDI-02/scCPDI-02 surface-modified particles (Section 3.3.2).

Average loading of OVA and of either CPDI-02 or scCPDI-02 into MPs (n=3 from at least two independent batches) was determined by first equilibrating ~2mg of each MP formulation to r.t. and dissolving in 125 μ L of DMSO in 8mL borosilicate glass vial, and incubating [r.t.] for 1hr with constant shaking. Digestion solution (NaOH [0.05 M]/SDS [0.5% w/w] in dH₂O) [1.25 mL] was added, and entire solution was stirred [650 RPM] in a capped vial overnight. Undissolved polymer was pelleted [10,000 RCF, 10 min] and supernatant was transferred to new vial, where 62.5 μ L of 10% trifluoroacetic acid (TFA) in dH₂O was added to neutralize the solution to a pH compatible with selected UPLC column (pH: 2-12). OVA alone, CPDI-02 alone, or scCPDI-02 alone were used as standards and treated under

identical digestion conditions as MP samples. Standards were serially diluted to be used as a standard curve using a diluent containing DMSO, NaOH [0.05 M]/SDS [0.5% w/w], and 10% TFA at identical concentrations to digestion solution. MP samples and OVA/CPDI-02/scCPDI-02 standards were then ran on an ACQUITY UPLC H-Class PLUS System (Waters, Milford, MA, USA) using a reversed-phase ACQUITY UPLC Protein BEH C4 Column (Waters, 300A, 1.7 μ m, 2.1 X 150 mm) under the same elution conditions. Solvent A was water containing 0.1% TFA (v/v) and Solvent B was acetonitrile containing 0.1% TFA (v/v). Samples were eluted from the columns by increasing the percentage of solvent B from 0 to 100% over 20 minutes, with continuous monitoring of column effluent at 214nm. Area under curve (AUC) of each OVA/CPDI-02/scCPDI-02 standard was calculated, and plotted against the respective OVA/CPDI-02/scCPDI-02 concentration. A linear regression curve was calculated for each standard species, and concentration of OVA, CPDI-02, or scCPDI-02 in digested MP sample determined from its measured AUC. Loading for either OVA, CPDI-02, or scCPDI-02 loading in the MP formulations was calculated as:

OVA or CPDI02 or scCPDI02 loading (wt%)

$$= \frac{\text{Calculated } \left[(\text{OVA or CPDI02 or scCPDI02}) \frac{\text{mg}}{\text{mL}} \right] \text{ from AUC} \times \text{Assay Sample Volume [1.4375mL]}}{\text{Starting Mass of MPs [2mg]}} \times 100$$

And percent encapsulation efficiency (EE%) was calculated as :

$$EE\%_{\text{OVA or CPDI02 or scCPDI02}} = \frac{[\text{Assayed mg (OVA or CPDI02 or scCPDI02)}] / \text{mg particles}}{[\text{Theoretical mg (OVA or CPDI02 or scCPDI02)}] / \text{mg particles}} \times 100$$

Note: For the quantification of CPDI-02/scCPDI-02 loading on the CPDI-02/scCPDI-02 surface-modified particles (Section 3.3.2), the following procedure was used:

Average loading of CPDI-02 or scCPDI-02 onto surface-modified MPs (n=3 from at least two independent batches) was determined by first enzymatically cleaving CPDI-02 or sc-CPDI-02 from MP surface by suspending 10mg of SM MPs into 0.1M Tris-HCl buffer [4mL, pH=8.5] containing 200µg of Kex2 protease (“kexin”; SignalChem Lifesciences, Richmond, BC, Canada). Kexin is a protease produced by *S. cerevisiae* yeast, that—like its mammalian/human homolog furin—is capable of cleaving the carboxyl side of Arg-Arg moieties in peptides and proteins.^{91,92} Treatment of MPs with excess kexin is thus expected to cleave the CGRR moiety linking CPDI-02 or scCPDI-02 to the MP surface, allowing complete liberation of all CPDI-02 or scCPDI-02 from the particles. Following treatment with Kexin according to manufacturer instructions, MP solution was pelleted [10,000 RCF, 10 min] and supernatant collected. Supernatant sample and serial dilutions of pure CPDI-02 or scCPDI-02 suspended in 0.1M Tris-HCl buffer for a standard curve were then ran on UPLC using an ACQUITY UPLC Peptide BEH C18 Column (Waters; 130A, 1.7 µm, 2.1 X 150 mm) with the same gradient conditions as previously stated above. AUC of each CPDI-02 or scCPDI-02 standard was calculated, and plotted against respective concentrations. A linear regression curve was calculated, and concentration of CPDI-02 or sc-CPDI-02 in kexin-treated surface-modified MP samples were determined from their measured AUC. CPDI-02 and scCPDI-02 loading then was calculated as:

CPDI02 or scCPDI02 loading (wt%)

$$= \frac{\text{Calculated } \left[\text{CPDI02 or scCPDI02} \frac{\text{mg}}{\text{mL}} \right] \text{ from AUC} \times \text{Assay Sample Volume [4mL]}}{\text{Starting Mass of MPs [10mg]}} \times 100$$

Percent encapsulation efficiency (EE%) was calculated as

$$EE\%_{CPDI02 \text{ or } scCPDI02} = \frac{(\text{Assayed mg CPDI02 or scCPDI02})/\text{mg particles}}{(\text{Theoretical mg CPDI02 or scCPDI02})/\text{mg particles}} \times 100$$

3.5.2 OVA burst release from microparticle formulations

Burst release of OVA from MPs (average percent of total OVA released from lyophilized NP 24 h after resuspension) \pm SD (n=3 from at least two independent batches) was determined as we previously described with modification.³³ MPs [10mg] from all formulations incorporating OVA were suspended in 1mL of PBST (PBS and Tween-20 [0.05% v/v]), vortexed [20 s], and incubated [37 °C] with shaking [200 rpm/min] (Vortemp 56 Shaking Incubator) for 24hr. Samples were pelleted [10,000 RCF, 5 min], and supernatants collected. Serial dilutions of OVA in PBST were prepared in the same manner, to be used as concentration standards. MP supernatants and OVA standards were then ran on UPLC using same conditions as stated above for total OVA loading in MPs, and concentration of released OVA in supernatant determined using AUC/linear regression. Burst release (% OVA released) was calculated as

$$\text{Burst release}_{OVA} = \left[\frac{\text{Calculated OVA [mg/mL]}_{\text{supernatant}} \times \text{Sample Volume [1mL]}}{\frac{\text{mass OVA [mg]}}{\text{mass of particles [mg]}} \times \text{mass of particles [10mg]}} \right] \times 100$$

3.6 Animals used in experimental procedures

All animal procedures were approved by the University of Nebraska Medical Center Institutional Animal Care and Use Committee (UNMC IACUC). Upon

receipt, naïve mice (C57BL/6, ~8-weeks old, Charles River Laboratories) were first acclimated in an ABSL-2 facility (UNMC Comparative Medicine) under pathogen-free conditions for one week before experiments.

3.7 Respiratory immunization with CPDI-02- or sc-CPDI-02-based OVA MPs

MP formulations were intranasally administered to naïve female C57BL/6 mice (~8-weeks old) on Day -14 (Prime), Day -7 (Boost #1), and Day 0 (Boost #2). Specific treatment groups are specified in each relevant figure in Chapters 4, 5 and 6, and include details such as formulation type, dose of OVA and CPDI-02 or scCPDI-02, and intranasal administration volume. Immediately prior to immunization, mice were anesthetized using an isoflurane-anesthetic chamber with vaporizer. Oxygen flow rate to the sealed induction chamber was set to 1.5L/min and vaporized isoflurane at 2.5%. Mice were sedated and visually monitored until they were in a recumbent position and breathing had stabilized at a slower rate (~5 minutes). Mice were removed from the chamber and held in a supine position while intranasally administering the relevant treatment dropwise, achieved by alternating drops between nares using a 2-20 μ L pipettor (10 μ L IAVs) or 20-200 μ L pipettor (50 μ L IAVs). Intranasal administration of 10 μ L volumes are expected to deposit MP treatments primarily in the nasal cavity, whereas 50 μ L volume is expected to deposit MP treatments in both the nasal cavity and lungs (i.e. respiratory immunization).⁸¹⁻⁸³

3.8 Isolation of murine lung lymphocytes and splenocytes

Mice were euthanized via isoflurane overdose followed by cervical dislocation at 6 days, 14 days, and 90 days after final immunization. Following euthanasia, lungs were surgically exposed and perfused by injecting PBS [5 mL] with a 25G needle

through the right ventricle of the heart. Lungs were minced using sterile surgical scissors and placed directly in a sterile gentleMACS C-Tube (Miltenyi) containing 5 mL complete RPMI containing collagenase IV at 1mg/mL (cRPMI: RPMI-1640 (Hyclone), HI-FBS (Atlanta Biologicals) [10% v/v], L-glutamine (GIBCO) [2 mM], sodium pyruvate (Gibco) [1 mM], non-essential amino acids (Hyclone) [0.1 mM], MEM vitamin solution (Hyclone) [1X], penicillin G/streptomycin sulfate (Gibco) [100 U/mL/100 µg/mL], β-mercaptoethanol (Sigma) [50 µM]). Lung fragments were then homogenized with a gentleMACS Tissue Dissociator (Miltenyi) using the “m_lung_02” setting, and incubated [37 °C, 30 minutes] in a shaking incubator (Vortem) [200 RPM]. Following incubation, digested lung fragments were homogenized again with the Tissue Dissociator using the same settings. Splenocytes were isolated using sterile forceps, minced with sterile surgical scissors, and then placed in sterile gentleMACS C tube containing 3mL cRPMI. Spleens were then homogenized with a gentleMACS Tissue Dissociator using the “m_spleen_01” setting. Digested spleen/lung cell suspensions were then passed through sterile 30 µm pre-separation filters (Miltenyi), then carefully overlaid onto 5mL Lympholyte M (Cedarlane Labs) in a sterile 15mL centrifuge tube. Cells were centrifuged at 1500 RCF, 20 mins, r.t., no brakes. Lung lymphocytes were then collected from the interphase with a sterile Pasteur pipette, and transferred to a sterile 15-mL centrifuge tube. Cells were diluted to 10mL with cRPMI, pelleted [800 RCF, r.t., 10 min], and supernatants aspirated. An additional wash step was completed by resuspending cells in 7mL cRPMI, pelleting [800 RCF, r.t., 10 min] and aspirating supernatants. Purified lung lymphocytes and splenocytes were then initially resuspended in 0.6mL and 1.2mL, respectively, of desired cell media (assay specific, indicated below accordingly), and then counted using a Cellometer

Auto T4 Automated Cell Counter. Suspensions were further diluted to desired concentrations, as later specified for each assay.

3.9 Collection of serum, BALF, and NLF from immunized mice

Serum was collected from immunized mice on Day 14 and Day 90. Briefly, serum was isolated by first collecting 0.2-0.3mL of whole blood via submandibular venipuncture with a 5mm lancet (MEDpoint) in a sterile 500 μ L centrifuge tube as previously described.⁹³ Samples were allowed to clot at room temperature for 30 minutes and then centrifuged [2000 RCF, 4°C, 10 minutes]. Serum was then isolated using a 20-200 μ L pipettor and transferred to a new sterile 500 μ L centrifuge tube. Bronchoalveolar lavage fluid (BALF) and nasal lavage fluid (NLF) were collected from immunized mice that were euthanized with isoflurane overdose on Day 14 and Day 90 using previously described methods.^{94,95} Briefly, the tracheas of immunized mice were surgically exposed, and an incision made below the larynx. A cannula was then inserted, and 1.0 mL of sterile PBS was instilled into the lungs and recovered by aspiration. For NLF collection, the cannula was then reoriented in the trachea to the cranial direction, and guided towards the nasopharynx. A 0.6mL aliquot of sterile PBS was then flushed through the nasal cavity and collected in a 6-well plate, before transferring to a sterile 500 μ L centrifuge tube. BALF and NLF samples were then centrifuged to remove cells [400 RCF, 4°C, 10 minutes]; supernatants were then isolated and transferred to new sterile 500 μ L centrifuge tubes. Serum, BALF, and NFL samples were stored at -80°C until later analyses.

3.10 IgA, IgG, IgM, and IFN- γ ELISpots (General)

All ELISpot assays were completed using Murine Single-Color ELISpot kits from CTL Immunospot according to manufacturer directions, with a few modifications (specified below) to enable assessment of epitope-specific antibody secreting cell (ASC) and cellular responses. All spots on ELISpot plates were measured and analyzed with an ImmunoSpot S6 MACRO Plate Analyzer (CTL), using the “Smart Count Wizard” function. The plate reader was adjusted to B cell (IgA, IgG, IgM) and T cell (IFN- γ) specific modes. Additional parameters included using the “Small Spots” setting, adjusting Spot Separation=1, Background Balance=10, and manually adjusting the positive spot gating threshold to a minimum size of 0.001mm² (IFN- γ), 0.0015mm² (IgA and IgG), or 0.0035 mm² (IgM). Once spot counts for each well were acquired, average spot count per sample (lung lymphocyte or splenocyte) was calculated, and adjusted to SFUs per 1x10⁶ cells.

3.10.1 OVA-specific IgA, IgG, and IgM ELISpots (Specific Considerations)

Murine lung lymphocytes and splenocytes were isolated at Day 6 to be utilized for OVA-specific IgA, IgG, and IgM ELISpots. Plates were coated with OVA [75 μ g/mL, 80 μ L/well] the day prior to cell isolations (Day 5), instead of capture antibody. Isolated lung lymphocytes and splenocytes (**Section 3.8**) were resuspended in serum-free CTL-Test Media [5x10⁶ cells/mL] and plated in triplicate [100 μ L/well] on Day 6, and incubated 37°C, 5% CO₂ for 18 hours.

3.10.2 OVA-specific CD4⁺ and CD8⁺ IFN- γ ELISpots (Specific Considerations)

Murine lung lymphocytes and splenocytes were isolated at Day 14 and Day 90 (**Section 3.8**). After purification, lung lymphocytes and splenocytes were suspended in serum-free CTL-Test media [5x10⁶ cells/mL] and plated in triplicate [100 μ L/well]. One of two OVA-specific epitopes was then added to plated cells

(100 μ L/well, for final volume of 200 μ L/well) at a final total concentration of 10 μ g/mL of OVA epitope. Epitopes used were specific either for CD4⁺ T Cells [ISQAVHAAHAEINEAGR, InvivoGen; binds to I-A(d) MHC class II protein]^{96,97} or for CD8⁺ T Cells [SIINFEKL, InvivoGen; binds to MHC class I H-2 K^b]^{98,99}. Plates were incubated for either 24 hours (Day 14 isolations) or 48 hours (Day 90 isolations) at 37°C, 5% CO₂, before completing assay as directed by manufacturer.

3.11 FACS analysis of OVA-specific CD4⁺ and CD8⁺ T-cells

Purified lung lymphocytes and splenocytes harvested on Day 14 and Day 90 (**Section 3.8**) were diluted to 1x10⁷ cells/mL in PBS, and plated (0.1mL/well) on a 96-well plate. Surface phenotype of OVA-specific CD4⁺ and CD8⁺ T cells was determined using flow cytometry as previously described.³³ Briefly, cells were incubated with MHC Class-I Tetramers-BV421 (H-2K^b/SIINFEKL, “Tet-OVA₂₅₇₋₂₆₄”) or MHC Class-II Tetramers-BV421 (I-Ab/HAAHAEINEA, “Tet-OVA₃₂₈₋₃₃₇”) (NIH Tetramer Core Facility at Emory University, Atlanta, GA, USA [1 μ g/10⁶ cells]. Staining for additional cell markers was applied using a cocktail containing half the manufacturer’s suggested amount of either FITC Anti-Mouse CD8a FITC (Clone 53–6.7; BioLegend) or Alexa Fluor 488 Anti-Mouse CD4 (Clone GK1.5; BioLegend); PE Anti-Mouse CD127 (Clone A7R34; BioLegend); APC Anti-Mouse KLRG1 (Clone 2F1; BioLegend); PE/Dazzle Anti-Mouse CD62L (Clone MEL-14; BioLegend); and PE/Cy5 Anti-Mouse CD44 (Clone IM7; BioLegend). Of note, the gating strategy was individualized to each T cell-type/organ-type pairing (ie, CD4⁺ in lungs, CD8⁺ in lungs, CD4⁺ in spleen, or CD8⁺ in spleen), and then kept constant between Day 14 and Day 90.

3.12 OVA-specific antibody titers of serum, BALF, and NLF

Indirect ELISA was used to assess OVA-specific titers of IgG1, IgG2b, IgG2c, and IgG3 in isolated serum, IgA and total IgG in BALF, and IgA in NLF (**Section 3.9**). Each isotype- or subclass-specific assay was completed according to manufacturer's instructions, with a few modifications. For all ELISAs, OVA was suspended in ELISA coating buffer (Thermo Scientific) [100µg/mL], coated on a 96-well clear flat-bottom polystyrene high bind microplate (Corning) [0.1mL/well], sealed in parafilm, and incubated at 4°C overnight. Plates were washed with PBST [300µL x 3 washes] using an automated plate washer (BioTek ELx50 Microplate Strip Washer), and blocked with 250µL/well of 2X ELISA Assay Diluent (Invitrogen) for 2 hours. Plates were washed again using same settings, and 15µL/well of 1X ELISA Assay Diluent was added to plate. Serial 10-fold dilutions (min. 6 dilutions) of sera, BALF, or NLF of each treatment group in 1X diluent were plated, and incubated on a plate shaker [400RPM] for 2 hours. Plates were washed with PBST [300µL x 3 washes] and HRP-conjugated detection antibodies for assay-specific isotype were diluted in 1X diluent and added to each plate [100 µL/well]. Plates were incubated on a plate shaker [400RPM] for 1 hour. Specific HRP-conjugated detection antibodies added were: goat anti-Mouse IgG1, HRP (Invitrogen, 1:500 dilution); goat anti-Mouse IgG2b, HRP (Invitrogen) [1:500 dilution]; goat anti-mouse IgG2c, HRP (Invitrogen) [1:500 dilution]; goat anti-mouse IgG3, HRP (Cell Signaling Technology) [1:250 dilution]; goat anti-mouse IgG (H+L), HRP (Invitrogen) [1:500 dilution]; or goat anti-mouse IgA (Invitrogen) [1:250 dilution]. Plates were washed with same settings, then TMB substrate solution (ThermoFisher Scientific) was added [100µL/well] and allowed to incubate in the dark for 20 minutes. Stop solution was then added [0.16M H₂SO₄ in H₂O, 100µL/well], and UV absorbance immediately read at 450nm and 570nm using a

microplate reader (Spectramax iD3, Molecular Devices, San Jose, CA, USA). Net absorbance reading (optical density, O.D.) of each well was calculated as:

$$\text{Net absorbance} = O.D._{450nm} - (O.D._{570nm} + \text{Average } O.D. \text{ of blank wells}_{\geq 6 \text{ wells}})$$

Any resulting net absorbance readings that were negative were set equal to 0. Positive antibody titer cutoff thresholds for individual dilution factors were then calculated statistically at the $\alpha=0.05$ level,¹⁰⁰ using the average net absorbance readings of mice from the vehicle-only treatment group (negative control). Net absorbance readings of mice from each specified MP treatment groups were then compared to positive titer cutoff thresholds, by plotting 4-parameter logistic (4PL) curves of net absorbances of individual mice (constraint were set on equations setting “bottom” value to 0), and plotting a 4PL curve of positive cutoff thresholds (constraint set on equations setting “bottom” value to be ≥ 0.01 , which is the margin of error of photometric accuracy for the Spectramax iD3 device). Individual titer values were then interpolated as the dilution factor at the intersection of the respective 4PL curve of each mouse and the 4PL curve of the positive titer cutoff thresholds.¹⁰¹ For NLF titers, calculated values were then multiplied by a factor of 18.75 to adjust for the volume of the nasal cavity (average nasal cavity volume of mice is $\sim 32\mu\text{L}$ ¹⁰²; nasal cavities were flushed with $600\mu\text{L}$ PBS during nasal lavage [$600 / 32 = 18.75$]).

3.13 Lung histology of immunized mice

To assess any potential long-term inflammatory responses and/or cytotoxicity of administered CPDI-02-SM MPs (Chapter 4 only), histologic analyses were completed on lungs of mice at Day 90 as previously described.¹⁰³ Briefly, lungs

were first perfused by injecting PBS [5 mL] with a 25G needle through the right ventricle of the heart. Whole lungs were removed and inflated to 10 cm H₂O pressure with a solution of 10% formalin to preserve anatomical structure. Fixed lungs were embedded in paraffin and sections (4–5 μm) were cut and stained with hematoxylin and eosin by the University of Nebraska Medical Center Tissue Sciences Facility (Omaha, NE, USA). Sample sections were then assessed for any pathology by a blinded, experienced grader (Dr. Todd Wyatt, Professor of Internal Medicine—Division of Pulmonary, Critical Care and Sleep, UNMC), using a scaling system that ranged from 1 to 5 (where 1 = “normal lung” and 5 = “severe inflammation”).

3.14 Statistics

All data comparisons where three or more treatment groups were present, results were analyzed using nonparametric Kruskal-Wallis one-way ANOVA with uncorrected Dunn's multiple comparisons post hoc test ($\alpha = 0.05$). For data comparisons with only two treatment groups, results were analyzed using the two-tailed, nonparametric Mann-Whitney U Test ($\alpha = 0.05$). ELISpot and antibody titer results were pooled from $n \geq 2$ independent experiments, with identical experimental parameters. Sample outliers in all experiments were identified through application of the ROUT method ($Q = 1\%$) and subsequently omitted in statistical comparisons. All statistical analyses were completed using GraphPad Prism software (Version 9.0). Any additional relevant statistical information is provided in the legends of related figures.

CHAPTER 4

Surface conjugation of the host-derived immunostimulant CPDI-02 to biodegradable microparticles increases short-term and long-term mucosal and systemic antibodies against encapsulated protein immunogen after IN administration to naïve mice

4.1 Introduction

Our lab group previously found that conjugation of CPDI-02 to the surface of biodegradable nanoparticles encapsulating OVA resulted in: (1) increased magnitudes of total T-cells and early-appearing memory subsets of OVA-specific CD4+ and CD8+ T cells in the lungs and spleen of intranasally immunized mice; and (2) decreased peak CFU of *L. monocytogenes* that ectopically express OVA in the lungs, liver, and spleen after respiratory challenge.³³ Although these findings indicate that CPDI-02 is an effective mucosal adjuvant for inducing immunogen-specific *cellular* immunity, it remains unclear whether intranasal administration of CPDI-02-surface-modified degradable particles encapsulating immunogen has a similar effect on *humoral* immunity.

The effect of CPDI-02 on the generation of humoral immunity in general is not wholly unknown, however. Previous research by Morgan et al found that administering an OVA-CPDI-02 conjugate via the intraperitoneal (IP) route to female C57BL/6 mice (young and aged) resulted in significantly higher serum titers of OVA-specific IgG1 and IgG2b compared to a vaccine using alum as the adjuvant.¹⁰⁴ Given that this study used an alternate route of administration and did not use biodegradable particles, it remains necessary to assess the humoral adjuvanticity of CPDI-02 in the context of both mucosal/intranasal administration and as a targeting ligand on the surface of a PLGA particle vaccine. In Chapter 4 of this dissertation, we aim to determine the effect of CPDI-02 surface conjugation, by evaluating humoral immune responses of C57BL/6 mice intranasally administered CPDI-02-surface-modified microparticles encapsulating the model protein OVA.

4.2 Results

4.2.1 Encapsulation of LPS-free OVA in biodegradable microparticles surface-conjugated with CPDI-02 or inactive, scrambled CPDI-02

To encapsulate LPS-free ovalbumin (OVA) in biodegradable microparticles (MP) surface-conjugated with CPDI-02 or inactive, scrambled CPDI-02 (scCPDI-02), we activated the surface of MP with maleimide (MAL) groups through 2 kDa PEG linkers by physically incorporating diblock copolymers of PLLA(10K)-PEG(2K)-MAL into PLGA 50:50 MP by interfacial activity assisted surface functionalization (IAASF) during $W_1/O/W_2$ encapsulation of LPS-free OVA at 10 wt% theoretical loading^{105,106} (**Section 3.3.2; Fig 4.1A**). We then conjugated sulfhydryl (cysteine)-activated CPDI-02 or scCPDI-02 to MAL-activated PEG on the MP surface through protease-labile N-terminal Cys-Gly-Arg-Arg linkers (**Fig 4.1B**). OVA was consistently encapsulated at ~5 to 6 wt% with minimal burst release (0.4 to 0.8%) in 1 μ m MP surface conjugated with 0.4 wt% CGRR-CPDI-02 ("CDPI-02-SM MP") or CGRR-scCPDI-02 ("scCPDI-02-SM MP") (**Table 4.1**).

4.2.2 Effect of surface conjugating CPDI-02 to biodegradable microparticles and IAV on the generation of short-term IgA, IgM, and IgG ASCs against encapsulated protein immunogen in the lungs of young, naïve mice

To provide an early indication that surface conjugating CPDI-02 to biodegradable microparticles increases the generation of mucosal antibodies against encapsulated protein immunogen, we intranasally administered vehicle alone (PBS, 50 μ L IAV) or vehicle containing an equivalent dose of LPS-free OVA [50 μ g] encapsulated in CPDI-02-SM MP or in inactive scCPDI-02-SM MP (**Table 1**) to young, naïve female C57BL/6

mice once every 7 days over 14 days (**Fig.4.2**). Magnitudes of generated epitope-specific ASCs at early timepoints (as measured by ELISpot) have previously been shown to correlate strongly with epitope-specific antibody titers at later timepoints.¹⁰⁷ We additionally used intranasal administration volumes (IAV) of 10 μ L or 50 μ L for CPDI-02-SM MP given that (i.) an IAV of 10 μ L restricts delivery of payloads to the nasal cavity and an IAV of 50 μ L has been shown to deliver payloads throughout nasal cavity and lower respiratory tracts of mice^{44,80,81} and (ii.) IAV can affect magnitudes of systemic antibodies in mice.^{82,108} We then compared magnitudes of OVA-specific IgA, IgG, and IgM antibody secreting cells (ASCs) in the lungs 6 days post-treatment by ELISpot (**Fig.4.2**).

CPDI-02-SM MP in 50 μ L IAV (**Fig.4.2**, black circles) increased OVA-specific IgA ASCs (767-fold) (**Fig.4.2A**), IgM ASCs (1120-fold) (**Fig.4.2B**), and IgG ASCs (275-fold higher) (**Fig.4.2C**) in the lungs compared to 50 μ L vehicle alone (**Fig.4.2**, white squares). CPDI-02-SM MP (**Fig.4.2**, black circles) also increased OVA-specific IgA ASCs (144-fold) (**Fig.4.2A**) and IgM ASCs (52-fold) (**Fig.4.2B**) with a trending, but statistically insignificant, 30-fold increase of OVA-specific IgG ASCs (**Fig.4.2C**) in the lungs compared to inactive scCPDI-02-SM MP in the same 50 μ L IAV (**Fig.4.2**, white circles). In contrast, CPDI-02-SM MP in 10 μ L IAV (**Fig.4.2**, white triangles) generated similar levels of OVA-specific IgA ASCs (**Fig.4.2A**), OVA-specific IgM ASCs (**Fig.4.2B**), and OVA-specific IgG ASCs (**Fig.4.2C**) in the lungs as 50 μ L of vehicle alone (**Fig.4.2**, white squares). Thus, given that a proportion of IgM B-cells will class-switch to IgG B-cells¹⁰⁹, conjugating CPDI-02 to the surface of \sim 1 μ m biodegradable microparticles and increasing delivery to the lungs likely increase the generation of mucosal antibodies against encapsulated protein immunogen in young, naïve mice.

4.2.3 Effect of surface conjugating CPDI-02 to biodegradable microparticles and IAV on generation of short-term and long-term mucosal antibodies against encapsulated protein immunogen in the nasal cavity and lungs of young, naïve mice

Given that CPDI-02-SM MP in 50 μ L IAV generated higher magnitudes of IgA and IgM ASCs against encapsulated LPS-free OVA in the lungs of mice 6 days post-treatment (**Fig.4.2**), we expected that CPDI-02-SM MP in 50 μ L IAV would also increase subsequent titers of OVA-specific mucosal antibodies. To first determine if surface conjugating CPDI-02 to biodegradable microparticles increases the generation of short-term mucosal antibodies against encapsulated protein immunogen, we intranasally administered vehicle alone (50 μ L), inactive scCPDI-02-SM MP in 50 μ L IAV, or CPDI-02-SM MP in 10 μ L or 50 μ L IAV as before (**Fig.4.2**) but compared titers of OVA-specific IgA in nasal lavage fluid (NLF) and titers of OVA-specific IgA and Total IgG in bronchoalveolar lavage fluid (BALF) normalized to vehicle alone 14 days post-treatment by ELISA (**Fig.4.3A-C**).

CPDI-02-SM MP in 50 μ L IAV (**Fig.4.3**, black circles) increased titers of OVA-specific IgA in the NLF (12-fold) (**Fig.4.3A**) and BALF ($10^{2.1}$ -fold) (**Fig.4.3B**) and OVA-specific IgG in the BALF ($10^{2.4}$ -fold) (**Fig.4.3C**) 14 days post-treatment compared to inactive scCPDI-02-SM MP in the same 50 μ L IAV (**Fig.4.3**, white circles). CPDI-02-SM MP in 50 μ L IAV (**Fig.4.3**, black circles) also increased titers of OVA-specific IgA in the NLF ($10^{2.7}$ -fold) (**Fig.4.3A**) and BALF ($10^{4.2}$ -fold) (**Fig.4.3B**) and OVA-specific IgG in the BALF ($10^{4.8}$ -fold) (**Fig.4.3C**) 14 days post-treatment compared to CPDI-02-SM MP in 10 μ L IAV (**Fig.4.3**, white triangles). Thus, surface conjugating CPDI-02 to ~ 1 μ m biodegradable microparticles and increasing delivery to the lungs (via a larger

IAV) increases the generation of short-term mucosal antibodies against encapsulated protein immunogen in young, naïve mice.

To next determine if conjugating CPDI-02 to the surface of biodegradable microparticles also increases the generation of long-term mucosal antibodies against encapsulated protein immunogen, we intranasally administered vehicle alone (50 μ L), inactive scCPDI-02-SM MP in 50 μ L IAV, or CPDI-02-SM MP in 10 μ L or 50 μ L IAV as before (**Fig.4.2**) but compared titers of OVA-specific IgA in nasal lavage fluid (NLF) and titers of OVA-specific IgA and IgG in bronchoalveolar lavage fluid (BALF) normalized to vehicle alone 90 days post-treatment by ELISA (**Fig.4.3D-F**).

At Day 90, CPDI-02-SM MP in 50 μ L IAV (**Fig.4.3**, black circles) also increased titers of OVA-specific IgA in the NLF ($10^{3.8}$ -fold) (**Fig.4.3D**) and BALF ($10^{3.8}$ -fold) (**Fig.4.3E**) and titers of OVA-specific IgG in the BALF ($10^{4.2}$ -fold) (**Fig.4.3F**) 90 days post-treatment compared to both scCPDI-02-SM MP in 50 μ L IAV (**Fig.4.3**, white circles) and CPDI-02-SM MP in 10 μ L IAV (**Fig.4.3**, white triangles). Thus, conjugating CPDI-02 to the surface of ~ 1 μ m biodegradable microparticles and increasing delivery to the lungs (via a larger IAV) increases the generation of long-term mucosal antibodies against encapsulated protein immunogen in young, naïve mice.

4.2.4 Effect of surface conjugating CPDI-02 to biodegradable microparticles and IAV on the generation of short-term IgA, IgM, and IgG ASCs against encapsulated protein immunogen in the spleens of young, naïve mice

Efficacious respiratory vaccines facilitate the stimulation of mucosal *and* systemic immunity. As referenced in **Figure 1.1**, when intranasally administered antigens or nanoparticulate vaccines penetrate nasal epithelia and/or lung epithelia, they are

taken up by DCs, which then migrate to lymph nodes and stimulate CD4⁺ T cells, which in turn activate and stimulate the generation of antigen-specific B Cells. The B cells generated in mucosal inductive sites are then able to localize to the spleen and propagate systemic immune responses.^{15,45,110,111} Because of this, and the fact that CPDI-02-SM MPs were able to generate mucosal humoral immune responses in the lungs, it is likely that CPDI-02-SM MPs are able to generate systemic humoral immune responses in the spleen.

To provide an early indication that conjugating CPDI-02 to the surface of biodegradable microparticles and increasing delivery to the lungs increases the generation of systemic antibodies against encapsulated protein immunogen, we intranasally administered vehicle alone (50 μ L), inactive scCPDI-02-SM MP in 50 μ L IAV, or CPDI-02-SM MP in 10 μ L or 50 μ L IAV as before (**Fig.4.2**) but compared the magnitudes of OVA-specific IgA, IgG, and IgM antibody secreting cells (ASCs) in the spleen 6 days post-treatment by ELISpot (**Fig.4.4**).

CPDI-02-SM MP in 50 μ L IAV (**Fig.4.4A&B**, black circles) generated similar levels of OVA-specific IgA and IgM ASCs in the spleen as 50 μ L of vehicle alone (**Fig.4.4A&B**, white squares), inactive scCPDI-02-SM MP in 50 μ L IAV (**Fig.4.4A&B**, white circles), and CPDI-02-SM MP in 10 μ L IAV (**Fig.4.4A&B**, white triangles). In contrast, CPDI-02-SM MP in 50 μ L IAV (**Fig.4.4C**, black circles) generated 17-fold higher levels of OVA-specific IgG than vehicle alone (**Fig.4.4C**, white squares), 41-fold higher levels of OVA-specific IgG than CPDI-02-SM MP in 10 μ L IAV (**Fig.4.4C**, white triangles), and 2.5-fold higher levels of OVA-specific IgG in the spleen as inactive scCPDI-02-SM MP in 50 μ L IAV (**Fig.4.4C**, white circles) 6 days post-treatment. Thus, based on differences between the magnitudes of ASCs in the spleen 6 days post-treatment, surface-conjugating CPDI-02 to \sim 1 μ m biodegradable microparticles and

increasing delivery to the lungs via larger IAV is likely to increase the generation of systemic antibodies against encapsulated protein immunogen in young, naïve mice.

4.2.5 Effect of CPDI-02 surface conjugation to biodegradable microparticles and IAV on the generation of short-term and long-term systemic antibodies against encapsulated protein immunogen in the serum of young, naïve mice

Given that CPDI-02-SM MP in 50 μ L IAV generated higher magnitudes of OVA-specific IgG ASCs than both inactive scCPDI-02-SM MP in 50 μ L IAV and CPDI-02-SM MP in 10 μ L in the spleens of mice at 6 days post-treatment (**Fig.4.4**), we expected CPDI-02-SM MP in 50 μ L IAV would also increase subsequent titers of OVA-specific systemic antibodies. To first determine if conjugating CPDI-02 to the surface of biodegradable microparticles increases the generation of short-term systemic antibodies against encapsulated protein immunogen, we intranasally administered vehicle alone (50 μ L), inactive scCPDI-02-SM MP in 50 μ L IAV, or CPDI-02-SM MP in 10 μ L or 50 μ L IAV as before (**Fig.2**) but compared titers of OVA-specific IgG subclasses in the serum normalized to vehicle alone at 14 days post-treatment by ELISA (**Fig.4.5A-D**).

CPDI-02-SM MP in 50 μ L IAV (**Fig.4.5**, black circles) generated $10^{2.9}$ -fold higher titers of OVA-specific IgG1 (**Fig.4.5A**), $10^{2.4}$ -fold higher titers of OVA-specific IgG2b (**Fig.4.5B**), $10^{4.8}$ -fold higher titers of OVA-specific IgG2c (**Fig.4.5C**), and $10^{4.9}$ -fold higher titers of OVA-specific IgG3 (**Fig.4.5D**) in the serum 14 days post-treatment than inactive scCPDI-02-SM MP in the same 50 μ L IAV (**Fig.4.5**, white circles). CPDI-02-SM MP in 50 μ L IAV (**Fig.4.5**, black circles) also generated $10^{3.8}$ -fold higher titers of OVA-specific IgG1 (**Fig.4.5A**), $10^{3.3}$ -fold higher titers of OVA-specific IgG2b (**Fig.4.5B**), $10^{5.4}$ -fold higher titers of OVA-specific IgG2c (**Fig.4.5C**), and $10^{4.9}$ -fold

higher titers of OVA-specific IgG3 (**Fig.4.5D**) in the serum 14 days post-treatment than CPDI-02-SM MP in 10 μ L IAV (**Fig.4.5**, white triangles). Thus, conjugating CPDI-02 to the surface of \sim 1 μ m biodegradable microparticles and increasing delivery to the lungs via larger IAV increases the generation of short-term systemic antibodies against encapsulated protein immunogen in young, naïve mice.

To next determine if conjugating CPDI-02 to the surface of biodegradable microparticles increases the generation of long-term systemic antibodies against encapsulated protein immunogen, we intranasally administered vehicle alone (50 μ L), inactive scCPDI-02-SM MP in 50 μ L IAV, or CPDI-02-SM MP in 10 μ L or 50 μ L IAV as before (**Fig.2**) but compared titers of OVA-specific IgG subclasses in the serum normalized to vehicle alone 90 days post-treatment by ELISA (**Fig.5E-H**).

CPDI-02-SM MP in 50 μ L IAV (**Fig.4.5**, black circles) generated $10^{3.4}$ -fold higher titers of OVA-specific IgG1 (**Fig.4.5E**), $10^{3.3}$ -fold higher titers of OVA-specific IgG2b (**Fig.4.5F**), $10^{2.2}$ -fold higher titers of OVA-specific IgG2c (**Fig.4.5G**), and $10^{4.6}$ -fold higher titers of OVA-specific IgG3 (**Fig.4.5H**) in the serum 90 days post-treatment than inactive scCPDI-02-SM MP in the same 50 μ L IAV (**Fig.4.5**, white circles). CPDI-02-SM MP in 50 μ L IAV (**Fig.4.5**, black circles) also generated $10^{3.0}$ -fold higher titers of OVA-specific IgG1 (**Fig.4.5E**), $10^{3.3}$ -fold higher titers of OVA-specific IgG2b (**Fig.4.5F**), $10^{3.0}$ -fold higher titers of OVA-specific IgG2c (**Fig.4.5G**), and $10^{1.6}$ -fold higher titers of OVA-specific IgG3 (**Fig.4.5H**) in the serum 90 days post-treatment than CPDI-02-SM MP in 10 μ L IAV (**Fig.4.5**, white triangles). Thus, conjugating CPDI-02 to the surface of \sim 1 μ m biodegradable microparticles and increasing delivery to the lungs via larger IAV increases the generation of long-term systemic antibodies against encapsulated protein immunogen in young, naïve mice.

4.2.6 Longitudinal analysis of Th1-Th2 profile of systemic antibodies in mice treated with CPDI-02-SM MPs in 50 μ L IAV

In C57BL/6 mice, the IgG1 antibody subclass has been shown to be associated with Th2-biased immunity, whereas IgG2b, IgG2c and IgG3 have been shown to be associated with Th1-biased responses.¹¹²⁻¹¹⁴ The ratio of subclasses of systemic antibodies to one another can serve as surrogate markers for overall determining Th1- or Th2-bias. Given that serum titers for mice treated with CPDI-02-SM MPs in 50 μ L IAV were significantly higher at both short- and long-term timepoints compared to mice treated with scCPDI-02-SM MPs in 50 μ L IAV and mice treated with CPDI-02-SM MPs in 10 μ L IAV (**Fig.4.5**), we next sought to assess whether these elevated titers were reflective of a Th1-biased or Th2-biased immune response.

Mice were treated with CPDI-02-SM MPs in 50 μ L IAV at Day -14, Day -7, and Day 0 as before (**Fig.2**), and IgG2b:IgG1, IgG2c:IgG1, and IgG3:IgG1 ratios were calculated at 14 days and 90 days post-treatment using the same titers depicted in **Fig.4.5**. A combined overall Th1:Th2 ratio ([IgG2b + IgG2c + IgG3] : IgG1) was also calculated. These ratios were not determined in the scCPDI-02-SM MPs in 50 μ L IAV and CPDI-02-SM MPs in 10 μ L IAV treatment groups due to very low and non-detectable titer levels of the majority of the mice in these cohorts (**Fig.4.5**).

From Day 14 to Day 90, the average ratio of IgG2b:IgG1 significantly increased from 0.08 to 2.04 (**Fig.4.6B**), as did the average ratio of IgG2c:IgG1 (from 0.02 to 1.10) (**Fig.4.6C**). The ratio of IgG3:IgG1 did not significantly change over the same time period (0.02 vs 0.04). The average combined [IgG2b + IgG2c + IgG3] : IgG1 ratio significantly increased from 0.16 to 3.18 from Day 14 to Day 90 (**Fig.4.6A**).

From Day 14 to Day 90, there was a non-significant, but appreciable decrease in average IgG1 titers for the CPDI-02-SM MPs in 50 μ L IAV treatment group ($10^{6.6}$ to $10^{6.1}$; $P=0.237$) (**Figs.4.5A&E**; statistical comparison not shown graphically), and

significant increases in average IgG2b titers ($10^{5.5}$ to $10^{6.3}$; $P < 0.0001$) (**Figs.4.5B & F**; statistical comparison not shown graphically) and IgG2c ($10^{5.4}$ to $10^{6.2}$; $P = 0.0004$) (**Figs.4.5C&G**; statistical comparison not shown graphically).

4.2.7 Effect of IAV and surface-conjugation of CPDI-02 to biodegradable microparticles encapsulating mucosal protein vaccine on long-term inflammatory changes in the lungs in naïve female C57BL/6 mice after respiratory immunization

Given that CPDI-02-SM MPs in 50 μ L IAV significantly increased the magnitudes of OVA-specific ASCs in the lungs at an early timepoint (**Fig.4.2**) and generated OVA-specific antibody titers that persisted from short-term to long-term timepoints, it is likely that there are long-term observable histologic changes in the lungs of mice treated with CPDI-02-SM MPs (50 μ L IAV). To determine whether CPDI-02-SM MPs indeed induces any histologic changes or indications of inflammatory responses in mice, we intranasally administered vehicle alone (50 μ L), inactive scCPDI-02-SM MP in 50 μ L IAV, or CPDI-02-SM MP in 10 μ L or 50 μ L IAV as before (**Fig.2**), and then on Day 90 surgically isolated, fixed, and stained the lungs of mice (Section 3.13) from all treatment groups.

Inflammation scores were given to the lungs of mice from each treatment group ($n=4$ per group), by an experienced, blinded grader using a scaling system that ranged from 1 to 5 (where 1 = “normal lung” and 5 = “severe inflammation”). Mice treated with CPDI-02-SM MPs in 50 μ L IAV had significantly higher indications of inflammation (mean score: 2.25) relative to the vehicle alone (mean score: 1.13) and CPDI-02-SM MPs in 10 μ L IAV (mean score: 1.25) (**Fig.4.7**). However, mice treated with CPDI-02-SM MPs in 50 μ L IAV had a similar average inflammation score compared to mice

treated with scCPDI-02-SM MPs in 50 μ L IAV (mean score: 1.63). The inflammation seen in mice treated with CPDI-02-SM MPs or scCPDI-02-SM MPs in 50 μ L IAV was mild in nature, and qualitatively described as having “few mild foci of perivascular inflammatory cells and alveolar macrophages.”

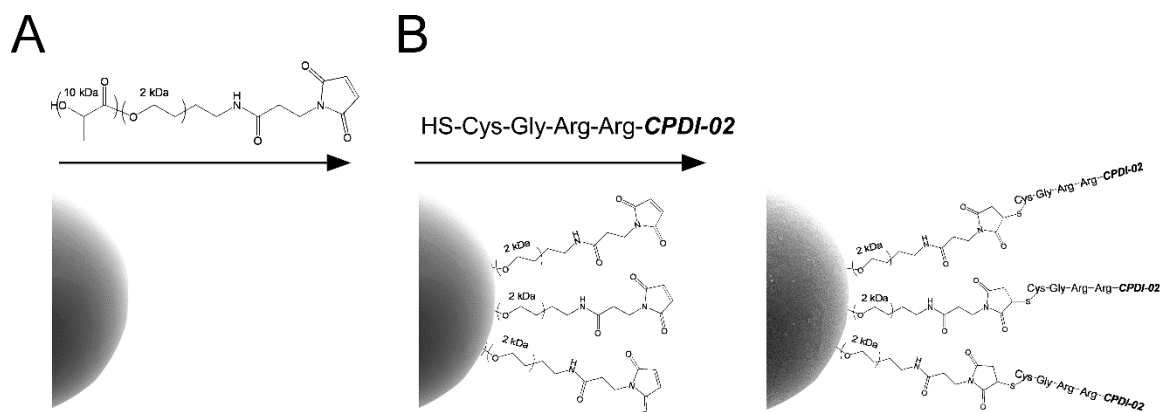


Fig 4.1. Synthetic strategy for conjugating CPDI-02 to the surface of biodegradable microparticles. PLGA 50:50 microparticles (MP) were (A) surface-activated with maleimide through 2 kDa PEG linkers by interfacial activity assisted surface functionalization (IAASF) with PLLA[10 kDa]-b-PEG[2 kDa]-maleimide diblock copolymers during encapsulation of LPS-free OVA by the W/O/W emulsification solvent extraction method (ESE), washed with deionized water, then lyophilized. (B) CPDI-02 was activated with sulfhydryl groups by the addition of an N-terminal Cys through a protease-labile Gly-Arg-Arg-linker during peptide synthesis, then reacted with the surfaces of maleimide-activated MP resuspended in PBS at a ratio of 0.07mg CGRR-CPDI-02 to every 1mg of MPs. Following activation of CPDI-02 to the linker, microparticles were washed (x3) with deionized water to remove residual unbound peptide, and lyophilized a second time.

Table 4.1

Formulation	OVA Loading ($\mu\text{g}/\text{mg}$ MP \pm SD)	Burst release ^a (% Loaded OVA)	CPDI-02 Conjugation ^b ($\mu\text{g}/\text{mg}$ MP \pm SD)	Diameter ^c (μm \pm SD)	Polydispersity Index ^c (PDI \pm SD)	Zeta Potential ^e (mV \pm SD)
CPDI-02-SM MP	62 \pm 13	0.8 \pm 0.2	4.0 \pm 0.6	1.12 \pm 0.17	0.26 \pm 0.15	-22.5 \pm 3.3
scCPDI-02-SM MP	52 \pm 13	0.4 \pm 0.1	3.9 \pm 0.2	1.21 \pm 0.02	0.36 \pm 0.08	-23.7 \pm 4.3

Table 4.1. Representative characteristics of OVA-encapsulated PLGA 50:50 microparticles (MP). ^aTotal encapsulated OVA released 24 hr after resuspension in PBS determined by UPLC AUC quantitation. ^bSurface conjugation of CPDI-02 or scCPDI-02 to MP determined by kexin-release / ultra-high performance liquid chromatography (UPLC). ^cDiameter, polydispersity index, and zeta potential determined using ZetaSizer Nano ZS90 (Malvern). Results are representative of at least two independent batches.

Fig.4.2

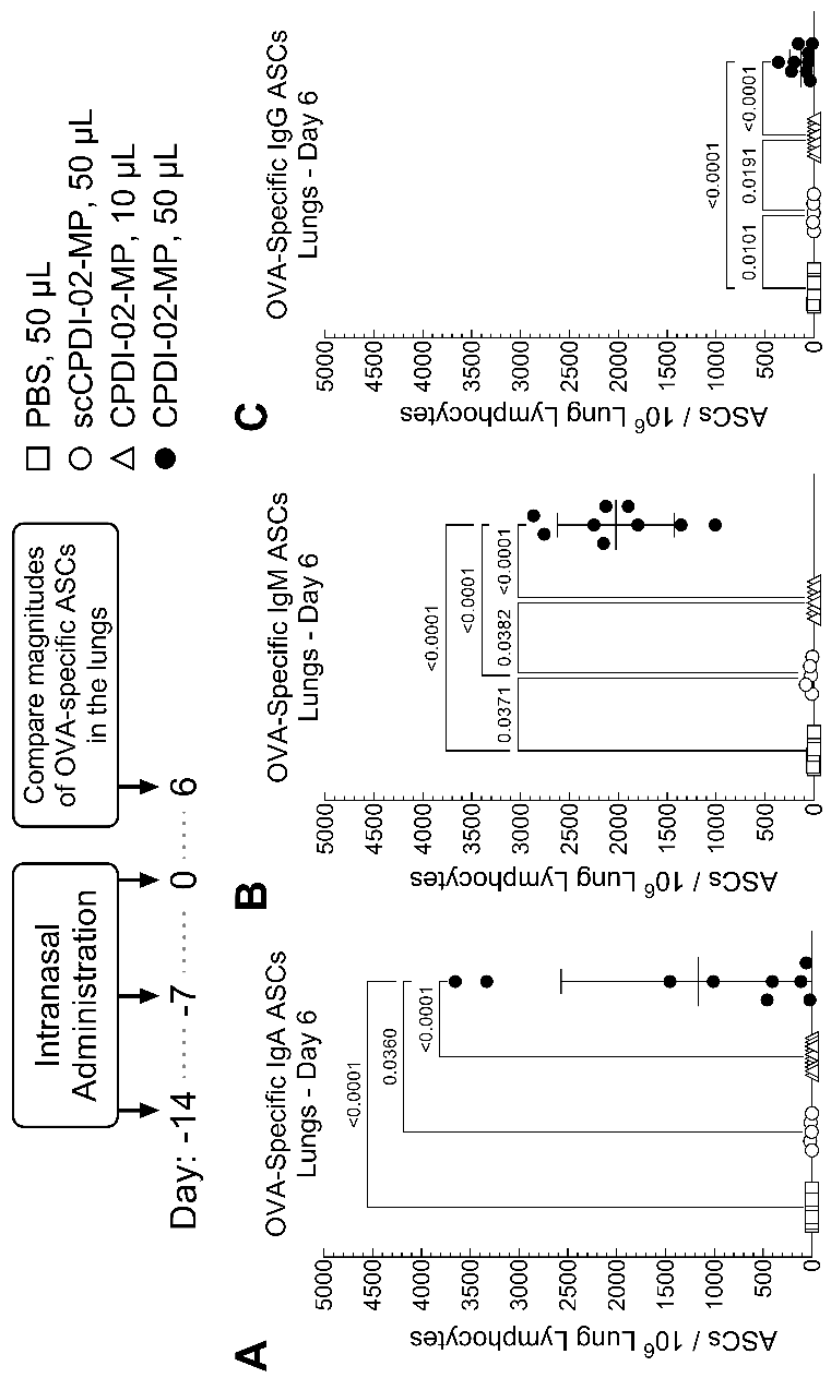


Fig.4.2. Effect of surface-conjugating CPDI-02 to biodegradable microparticles and intranasal administration volume (IAV) on magnitudes of short-term OVA-specific antibody-secreting cells (ASCs) in the lungs of naïve female C57BL/6 mice after respiratory immunization with encapsulated LPS-free OVA. Vehicle alone (PBS [50 μ L], white squares) or vehicle containing an equivalent dose of LPS-free OVA [50 μ g] encapsulated in PLGA 50:50 microparticles (~1 μ m diam.) with 0.39 wt% surface-conjugated inactive, scrambled CPDI-02 (scCPDI-02-SM MP [50 μ L], white circles) or 0.40 wt% CPDI-02 (CPDI-02-SM MP [10 μ L], white triangles or CPDI-02-SM MP [50 μ L], black circles) through 2 kDa PEG linkers (**Table 4.1**) was intranasally administered to naive female C57BL/6 mice (n=10 mice total from two independent studies) on Days -14, -7, and 0. Average OVA-specific (**A**) IgA, (**B**) IgM, and (**C**) IgG antibody secreting cell (ASC) spots / 10^6 lung lymphocytes \pm SD (n=3 replicates per mouse) in the lungs were determined 6 days post-IN administration by ELISpot and compared by Kruskal-Wallis nonparametric one-way ANOVA with uncorrected Dunn's post-test.

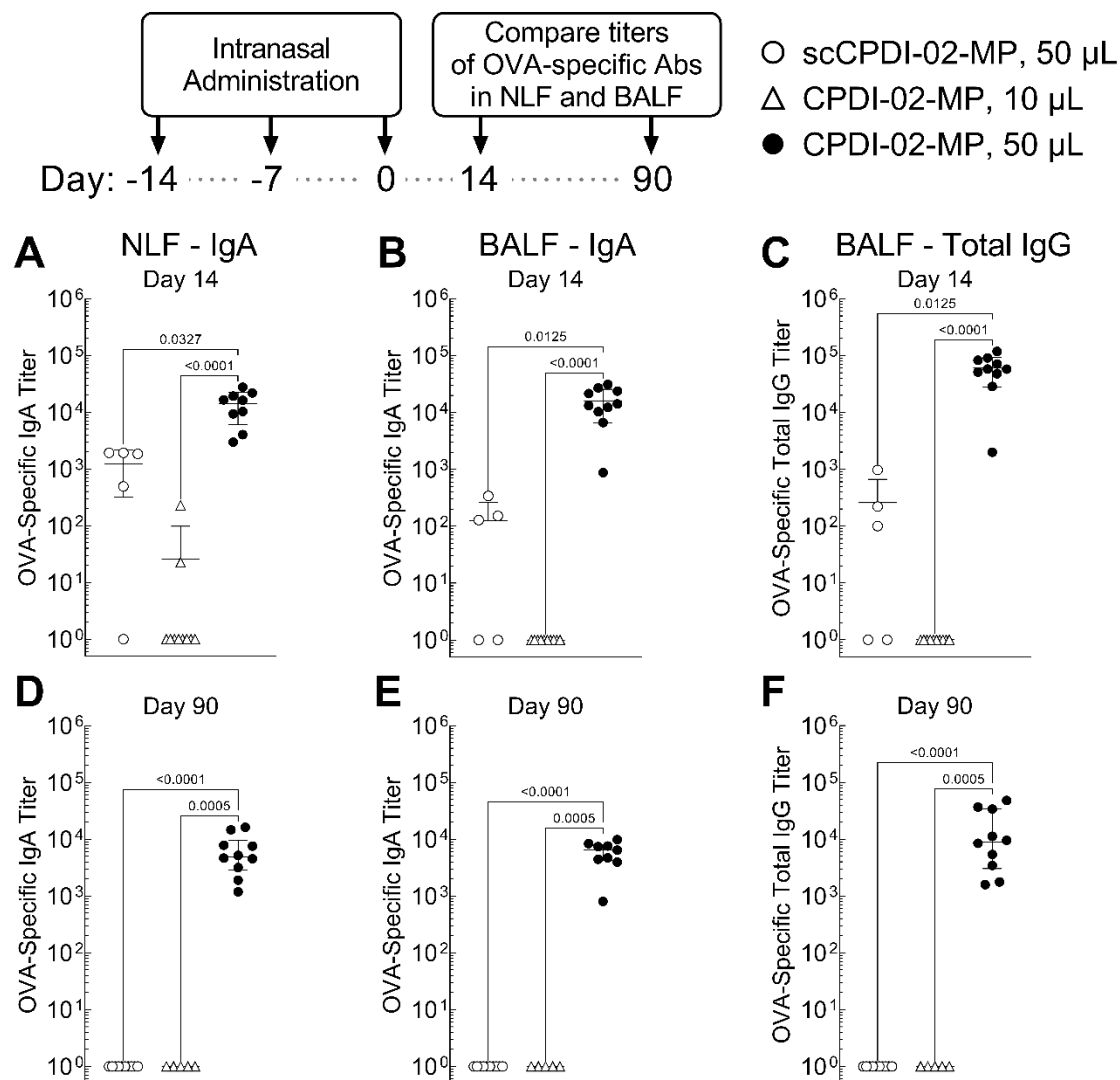


Fig.4.3. Effect of surface-conjugating CPDI-02 to biodegradable microparticles and intranasal administration volume (IAV) on titers of short-term and long-term OVA-specific antibodies in the nasal cavities and lungs of naïve female C57BL/6 mice after respiratory immunization with encapsulated LPS-free OVA. Vehicle alone (PBS, 50 μ L) or vehicle containing an equivalent dose of LPS-free OVA [50 μ g] encapsulated in PLGA 50:50 microparticles (~1 μ m diam.) with 0.39 wt% surface-conjugated inactive, scrambled scCPDI-02 (scCPDI-02, 50 μ L) or 0.40 wt% CPDI-02 (CPDI-02, 10 or 50 μ L) through 2 kDa PEG linkers (**Table 4.1**) was intranasally administered to naïve female

C57BL/6 mice (~8 weeks old; n=5 mice for Day 14 scCPDI-02-SM MP treatment group, and n=10 for all other treatment groups) on Days -14, -7, and 0. Average OVA-specific titers \pm SD of IgA in the nasal lavage fluid (NLF) (**A, D**) and bronchial lavage fluid (BALF) (**B, E**) or total IgG in the BALF (**C,F**) 14 days (**A-C**) and 90 days (**D-F**) post-IN administration were determined by ELISA, normalized to vehicle alone by “positive titer cutoff threshold method,”¹⁰⁰ and compared by Kruskal-Wallis nonparametric one-way ANOVA with uncorrected Dunn’s post-test. Outliers identified by the ROUT method (Q = 1%) were omitted. Non-detectable titers below the positive titer cutoff threshold are shown as 10⁰. Day 14 results are representative of at least two independent studies.

Fig.4.4

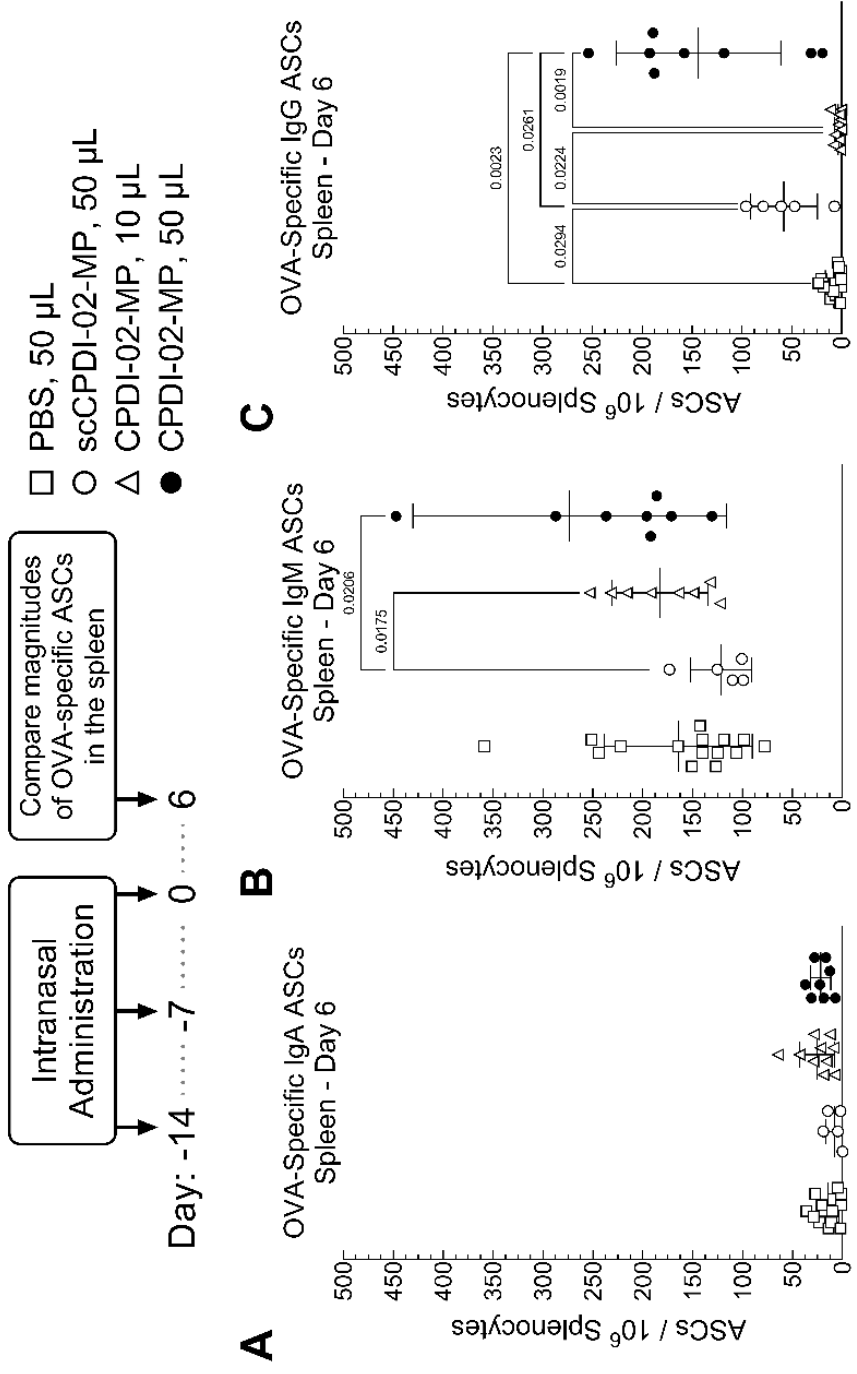


Fig.4.4. Effect of surface-conjugating CPDI-02 to biodegradable microparticles and intranasal administration volume (IAV) on magnitudes of short-term systemic OVA-specific antibody-secreting cells (ASCs) in the spleens of naïve female C57BL/6 mice after respiratory immunization with encapsulated LPS-free OVA. Vehicle alone (PBS, 50 μ L) or vehicle containing an equivalent dose of LPS-free OVA [50 μ g] encapsulated in PLGA 50:50 microparticles (~1 μ m diam.) with 0.39 wt% surface-conjugated inactive, scrambled scCPDI-02 (scCPDI-02, 50 μ L) or 0.40 wt% CPDI-02 (CPDI-02, 10 or 50 μ L) through 2 kDa PEG linkers (**Table 4.1**) was intranasally administered to naive female C57BL/6 mice (~8 weeks old; n=5 mice for vehicle alone, 5 mice for scCPDI-02-SM MP treatment group, and 10 mice for both 10 μ L and 50 μ L CPDI-02-SM MP treatment groups) on Days -14, -7, and 0. Average OVA-specific IgA (**A**), IgM (**B**), and IgG (**C**) antibody secreting cell (ASC) spots / 10^6 splenocytes \pm SD (n=3 replicates per mouse) were determined 6 days post-IN administration by ELISpot and compared by Kruskal-Wallis nonparametric one-way ANOVA with uncorrected Dunn's post-test. Outliers identified by the ROUT method (Q = 1%) were omitted.

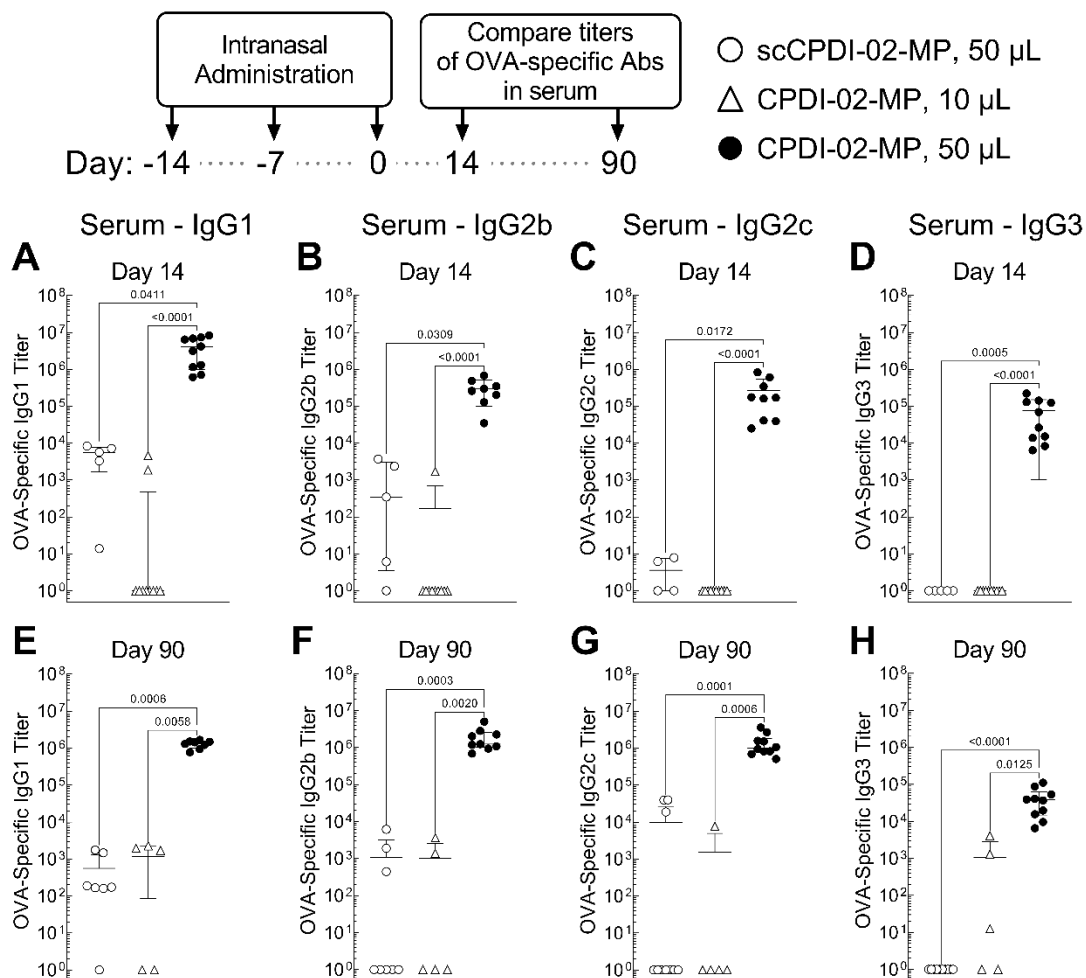


Fig.4.5. Effect of surface-conjugating CPDI-02 to biodegradable microparticles and intranasal administration volume (IAV) on the titers of short-term and long-term systemic OVA-specific Th1 and Th2 subclasses of IgG in the serum of naïve female C57BL/6 mice after respiratory immunization with encapsulated LPS-free OVA. Vehicle alone (PBS, 50 µL) or vehicle containing an equivalent dose of LPS-free OVA [50µg] encapsulated in PLGA 50:50 microparticles (~1 µm diam.) with 0.39 wt% surface-conjugated inactive, scrambled scCPDI-02 (scCPDI-02, 50 µL) or 0.40 wt% CPDI-02 (CPDI-02, 10 or 50 µL) through 2 kDa PEG linkers (**Table 4.1**) was intranasally administered to naive female C57BL/6 mice (~8 weeks old; n=5 mice for Day 14 scCPDI-02-SM MP treatment group, and n=10 for all other treatment groups) on Days -14, -7, and

0. Average OVA-specific titers \pm SD of IgG1 Th2 antibodies (**A&E**) and IgG2b (**B&F**), IgG2c (**C&G**), and IgG3 (**D&H**) Th1 antibodies in the serum were determined 14 days (**A-D**) and 90 days (**E-H**) post-immunization by ELISA, normalized to vehicle alone by “positive titer cutoff threshold method,”¹⁰⁰ and compared by Kruskal-Wallis nonparametric one-way ANOVA with uncorrected Dunn’s post-test. Outliers identified by the ROUT method (Q = 1%) were omitted. Non-detectable titers below the positive titer cutoff threshold are shown as 10^0 . Results are representative of at least two independent studies.

Fig.4.6

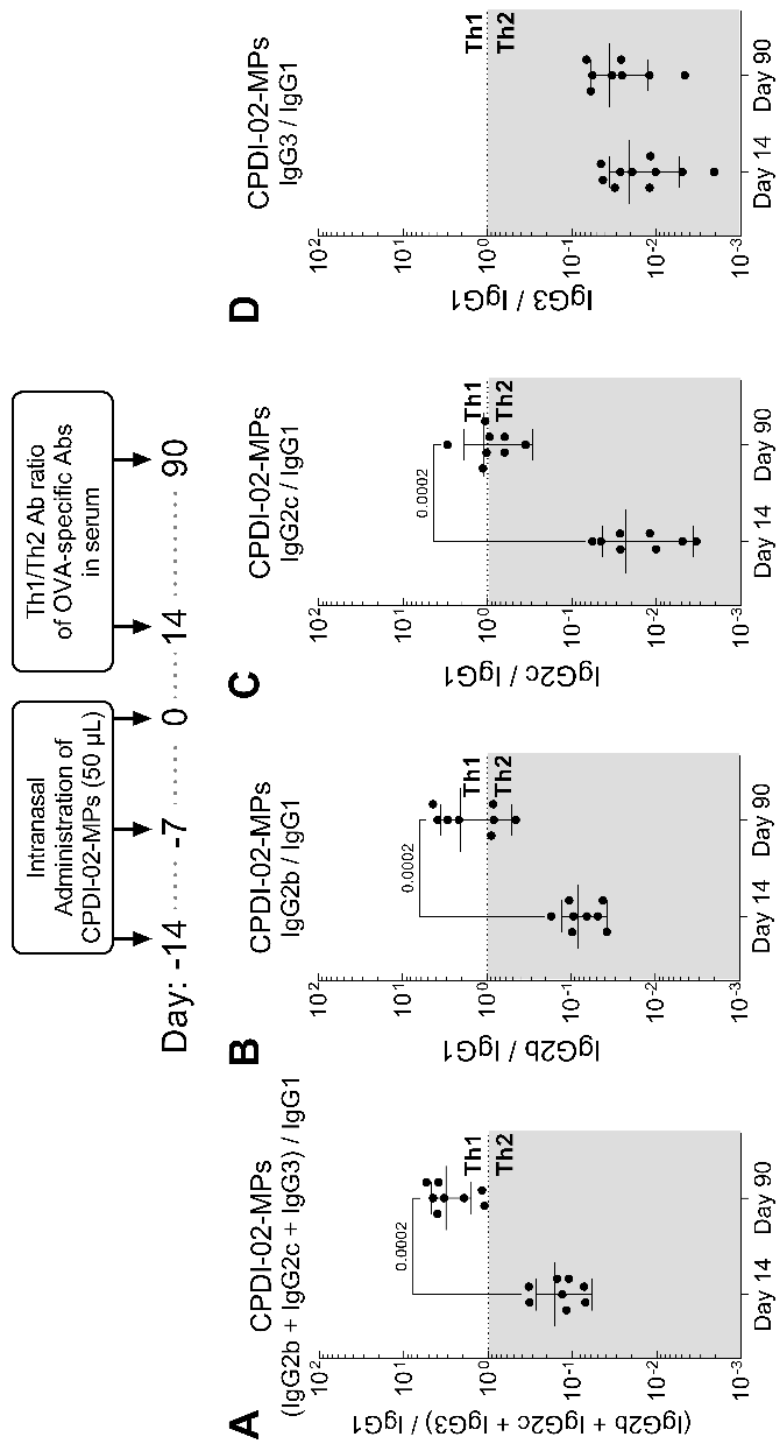


Fig.4.6. Longitudinal analysis of Th1-Th2 profile of systemic antibodies in mice treated with CPDI-02-SM MPs in 50 μ L IAV. Vehicle [50 μ L] containing a 50 μ g dose equivalent of LPS-free OVA encapsulated in PLGA 50:50 microparticles (~1 μ m diam.) surface-modified with 0.4 wt% CPDI-02 through 2 kDa PEG linkers (**Table 4.1**) was intranasally administered to naive female C57BL/6 mice (~8 weeks old; n=10 mice) on Days -14, -7, and 0. Average ratios of Th1/Th2 antibody titers \pm SD on Day 14 and Day 90 post-immunization of **(A)** total Th1 antibodies (IgG2b + IgG2c + IgG3) / Th2 antibodies (IgG1), **(B)** IgG2b / IgG1, **(C)** IgG2c / IgG1, or **(D)** IgG3 / IgG1 were determined by ELISA and compared by two-tailed, nonparametric Mann-Whitney U Test. Outlier ratios identified by the ROUT method (Q = 1%) were omitted. Results are representative of at least two independent studies.

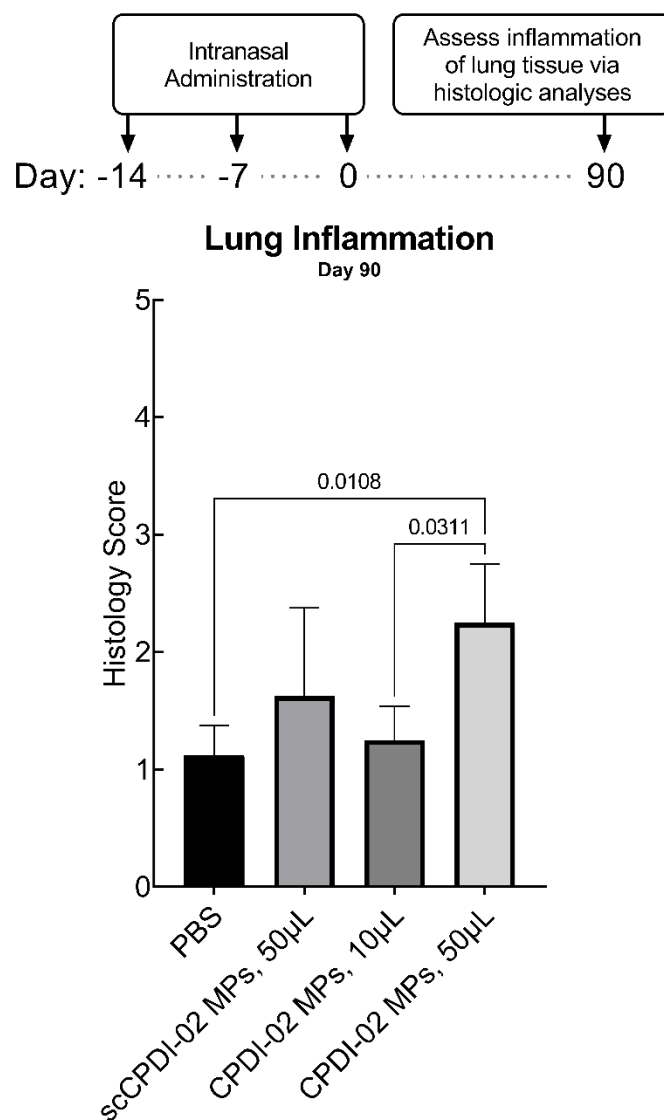


Fig.4.7. Effect of surface-conjugating CPDI-02 to biodegradable microparticles and intranasal administration volume (IAV) on long-term inflammatory changes in the lungs of naïve female C57BL/6 mice after respiratory immunization with encapsulated LPS-free OVA. Vehicle alone (“PBS,” 50 µL) or vehicle containing an equivalent dose of LPS-free OVA [50µg] encapsulated in PLGA 50:50 microparticles (~1 µm diam.) with 0.39 wt% surface-conjugated inactive, scrambled scCPDI-02 (scCPDI-02 MPs, 50 µL) or 0.40 wt% CPDI-02 (“CPDI-02 MPs, 10 µL” or “CPDI-02 MPs, 50 µL”) through 2 kDa PEG linkers (**Table 4.1**) was intranasally administered to naive female

C57BL/6 mice (~8 weeks old; n=4 mice per treatment group) on Days -14, -7, and 0. On Day 90, perfused lungs were excised and inflated with 10% formalin. Fixed lungs were embedded in paraffin and cut sections stained with hematoxylin and eosin, before being graded by an experienced, blinded grader using a scaling system that ranged from 1 to 5 (where 1 = “normal lung” and 5 = “severe inflammation”). Results were compared by Kruskal-Wallis nonparametric one-way ANOVA with uncorrected Dunn’s post-test. No outliers were identified by the ROUT method (Q = 1%).

CHAPTER 5

The effect of intranasal administration volume on short- and long-term memory T-cells generated in naïve mice by intranasal immunization with protein vaccine encapsulated in CPDI-02-surface-modified biodegradable microparticles

5.1 Introduction

Intranasal vaccines are typically deployed in a liquid formulation or as a dry powder. While each of these approaches offers distinct advantages, liquid formulations are by far the most common, due to their simplistic and flexible application, reduced nasal mucosal irritation, and lower production costs. The only FDA-approved intranasal vaccine currently on the market—FluMist Quadrivalent—is administered as a liquid suspension. Overall, intranasal vaccines using a liquid-based administration are becoming increasingly prevalent and are readily translatable to the clinic.

Despite recent scientific interest and advances in intranasal vaccination strategies, many questions remain and areas unexplored. One such area is the elucidation of the “ideal” volume of intranasal delivery vehicle for drug and vaccines in liquid suspensions/solutions. CPDI-02-protein conjugate vaccines (non-encapsulated) have shown efficacy when administered using a 15 μ L intranasal administration volume (IAV),⁶⁶ whereas incorporating CPDI-02 and protein vaccine into biodegradable particles have shown efficacy using 50 μ L IAVs.^{32,33} It remains unclear, however, whether the formulations utilizing biodegradable particles will maintain efficacy being deployed using a smaller IAV in the range of 10-15 μ L.

The varied IAVs of CPDI-02-based intranasal vaccines in these previously reported studies reflect a more universal trend across literature sources pertaining to intranasal immunization: there is a current lack of uniformity in terms of the IAV of mucosal vaccines in murine models. The noted differences in IAV across literature sources prompted several groups to assess the impact of IAV on biodistribution. Eyles et al. showed that instillation of scandium-46 labelled styrene-divinyl benzene 7- μ m-diameter microspheres in comparatively large (50 μ L) IAVs resulted in substantial bronchopulmonary deposition, whereas intranasal instillation of microspheres suspended

in 10 μ L volumes tended to restrict particle deposition initially to the nasal cavity.⁸¹ Southam et al confirmed these findings by instilling radioactive particles intranasally in volumes ranging from 5 μ L to 75 μ L, and showing a strong correlation between IAV and levels of radiation in the lower respiratory tracts.⁸⁰ In general, these studies indicated that smaller volumes of vehicle (typically 10-15 μ L) deposit payloads primarily in the nasal passages, whereas larger volumes (typically 40-50 μ L) are able to deposit payloads throughout the nasal passages and lower respiratory tracts.^{44,80-83}

What these biodistribution studies and others have failed to fully characterize, however, is the specific *immunologic* impact of restricting vaccines to the nasal cavity (ie, small IAVs) versus deployment of vaccines throughout the respiratory tract (large IAVs). With regards to the relationship between IAV of mucosal vaccines and corresponding immunologic responses, immunologic characterization data has been limited to only *short-term* antigen-specific antibody titers in serum (IgG) and bronchoalveolar lavage fluid (“BALF;” IgA, IgG) generated by tetanus toxoid encapsulated in poly-(L-lactide) microparticles.⁸² To our knowledge, characterization of *cellular* immune responses to mucosal vaccines as they specifically relate to varied IAV is non-existent, as is any characterization of immunologic responses to vaccines in varied IAV at long-lived timepoints (≥ 90 days post-treatment). Further, the impact of administering adjuvants in the context of intranasal vaccines in varied IAV is also unclear, given that immune responses measured in the Eyles 1999 study did not incorporate adjuvant into their formulations. In short, there is a significant gap in knowledge for how varying the vehicle volume of intranasal vaccines impacts immunoresponsiveness.

In Chapter 5 of this dissertation, we seek to address this gap in knowledge, by more fully characterizing the impact that IAV may have on the generation of cellular immunity—utilizing the CPDI-02-SM MPs developed Chapter 4—at both short-term and long-term timepoints.

5.2 Results

5.2.1 Effect of IAV on the magnitude of early-memory CD127/KLRG1 subsets and late-memory CD127/CD62L subsets of mucosal CD4⁺ T cells in the lungs generated by protein vaccine encapsulated in CPDI-02-SM MPs

We previously demonstrated that surface conjugation of CPDI-02 to PLGA 50:50 NPs (~380nm diameter) increases the magnitude of memory subsets of mucosal and systemic CD4⁺ and CD8⁺ T cells generated by encapsulated protein vaccines at a short-lived timepoint (14 days post final immunization).³³ It was thus expected that our ~1µm diameter CPDI-02-SM MPs would similarly increase memory subsets of CD4⁺ and CD8⁺ T cells at an early timepoint. To assess the effect of IAV on the generation of these CD4⁺ T cell memory subsets in the lungs, we intranasally administered 50µL vehicle only, or vehicle (10µL or 50µL) containing an equivalent of 50µg LPS-free OVA encapsulated in CPDI-02-SM MPs to C57BL/6 mice on Day -14, Day -7, and Day 0 (**Fig.5.1**). On Day 14, we measured the magnitude of memory subsets of CD4⁺ T Cells in the lungs by flow cytometry. Specific early memory T cell subsets include: (i) “early effector cells” (EEC: CD44^{HI}CD127⁻KLRG1⁻)¹¹⁵; (ii) long-lived memory precursor cells (MPEC: CD44^{HI}CD127⁺KLRG1⁻)¹¹⁶; (iii) short-lived effector cells (SLEC: CD44^{HI}CD127⁻KLRG1⁺);¹¹⁷ and (iv) “intermediate-lived” (SLEC < DPEC < MPEC) double-positive effector cells (DPEC: CD44^{HI}CD127⁺KLRG1⁺).¹¹⁸⁻¹²²

Compared to vehicle alone and CPDI-02-SM MPs in 10µL at Day 14, mice administered CPDI-02-SM MPs in 50µL had 5.0-fold and 3.8-fold more total activated OVA-specific CD4⁺ T cells (CD44^{HI}Tet-OVA₃₂₈₋₃₃₇⁺), respectively, in the lungs; mice treated with vehicle alone and CPDI-02-SM MPs in 10µL had similar magnitudes of activated OVA-specific CD4⁺ T Cells (**Fig.5.1A**).

Compared to vehicle alone, at Day 14 mice administered CPDI-02-SM MPs in 50 μ L had 5.1-fold more long-lived CD4⁺ MPEC (**Fig.5.1B**), 2.8-fold more intermediate-lived CD4⁺ DPEC (**Fig.5.1C**), 5.8-fold more short-lived CD4⁺ SLEC (**Fig.5.1D**), and 7.2-fold more CD4⁺ EEC (**Fig.5.1E**) within total CD4⁺CD44^{HI}Tet-OVA₃₂₈₋₃₃₇⁺ cells in the lungs (**Fig. 5.1A**). Conversely, compared to vehicle alone, mice administered CPDI-02-SM MPs in 10 μ L had 1.3-fold more CD4⁺ MPEC (**Fig.5.1B**), similar levels of CD4⁺ DPEC (**Fig.5.1C**), similar levels of CD4⁺ SLEC (**Fig.5.1D**), and 1.6-fold more CD4⁺ EEC (**Fig.5.1E**) within total CD4⁺CD44^{HI}Tet-OVA₃₂₈₋₃₃₇⁺ cells in the lungs (**Fig. 5.1A**). Compared to CPDI-02-SM MPs in 10 μ L, mice administered CPDI-02-SM MPs in 50 μ L had 3.9-fold more long-lived CD4⁺ MPEC (**Fig.5.1B**), 2.4-fold more intermediate-lived CD4⁺ DPEC (**Fig.5.1C**), 3.8-fold more short-lived CD4⁺ SLEC (**Fig.5.1D**), and 4.6-fold more CD4⁺ EEC (**Fig.5.1E**) within total CD4⁺CD44^{HI}Tet-OVA₃₂₈₋₃₃₇⁺ cells in the lungs (**Fig. 5.1A**). Taken together, the results indicate that IAV affects the generation of memory subsets of CD4⁺ T cells in the lungs by protein vaccine encapsulated in CPDI-02 MPs at an early (14 days post-treatment) timepoint.

The CD127/KLRG1 subsets at a Day 14 timepoint provide an indication of memory response at a long-term timepoint. To assess whether the differences in magnitude of CD4⁺ memory T cell populations in the lungs due to IAV persisted at a long-term timepoint, CD4⁺ T cells in the lungs of immunized mice were assessed by FACS at Day 90 (**Fig.5.1**). Surface expression of CD44 and CD127 are general markers for long-living CD4⁺ and CD8⁺ memory T cells.^{123,124} Memory CD4⁺ and CD8⁺ T cell populations of cells can be further delineated into effector memory T cells (TEM)—which are relatively more abundant in peripheral non-lymphoid tissues such as the lungs—by the absence of the cell surface marker CD62L (ie, CD44⁺CD127⁺CD62L⁻ phenotype).¹²⁵ While downregulation of KLRG1 at early timepoints is indicative of a

long-lived memory phenotype, studies have recently shown that at later timepoints, KLRG1 downregulation is not an absolute requirement to be considered a long-lived memory T cell.¹²⁶ This marker was thus excluded from Day 90 assessments.

Compared to vehicle alone at Day 90, mice administered CPDI-02-SM MPs in 50 μ L had 2.0-fold more total Tet-OVA₃₂₈₋₃₃₇⁺CD127⁺ memory T cells (**Fig.5.1F**) and 2.0-fold more long-lived CD4⁺ TEM (**Fig.5.1G**). In contrast, compared to vehicle alone at Day 90, mice administered CPDI-02-SM MPs in 10 μ L had only 1.5-fold more total Tet-OVA₃₂₈₋₃₃₇⁺CD127⁺ memory T cells (**Fig.5.1F**) and a similar magnitude of CD4⁺ TEM (**Fig.5.1G**). Compared to CPDI-02-SM MPs in 10 μ L at Day 90, mice administered CPDI-02-SM MPs in 50 μ L had 1.3-fold more total Tet-OVA₃₂₈₋₃₃₇⁺CD127⁺ memory T cells (**Fig.5.1F**) and 2.1-fold more long-lived CD4⁺ TEM (**Fig.5.1G**). Taking results from Day 14 and Day 90 together, IAV affects the magnitude of antigen-specific memory CD4⁺ T cells in the lungs generated by protein vaccine encapsulated in CPDI-02-SM MPs at both short-term and long-term timepoints.

5.2.2 Effect of IAV on the magnitude of early-memory CD127/KLRG1 subsets and late memory CD127/CD62L subsets of mucosal CD8⁺ T cells in the lungs generated by protein vaccine encapsulated in CPDI-02-SM MPs

Because IAV affected the generation of memory subsets of CD4⁺ T cells in the lungs, we next sought to determine whether it had a similar impact on the generation of memory subsets of CD8⁺ T cells in the lungs. To assess the effect of IAV on the generation of CD8⁺ T cell memory subsets in the lungs, we intranasally administered 50 μ L vehicle only, or vehicle (10 μ L or 50 μ L) containing an equivalent of 50 μ g LPS-free OVA encapsulated in CPDI-02-SM MPs to C57BL/6 mice on Day -14, Day -7, and Day 0 as before (**Fig.5.2**). On Day 14, we measured the magnitude of memory subsets of CD8⁺ T Cells (MPEC, DPEC, EEC, SLEC) in the lungs by flow cytometry.

Compared to vehicle alone and CPDI-02-SM MPs in 10 μ L at Day 14, mice administered CPDI-02-SM MPs in 50 μ L had 37-fold and 31-fold more total activated OVA-specific CD8⁺ T Cells (CD44^{HI}Tet-OVA₂₅₇₋₂₆₄⁺), respectively, in the lungs; mice treated with vehicle alone and CPDI-02-SM MPs in 10 μ L had similar magnitudes of activated OVA-specific CD8⁺ T cells (**Fig.5.2A**).

Compared to vehicle alone, mice administered CPDI-02-SM MPs in 50 μ L had 9.5-fold more long-lived CD8⁺ MPEC (**Fig.5.2B**), similar levels of intermediate-lived CD8⁺ DPEC (**Fig.5.2C**), significantly more short-lived CD8⁺ SLEC (fold-increase unspecified due to undetectable amounts for vehicle only treatment group) (**Fig.5.2D**), and 262-fold more CD8⁺ EEC (**Fig.5.2E**) within total CD8⁺CD44^{HI}Tet-OVA₂₅₇₋₂₆₄⁺ cells in the lungs (**Fig. 5.2A**). Conversely, compared to vehicle alone, mice administered CPDI-02-SM MPs in 10 μ L had similar levels of CD8⁺ MPEC (**Fig.5.2B**), CD8⁺ DPEC (**Fig.5.2C**), CD8⁺ SLEC (**Fig.5.2D**), and CD8⁺ EEC (**Fig.5.2E**) within total CD8⁺CD44^{HI}Tet-OVA₂₅₇₋₂₆₄⁺ cells in the lungs (**Fig. 5.2A**). Further, compared to CPDI-02-SM MPs in 10 μ L, mice administered CPDI-02-SM MPs in 50 μ L had 11-fold more long-lived CD8⁺ MPEC (**Fig.5.2B**), similar levels of intermediate-lived CD8⁺ DPEC (**Fig.5.2C**), 103-fold more short-lived CD8⁺ SLEC (**Fig.5.2D**), and 172-fold more CD8⁺ EEC (**Fig.5.2E**) within total CD8⁺CD44^{HI}Tet-OVA₂₅₇₋₂₆₄⁺ cells in the lungs (**Fig. 5.2A**). Taken together, the results indicate that IAV affects the generation of memory subsets of CD8⁺ T Cells (EEC, SLEC, and MPEC) in the lungs by protein vaccine encapsulated in CPDI-02 MPs at an early (14 days post-treatment) timepoint.

To assess whether the differences in magnitude of CD8⁺ memory T cell populations in the lungs due to IAV persisted at a long-term timepoint, CD8⁺ T cells in the lungs of immunized mice were assessed by FACS at Day 90 (**Fig.5.2**). Compared to vehicle alone at Day 90, mice administered CPDI-02-SM MPs in 50 μ L had 2.5-fold more total Tet-OVA₂₅₇₋₂₆₄⁺CD127⁺ memory T cells (**Fig.5.2F**) and 6.5-fold more long-

lived CD8⁺ TEM (**Fig.5.2G**). In contrast, compared to vehicle alone at Day 90, mice administered CPDI-02-SM MPs in 10 μ L had similar levels of total Tet-OVA₂₅₇₋₂₆₄⁺CD127⁺ memory T cells (**Fig.5.2F**) and CD8⁺ TEM (**Fig.5.2G**). Compared to CPDI-02-SM MPs 10 μ L at Day 90, mice administered CPDI-02-SM MPs in 50 μ L had 2.7-fold more total Tet-OVA₂₅₇₋₂₆₄⁺CD127⁺ memory T cells (**Fig.5.2F**) and 5.0-fold more long-lived CD8⁺ TEM (**Fig.5.2G**). Taking results from Day 14 and Day 90 together, IAV affects the magnitude of antigen-specific memory CD8⁺ T cells in the lungs generated by protein vaccine encapsulated in CPDI-02-SM MPs at both short-term and long-term timepoints.

5.2.3 Effect of IAV on the magnitude of mucosal OVA-specific CD4⁺ and CD8⁺ T cells generated in the lungs by protein vaccine encapsulated in CPDI-02-SM MPs, as measured by IFN- γ ELISpot

FACS analyses revealed that IAV affected the magnitude and phenotypic profile of OVA-specific CD4⁺ and CD8⁺ T cells in the lungs. We next sought to determine whether these findings would correlate with the magnitude of cellular responsiveness of OVA-specific CD4⁺ and CD8⁺ T cells in the lungs. We thus intranasally administered vehicle alone (50 μ L PBS), or vehicle (10 μ L or 50 μ L) containing an equivalent amount of LPS-free OVA encapsulated in CPDI-02-SM MPs to C57BL/6 mice (**Fig.5.3**). At Day 14, we then measured magnitudes of lung-derived, IFN- γ secreting T cells via ELISpot which were specific for either OVA₃₂₃₋₃₃₉ (“ISQAVHAAHAEINEAGR;” binds to I-A(d) MHC class II molecule and is specific for CD4⁺ T cells ^{96,97}) or OVA₂₅₇₋₂₆₄ (“SIINFEKL;” binds to MHC class I molecule and is specific to CD8⁺ T Cells ^{98,99}).

Compared to vehicle alone, mice administered CPDI-02-SM MPs in 50 μ L had a 94-fold increase in ISQAVHAAHAEINEAGR-specific IFN- γ SFUs/10⁶ lung

lymphocytes (**Fig.5.3A**) and 71-fold increase in SIINFEKL-specific IFN- γ SFUs/ 10^6 lung lymphocytes (**Fig.5.3B**). Compared to vehicle alone, mice administered CPDI-02-SM MPs in 10 μ L had a 3.6-fold increase in ISQAVHAAHAEINEAGR-specific IFN- γ SFUs/ 10^6 lung lymphocytes (**Fig.5.3A**) and similar magnitudes of SIINFEKL-specific IFN- γ SFUs/ 10^6 lung lymphocytes (**Fig.5.3B**). Finally, compared to CPDI-02-SM MPs in 10 μ L, mice administered CPDI-02-SM MPs in 50 μ L had a 26-fold increase in ISQAVHAAHAEINEAGR-specific IFN- γ SFUs/ 10^6 lung lymphocytes (**Fig.5.3A**) and 23-fold increase in SIINFEKL-specific IFN- γ SFUs/ 10^6 lung lymphocytes (**Fig.5.3B**). These data suggest concurrence with Day 14 FACS analyses; the greater magnitude of OVA-specific CD4 $^+$ and CD8 $^+$ T Cells observed with greater IAV via flow cytometry correlates with greater magnitudes of functional cellular responses of CD4 $^+$ and CD8 $^+$ T cells as measured by IFN- γ ELISpot at Day 14.

To determine whether functional differences in CD4 $^+$ and CD8 $^+$ T cells due to varying IAV were long-lived in the lungs, C57BL/6 mice were similarly intranasally immunized (**Fig.5.3**) and the magnitude of cellular responsiveness of OVA-specific CD4 $^+$ and CD8 $^+$ T cells in the lungs was measured via IFN- γ ELISpot at Day 90. Compared to vehicle alone, mice administered CPDI-02-SM MPs in 50 μ L had similar levels of ISQAVHAAHAEINEAGR-specific IFN- γ SFUs/ 10^6 lung lymphocytes (**Fig.5.3C**) and a 31-fold increase in SIINFEKL-specific IFN- γ SFUs/ 10^6 lung lymphocytes (**Fig.5.3D**). Compared to vehicle alone, mice administered CPDI-02-SM MPs in 10 μ L had similar levels of ISQAVHAAHAEINEAGR-specific IFN- γ SFUs/ 10^6 lung lymphocytes (**Fig.5.3C**) and SIINFEKL-specific IFN- γ SFUs/ 10^6 lung lymphocytes (**Fig.5.3D**). Finally, compared to CPDI-02-SM MPs in 10 μ L, mice administered CPDI-02-SM MPs in 50 μ L had similar levels of ISQAVHAAHAEINEAGR-specific IFN- γ

SFUs/ 10^6 lung lymphocytes (**Fig.5.3C**), but a 17-fold increase in SIINFEKL-specific IFN- γ SFUs/ 10^6 lung lymphocytes (**Fig.5.3D**).

As expected, magnitudes of ISQAVHAAHAEINEAGR-specific and SIINFEKL-specific IFN- γ SFUs decreased over time (from Day 14 to Day 90) for mice intranasally administered CPDI-02-SM MPs in both 10 μ L and 50 μ L, which is reflective of the contraction of antigen-specific T cell populations into more strictly memory phenotypes.¹²⁷ There was strong correlation between the magnitudes of CD4+/CD8+ T Cell populations observed via FACS and the functional magnitude of IFN- γ secretion from OVA-specific CD4+/CD8+ T cells observed via ELISpot. Interestingly, despite appreciable CD4+ T cell phenotypic/magnitude differences being observed between treatment groups via FACS at Day 90 (**Figs.5.1F-G**), these differences did not correspond to statistically significant functional differences in terms of CD4+-specific IFN- γ activity (SFUs) for the same cell populations at the same timepoint (**Fig.5.3C**).

5.2.4 Effect of IAV on the magnitude of late-memory CD127/CD62L subsets of systemic CD4+ T cells in the spleen generated by protein vaccine encapsulated in CPDI-02-SM MPs

Given that CPDI-02-SM MPs were able to generate memory CD4+ T cells in mucosal tissues (lungs) and that IAV was shown to affect the magnitude of generated antigen-specific memory CD4+ T cells, it is likely that IAV would similarly impact generation of *systemic* antigen-specific memory subsets of CD4+ T cells. To assess the systemic effect of IAV on the generation of CD4+ T cell memory subsets, we intranasally administered 50 μ L vehicle only, or vehicle (10 μ L or 50 μ L) containing an equivalent of 50 μ g LPS-free OVA encapsulated in CPDI-02-SM MPs to C57BL/6 mice and measured the magnitude of memory subsets of CD4+ T cells in the spleen by flow

cytometry on Day 14 (**Fig.5.4**). Similar to lungs (**Fig.5.1**), specific CD4⁺ T cell subsets analyzed in the spleen included effector cells (“TEFFs”, similar to EECs; CD44^{HI}CD127⁻KLRG1⁻CD62L⁻), SLECs (CD44^{HI}CD127⁻KLRG1⁺CD62L⁻), and DPECs (CD44^{HI}CD127⁺KLRG1⁺). MPECs were further delineated by the presence of CD62L cell marker into either effector memory T Cells (“TEM;” CD44^{HI}CD127⁺KLRG1⁻CD62L⁻) or central memory T Cells (“TCM;” CD44^{HI}CD127⁺KLRG1⁻CD62L⁺).^{128,129}

Mice treated with vehicle alone, CPDI-02-SM MPs in 10μL, and CPDI-02-SM MPs in 50μL all had non-significantly different total activated OVA-specific CD4⁺ T Cells (CD44^{HI}Tet-OVA₃₂₈₋₃₃₇⁺), respectively, in the lungs (**Fig.5.4A**).

Compared to vehicle alone at Day 14, mice administered CPDI-02-SM MPs in 50μL consistently averaged higher magnitudes for each CD4⁺ memory subset, but these differences were non-significant for OVA-specific CD4⁺ TEM (**Fig.5.4B**), CD4⁺ TCM (**Fig.5.4C**), CD4⁺ TEFF (**Fig.5.4E**), and CD4⁺ SLEC (**Fig.5.4F**). Only OVA-specific CD4⁺ DPEC showed a statistically higher magnitude (**Fig.5.4D**) within total CD4⁺CD44^{HI}Tet-OVA₃₂₈₋₃₃₇⁺ cells in the spleen (**Fig.5.4A**). Compared to vehicle alone at Day 14, mice administered CPDI-02-SM MPs in 10μL consistently averaged similar or higher magnitudes for each CD4⁺ memory subset, however these differences were also all non-significant.

When comparing mice administered CPDI-02-SM MPs in 50μL to 10μL, mice administered CPDI-02-SM MPs in 50μL consistently averaged higher magnitudes for each CD4⁺ memory subset, but these differences were non-significant for OVA-specific CD4⁺ TEM (**Fig.5.4B**), CD4⁺ TCM (**Fig.5.4C**), CD4⁺ TEFF (**Fig.5.4E**), and CD4⁺ SLEC (**Fig.5.4F**). Again, only OVA-specific CD4⁺ DPEC showed a statistically higher magnitude (**Fig.5.4D**). In general, FACS data indicated that CPDI-02-SM MPs fails to generate appreciable numbers of epitope-specific CD4⁺ T cells in the spleen regardless of IAV when compared to negative control. The lone notable exception was

the significant level of OVA-specific DPEC generated by CPDI-02-SM MPs administered in 50 μ L compared to vehicle alone and CPDI-02-SM MPs in 10 μ L treatment groups.

Given that significant differences between vehicle only, the CPDI-02-SM MPs in 10 μ L, and the CPDI-02-SM MPs in 50 μ L treatment groups were only observed for OVA-specific CD4+ DPEC, we expected that differences in magnitudes between OVA-specific CD4+ memory subsets in the spleen would remain minimal at a long-lived timepoint (90 Days post-treatment). To assess this relationship, C57BL/6 mice (n=5 mice per treatment group) were intranasally administered 50 μ L of vehicle only, or vehicle (10 μ L or 50 μ L) containing an equivalent of 50 μ g LPS-free OVA encapsulated in CPDI-02-SM MPs, and magnitudes of long-lived OVA-specific CD4+ T Cells (Tet-OVA₃₂₈₋₃₃₇⁺CD127⁺ memory T cells, CD4+ TCM, and CD4+ TEM) were assessed by FACS at Day 90 (**Fig.5.4**).

Compared to vehicle alone at Day 90, mice administered CPDI-02-SM MPs in 50 μ L had 1.7-fold more total Tet-OVA₃₂₈₋₃₃₇⁺CD127⁺ memory T cells (**Fig.5.4G**), 1.5-fold more long-lived CD4+ TEM (**Fig.5.4H**), and 2.4-fold more long-lived CD4+ TCM (**Fig.5.4I**). Compared to vehicle alone at Day 90, mice administered CPDI-02-SM MPs in 10 μ L had similar magnitudes of total Tet-OVA₃₂₈₋₃₃₇⁺CD127⁺ memory T cells (**Fig.5.4G**), CD4+ TEM (**Fig.5.4H**), and CD4+ TCM (**Fig.5.4I**). Compared to CPDI-02-SM MPs in 10 μ L at Day 90, mice administered CPDI-02-SM MPs in 50 μ L had 1.3-fold more total Tet-OVA₃₂₈₋₃₃₇⁺CD127⁺ memory T cells (**Fig.5.4G**) and 1.3-fold more long-lived CD4+ TEM (**Fig.5.4H**). While 50 μ L showed a higher average magnitude of long-lived CD4+ TCM compared to 10 μ L, this difference was non-significant (**Fig.5.4I**).

Overall, IAV had only a modest effect on the generation of OVA-specific CD4+ T Cells at the Day 14 timepoint (specifically on DPECs), however a more robust effect

was observed at a long-lived timepoint (Day 90), with respect to the generation of total CD127⁺ memory T cells and TEMs.

5.2.5 Effect of IAV on the magnitude of early-memory CD127/KLRG1/CD62L subsets and late-memory CD127/CD62L subsets of systemic CD8⁺ T cells in the spleen generated by protein vaccine encapsulated in CPDI-02-SM MPs

Given that IAV affected the generation of memory subsets of CD4⁺/CD8⁺ T cells in the lungs, and to a moderate degree CD4⁺ T cells in the spleen, we next sought to determine whether IAV affects generation of systemic memory subsets of CD8⁺ T cells in the spleen. We intranasally administered 50 μ L vehicle only, or vehicle (10 μ L or 50 μ L) containing an equivalent of 50 μ g LPS-free OVA encapsulated in CPDI-02-SM MPs to C57BL/6 mice and measured the magnitude of memory subsets of CD4⁺ T cells in the spleen by flow cytometry on Day 14 (**Fig.5.5**). Similar to CD4⁺ T cells in the spleen (**Fig.5.4**), specific subsets that were analyzed included CD8⁺ TEFFs, SLECs, DPECs, TEMs, and TCMs.

Compared to vehicle alone and CPDI-02-SM MPs in 10 μ L at Day 14, mice administered CPDI-02-SM MPs in 50 μ L had 3.6-fold and 3.3-fold more total activated OVA-specific CD8⁺ T cells (CD44^{HI}Tet-OVA₂₅₇₋₂₆₄⁺), respectively, in the spleen; mice treated with vehicle alone and CPDI-02-SM MPs in 10 μ L had similar magnitudes of activated OVA-specific CD8⁺ T cells in the spleen (**Fig.5.5A**).

Compared to vehicle alone at Day 14, mice administered CPDI-02-SM MPs in 50 μ L had 4.1-fold more CD8⁺ TEM (**Fig.5.5B**), similar levels of CD8⁺ TCM (**Fig.5.5C**), similar levels of CD8⁺ DPEC (**Fig.5.5D**), 3.2-fold more CD8⁺ TEFFs (**Fig.5.5E**), and 8.4-fold more CD8⁺ SLEC (**Fig.5.5F**) within total CD8⁺CD44^{HI}Tet-OVA₂₅₇₋₂₆₄⁺ cells in the spleen (**Fig. 5.5A**). Conversely, compared to vehicle alone, mice administered CPDI-02-SM MPs in 10 μ L had similar levels of CD8⁺ TEM (**Fig.5.5B**), CD8⁺ TCM

(**Fig.5.5C**), CD8⁺ DPEC (**Fig.5.5D**), CD8⁺ TEFFs (**Fig.5.5E**), and CD8⁺ SLEC (**Fig.5.5F**) within total CD8⁺CD44^{HI}Tet-OVA₂₅₇₋₂₆₄⁺ cells in the lungs (**Fig.5.5A**). Finally, compared to CPDI-02-SM MPs in 10 μ L, mice administered CPDI-02-SM MPs in 50 μ L had 3.0-fold more CD8⁺ TEM (**Fig.5.5B**), similar levels of CD8⁺ TCM (**Fig.5.5C**), similar levels of CD8⁺ DPEC (**Fig.5.5D**), 3.6-fold more CD8⁺ TEFFs (**Fig.5.5E**), and 12.7-fold more CD8⁺ SLEC (**Fig.5.5F**). Overall, the results indicate that a larger IAV is required to induce generation of several memory subsets of CD8⁺ T Cells (TEM, TEFF, SLEC) in the spleen by protein vaccine encapsulated in CPDI-02-SM MPs at short-lived (Day 14) timepoint.

To assess whether the differences in magnitude of CD8⁺ memory T cell subsets in the spleen due to IAV persisted at a long-term timepoint, CD8⁺ T cells in the spleens of immunized mice were also assessed by FACS at Day 90 (**Fig.5.5**). Compared to vehicle alone at Day 90, mice administered CPDI-02-SM MPs in 50 μ L had 2.0-fold more total Tet-OVA₂₅₇₋₂₆₄⁺CD127⁺ memory T cells (**Fig.5.5G**), 2.4-fold more CD8⁺ TEM (**Fig.5.5H**), and 1.7-fold more CD8⁺ TCM (**Fig.5.5I**). In contrast, compared to vehicle alone at Day 90, mice administered CPDI-02-SM MPs in 10 μ L had only 1.2-fold more total Tet-OVA₂₅₇₋₂₆₄⁺CD127⁺ memory T cells (**Fig.5.5G**), similar levels of CD8⁺ TEM (**Fig.5.5H**), and similar levels of CD8⁺ TCM (**Fig.5.5I**). Finally, compared to CPDI-02-SM MPs in 10 μ L, mice administered CPDI-02-SM MPs in 50 μ L had 1.6-fold more total Tet-OVA₂₅₇₋₂₆₄⁺CD127⁺ memory T cells (**Fig.5.5G**), 1.9-fold more CD8⁺ TEM (**Fig.5.5H**), and 1.5-fold more CD8⁺ TCM (**Fig.5.5I**). Taking FACS results from Day 14 and Day 90 together, IAV affects the magnitude of antigen-specific memory CD8⁺ T cells in the spleen generated by protein vaccine encapsulated in CPDI-02-SM MPs, with greater IAV volume being associated with more robust short- and long-term OVA-specific CD8⁺ T cell magnitudes.

5.2.6 Effect of IAV on the magnitude of systemic OVA-specific CD4+ and CD8+ T cells generated in the spleen by protein vaccine encapsulated in CPDI-02-SM MPs, as measured by IFN- γ ELISpot

FACS analyses revealed that IAV affects the magnitude of short- and long-lived systemic OVA-specific T cell subsets (CD8⁺ more so than CD4⁺ T cells) in the spleen. We next sought to determine whether these findings would correlate with the magnitude of cellular responsiveness of CD4⁺ and CD8⁺ T cells in the spleen to OVA-specific epitopes. We thus intranasally administered vehicle alone (50 μ L PBS), or vehicle (10 μ L or 50 μ L) containing an equivalent amount of LPS-free OVA encapsulated in CPDI-02-SM MPs to C57BL/6 mice (**Fig.5.6**). At Day 14, we then measured magnitudes of spleen-derived, IFN- γ secreting T cells via ELISpot which were specific for either OVA₃₂₃₋₃₃₉ (ISQAVHAAHAEINEAGR) or OVA₂₅₇₋₂₆₄ (SIINFEKL).

Compared to vehicle alone, mice administered CPDI-02-SM MPs in 50 μ L had 98-fold more ISQAVHAAHAEINEAGR-specific IFN- γ SFUs/10⁶ splenocytes (**Fig.5.6A**) and 71-fold more SIINFEKL-specific IFN- γ SFUs/10⁶ splenocytes (**Fig.5.6B**). Compared to vehicle alone, mice administered CPDI-02-SM MPs in 10 μ L had 9.7-fold more ISQAVHAAHAEINEAGR-specific IFN- γ SFUs/10⁶ splenocytes (**Fig.5.6A**) and 5.7-fold more SIINFEKL-specific IFN- γ SFUs/10⁶ splenocytes (**Fig.5.6B**). Finally, when compared to CPDI-02-SM MPs in 10 μ L, mice administered CPDI-02-SM MPs in 50 μ L had 10-fold more ISQAVHAAHAEINEAGR-specific IFN- γ SFUs/10⁶ splenocytes (**Fig.5.6A**) and 13-fold more SIINFEKL-specific IFN- γ SFUs/10⁶ splenocytes (**Fig.5.6B**). These data indicate that IAV has an effect on the ability of protein vaccine encapsulated in CPDI-02-SM MPs to generate systemic epitope-specific IFN- γ T cell responses in the spleen at a short-lived timepoint. Further, it aligns with FACS data, which suggests that systemic CD8⁺ response in the spleen outweighs CD4⁺ response

(in terms of magnitude of generated OVA-specific T Cells and cellular responsiveness) by CPDI-02-SM MPs.

To determine whether functional differences in CD4⁺ and CD8⁺ T cells due to varying IAV were long-lived, CD4⁺ and CD8⁺ T cells in the spleens of immunized C57BL/6 mice were similarly assessed via IFN- γ ELISpot at Day 90 (**Fig.5.6**). At 90 days, compared to vehicle alone, mice administered CPDI-02-SM MPs in 50 μ L averaged 4.5-fold greater (but not statistically significant) levels of ISQAVHAAHAEINEAGR-specific IFN- γ SFUs/10⁶ splenocytes (**Fig.5.6C**) and 139-fold more (statistically significant) SIINFEKL-specific IFN- γ SFUs/10⁶ splenocytes (**Fig.5.6D**). Compared to vehicle alone, mice given CPDI-02-SM MPs in an IAV of 10 μ L had similar levels of ISQAVHAAHAEINEAGR-specific IFN- γ SFUs/10⁶ splenocytes (**Fig.5.6C**), but 10.7-fold more SIINFEKL-specific IFN- γ SFUs/10⁶ splenocytes (**Fig.5.6D**). Compared to CPDI-02-SM MPs in 10 μ L, mice administered CPDI-02-SM MPs in an IAV of 50 μ L had similar levels of ISQAVHAAHAEINEAGR-specific IFN- γ SFUs/10⁶ splenocytes (**Fig.5.6C**), but 13-fold more SIINFEKL-specific IFN- γ SFUs/10⁶ splenocytes (**Fig.5.6D**).

As expected, magnitudes of ISQAVHAAHAEINEAGR-specific and SIINFEKL-specific IFN- γ SFUs decreased over time (from Day 14 to Day 90) for mice given CPDI-02-SM MPs in IAVs of both 10 μ L and 50 μ L. This is reflective of the contraction of T Cell populations into memory phenotypes. For the 50 μ L treatment group, there was strong correlation between the greater magnitudes of CD8⁺ T cell subset populations observed via FACS (**Fig.5.5**) with the greater magnitude of epitope-specific IFN- γ secreting T cells observed via ELISpot (**Fig.5.6**).

Fig.5.1

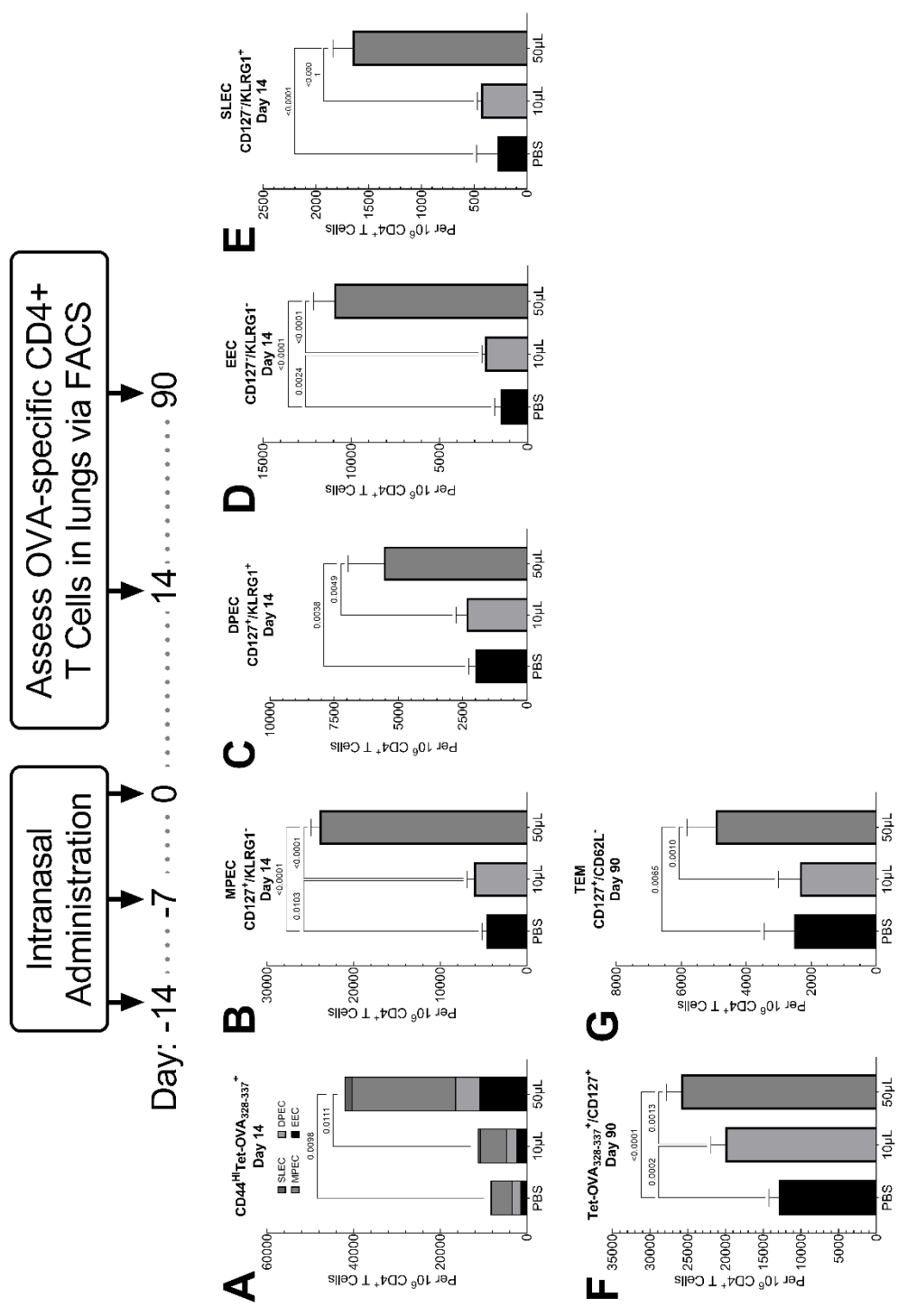


Fig.5.1. Short- and long-term effects of IAV on generation of CD4⁺ memory T cell subsets in the lungs of C57BL/6 mice. Vehicle alone (PBS, 50 μ L) or vehicle containing an equivalent dose of LPS-free OVA [50 μ g] encapsulated in PLGA 50:50 microparticles (~1 μ m diam.) with 0.40 wt% CPDI-02 (CPDI-02, 10 or 50 μ L) through 2 kDa PEG linkers (**Table 4.1**) was intranasally administered to naive female C57BL/6 mice (~8 weeks old; n=5 mice per treatment group) on Days -14, -7, and 0. Lungs were isolated on Day 14 (**A-E**) and Day 90 (**F-G**) and OVA-specific CD4⁺ T cells analyzed via flow cytometry. Average proportions of (**A**) total CD4⁺CD44^{HI}Tet-OVA₃₂₈₋₃₃₇⁺ T cells in the lungs and proportions of (**B-E**) CD127/KLRG1 memory subsets within CD4⁺CD44^{HI}Tet-OVA₃₂₈₋₃₃₇⁺ T cells \pm SD (n = 5 mice) per 10⁶ CD4⁺ T cells at Day 14 were compared between treatment groups. At Day 90, (**F**) total CD44^{HI}Tet-OVA₃₂₈₋₃₃₇⁺CD127⁺ in the lungs and proportion of (**G**) CD4⁺ effector memory T cells (CD127⁺CD62L⁻) within CD4⁺CD44^{HI} Tet-OVA₃₂₈₋₃₃₇⁺ T cells per 10⁶ CD4⁺ T cells were compared. Results were compared by Kruskal-Wallis nonparametric one-way ANOVA with uncorrected Dunn's post-test. Outliers identified by the ROUT method (Q = 1%) were omitted.

Fig.5.2

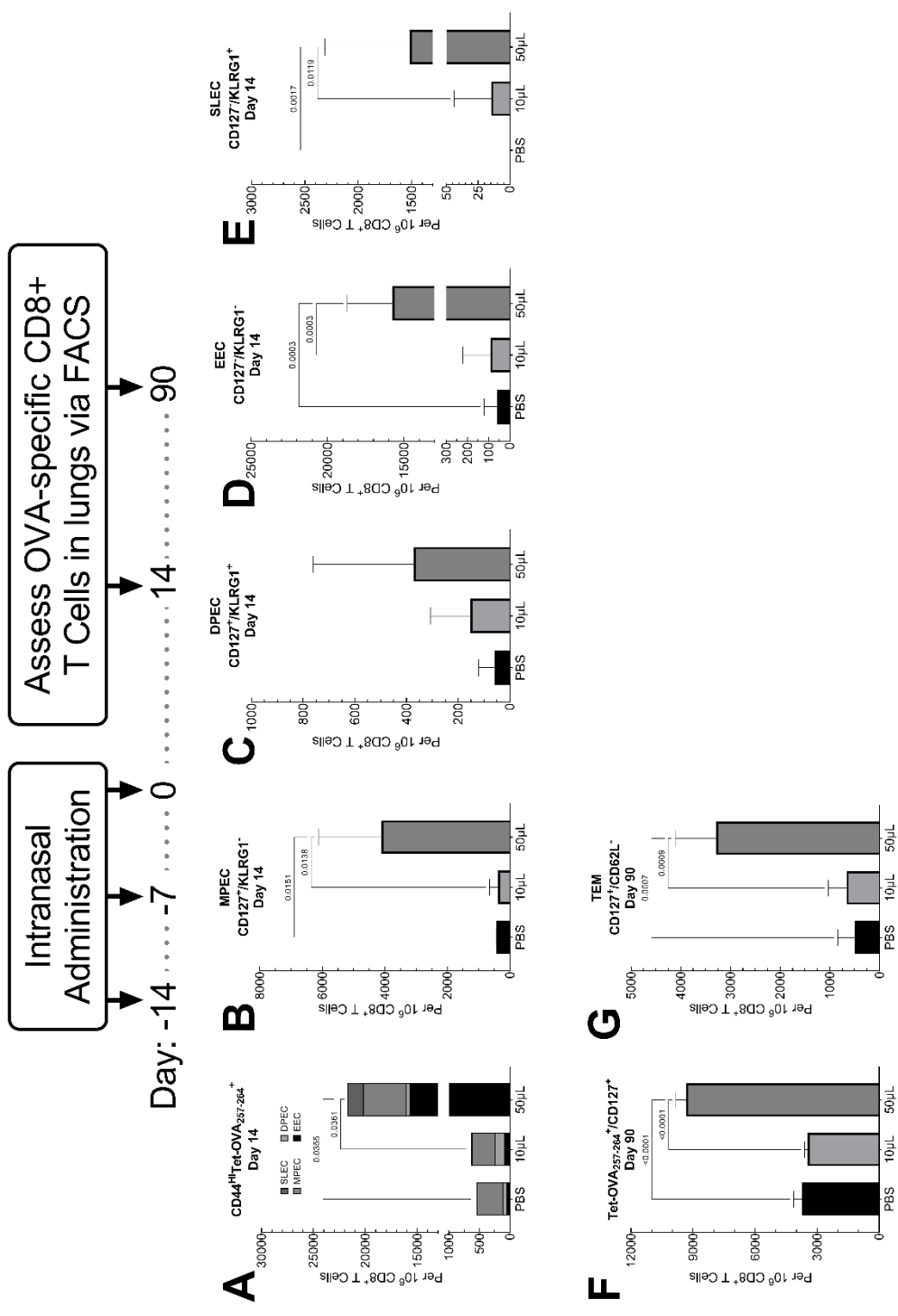


Fig.5.2. Short- and long-term effects of IAV on generation of CD8⁺ memory T cell subsets in the lungs of C57BL/6 mice. Vehicle alone (PBS, 50 μ L) or vehicle containing an equivalent dose of LPS-free OVA [50 μ g] encapsulated in PLGA 50:50 microparticles (~1 μ m diam.) with 0.40 wt% CPDI-02 (CPDI-02, 10 or 50 μ L) through 2 kDa PEG linkers (**Table 4.1**) was intranasally administered to naive female C57BL/6 mice (~8 weeks old; n=5 mice per treatment group) on Days -14, -7, and 0. Lungs were isolated on Day 14 (**A-E**) and Day 90 (**F-G**) and OVA-specific CD8⁺ T cells analyzed via flow cytometry. Average proportions of (**A**) total CD8⁺CD44^{HI}Tet-OVA₂₅₇₋₂₆₄⁺ T cells in the lungs and proportions of (**B-E**) CD127/KLRG1 memory subsets within CD8⁺CD44^{HI}Tet-OVA₂₅₇₋₂₆₄⁺ T cells \pm SD (n = 5 mice) per 10⁶ CD8⁺ T cells at Day 14 were compared between treatment groups. At Day 90, (**F**) total CD44^{HI}Tet-OVA₂₅₇₋₂₆₄⁺CD127⁺ in the lungs and proportion of (**G**) CD8⁺ effector memory T cells (CD127⁺CD62L⁻) within CD8⁺CD44^{HI}Tet-OVA₂₅₇₋₂₆₄⁺ T cells per 10⁶ CD8⁺ T cells were compared. Results were compared by Kruskal-Wallis nonparametric one-way ANOVA with uncorrected Dunn's post-test. Outliers identified by the ROUT method (Q = 1%) were omitted.

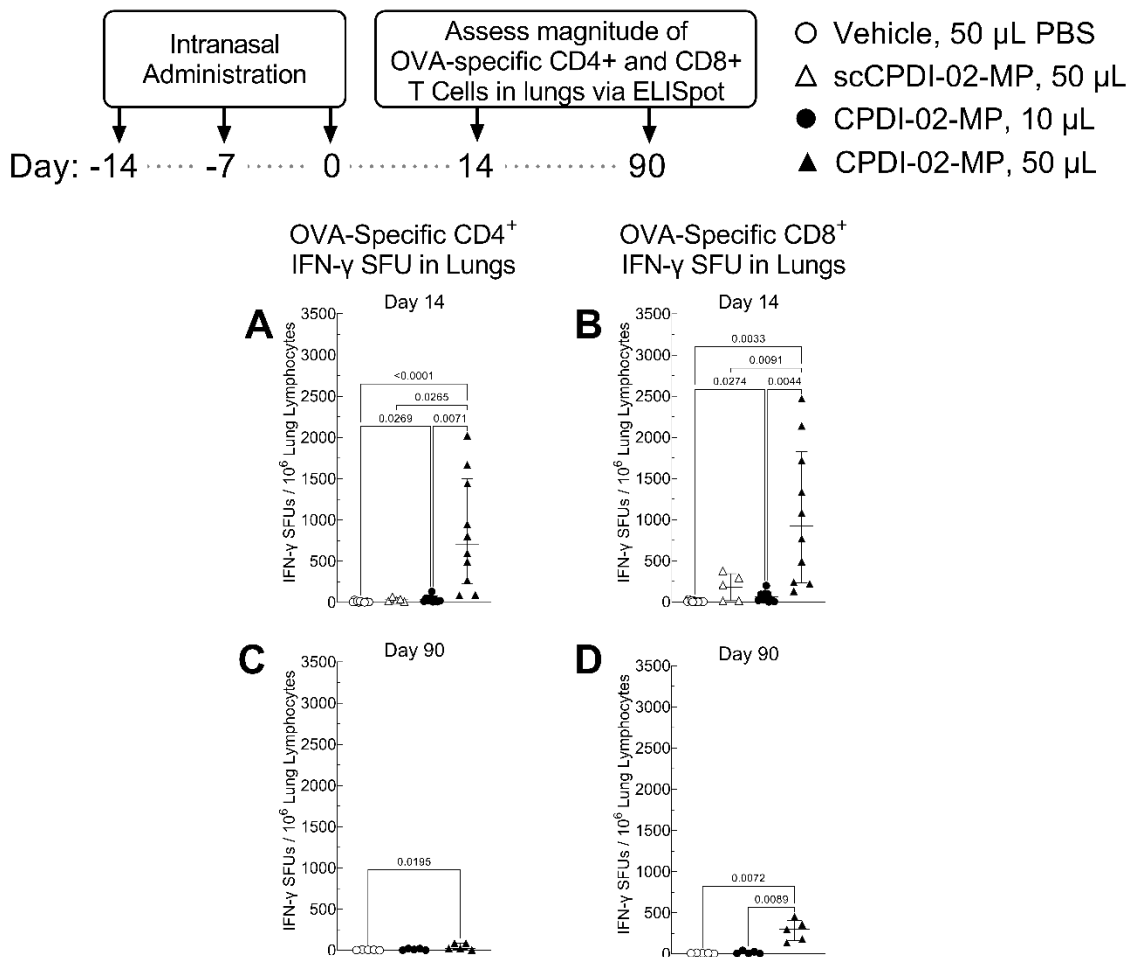


Fig.5.3. Effect of surface-conjugating CPDI-02 to biodegradable microparticles and intranasal administration volume on the magnitude of IFN- γ secretion of mucosal OVA-specific CD4⁺ and CD8⁺ T cells in the lungs generated in naïve female C57BL/6 mice after respiratory immunization with encapsulated LPS-free OVA. Vehicle alone (PBS, 50 μ L) or vehicle containing an equivalent dose of LPS-free OVA [50 μ g] encapsulated in PLGA 50:50 microparticles (~1 μ m diam.) with 0.39 wt% surface-conjugated inactive, scrambled scCPDI-02 (scCPDI-02, 50 μ L; Day 14 results only) or 0.40 wt% CPDI-02 (CPDI-02, 10 or 50 μ L) through 2 kDa PEG linkers (Table 4.1) was intranasally administered to naïve female C57BL/6 mice (~8 weeks old; n=5 mice for scCPDI-02-SM MP treatment group, and 10 mice for both 10 μ L and 50 μ L CPDI-02-SM MP treatment groups) on Days -14, -7, and 0. On Day 14 or Day 90, lung lymphocytes

were isolated, purified, and plated in triplicate on pre-coated IFN- γ ELISpot plates in serum-free CTL-Test Media. Cells were co-incubated with 10 μ g/mL of either ISQAVHAAHAEINEAGR [CD4-specific OVA epitope; **(A)** and **(C)**] or SIINFEKL [CD8-specific OVA epitope; **(B)** and **(D)**]. Incubations were for 24 hrs [Day 14 experiments; **(A)** and **(B)**] or 48 hours [Day 90 experiments; **(C)** and **(D)**] at 37°C and 5% CO₂. IFN- γ SFUs for each sample were counted using ImmunoSpot S6 MACRO Plate Analyzer (CTL), averaged, and normalized to SFUs/10⁶ lung lymphocytes. Results were compared by Kruskal-Wallis nonparametric one-way ANOVA with uncorrected Dunn's post-test. Outliers identified by the ROUT method (Q = 1%) were omitted.

Fig.5.4

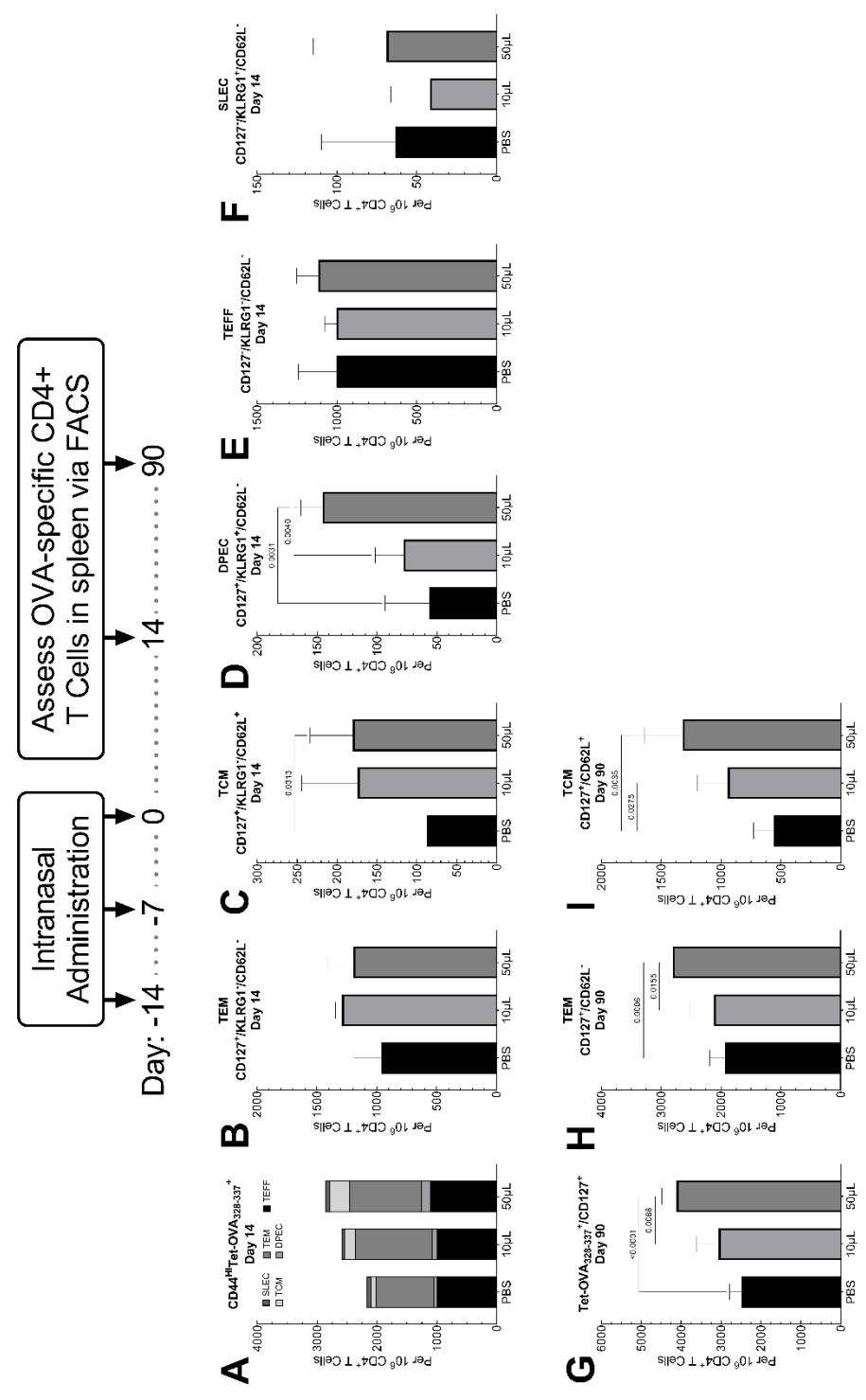


Fig.5.4. Short- and long-term effects of IAV on generation of systemic CD4⁺ memory T cell subsets in the spleens of C57BL/6 mice. Vehicle alone (PBS, 50 μ L) or vehicle containing an equivalent dose of LPS-free OVA [50 μ g] encapsulated in PLGA 50:50 microparticles (~1 μ m diam.) with 0.40 wt% CPDI-02 (CPDI-02, 10 or 50 μ L) through 2 kDa PEG linkers (**Table 4.1**) was intranasally administered to naive female C57BL/6 mice (~8 weeks old, n=5 mice per treatment group) on Days -14, -7, and 0. Spleens were isolated on Day 14 (**A-F**) and Day 90 (**G-I**) and OVA-specific CD4⁺ T cells analyzed via flow cytometry. Average proportions of (**A**) total CD4⁺CD44^{HI} Tet-OVA₃₂₈₋₃₃₇⁺ T cells in the spleen and proportions of (**B-F**) CD127/KLRG1/CD62L memory subsets within CD4⁺CD44^{HI} Tet-OVA₃₂₈₋₃₃₇⁺ T cells \pm SD (n = 5 mice) per 10⁶ CD4⁺ T cells at Day 14 were compared between treatment groups. At Day 90, (**G**) total CD44^{HI}Tet-OVA₃₂₈₋₃₃₇⁺CD127⁺ in the spleen and proportion of (**H-I**) long-lived CD127/CD62L subsets within CD4⁺CD44^{HI} Tet-OVA₃₂₈₋₃₃₇⁺ T cells per 10⁶ CD4⁺ T cells were compared. Results were compared by Kruskal-Wallis nonparametric one-way ANOVA with uncorrected Dunn's post-test. Outliers identified by the ROUT method (Q = 1%) were omitted.

Fig.5.5

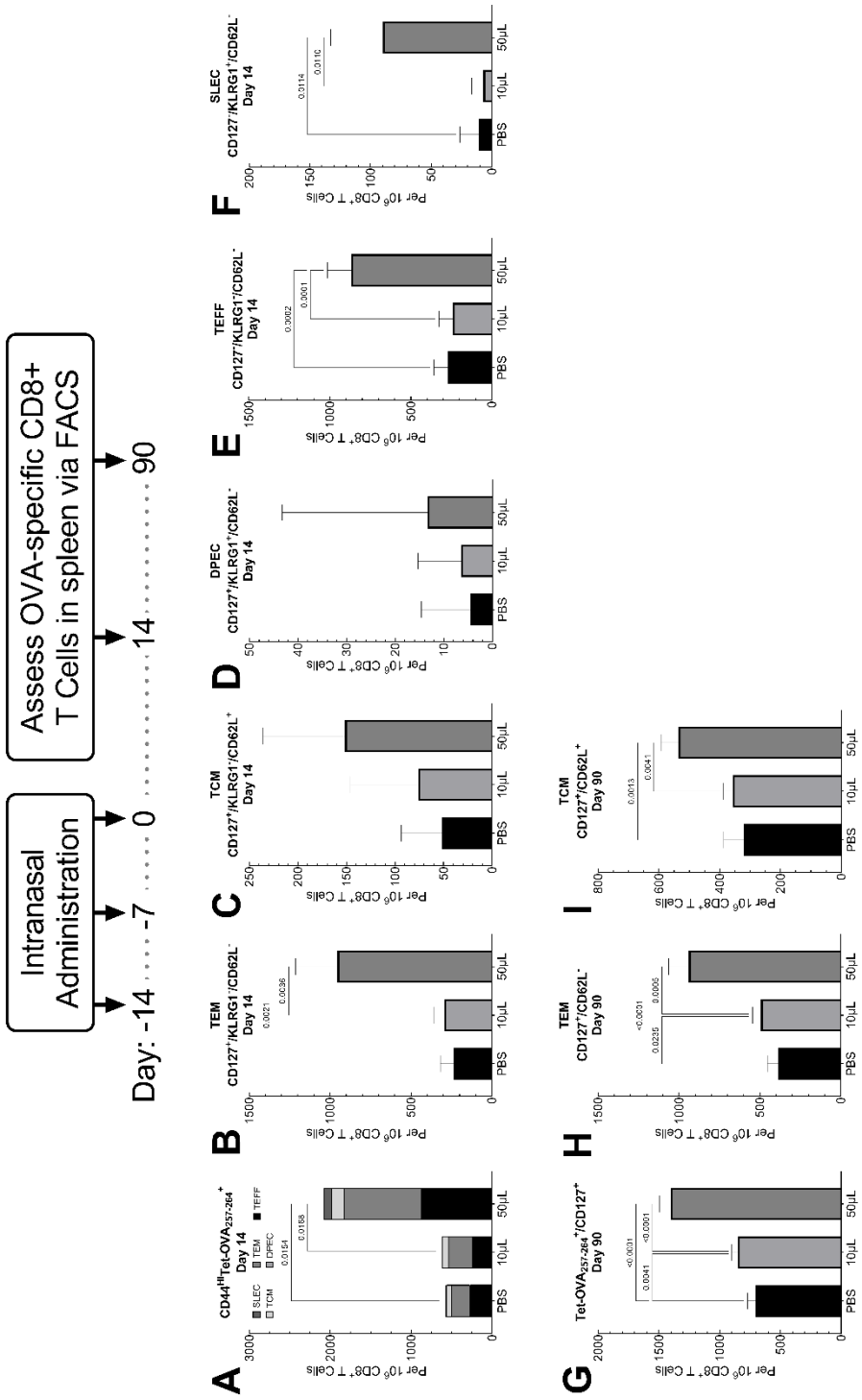


Fig.5.5. Short- and long-term effects of IAV on generation of systemic CD8⁺ memory T cell subsets in the spleens of C57BL/6 mice. Vehicle alone (PBS, 50 μ L) or vehicle containing an equivalent dose of LPS-free OVA [50 μ g] encapsulated in PLGA 50:50 microparticles (~1 μ m diam.) with 0.40 wt% CPDI-02 (CPDI-02, 10 or 50 μ L) through 2 kDa PEG linkers (**Table 4.1**) was intranasally administered to naive female C57BL/6 mice (~8 weeks old, n=5 mice per treatment group) on Days -14, -7, and 0. Spleens were isolated on Day 14 (**A-F**) and Day 90 (**G-I**) and OVA-specific CD8⁺ T cells analyzed via flow cytometry. Average proportions of (**A**) total CD8⁺CD44^{HI}Tet-OVA₂₅₇₋₂₆₄⁺ T cells in the spleen and proportions of (**B-F**) CD127/KLRG1/CD62L memory subsets within CD8⁺CD44^{HI}Tet-OVA₂₅₇₋₂₆₄⁺ T cells \pm SD (n = 5 mice per treatment group) per 10⁶ CD8⁺ T cells at Day 14 were compared between treatment groups. At Day 90, (**G**) total CD44^{HI}Tet-OVA₂₅₇₋₂₆₄⁺CD127⁺ in the spleen and proportion of (**G-I**) long-lived CD127/CD62L subsets within CD8⁺CD44^{HI}Tet-OVA₂₅₇₋₂₆₄⁺ T cells per 10⁶ CD8⁺ T cells were compared. Results were compared by Kruskal-Wallis nonparametric one-way ANOVA with uncorrected Dunn's post-test. Outliers identified by the ROUT method (Q = 1%) were omitted.

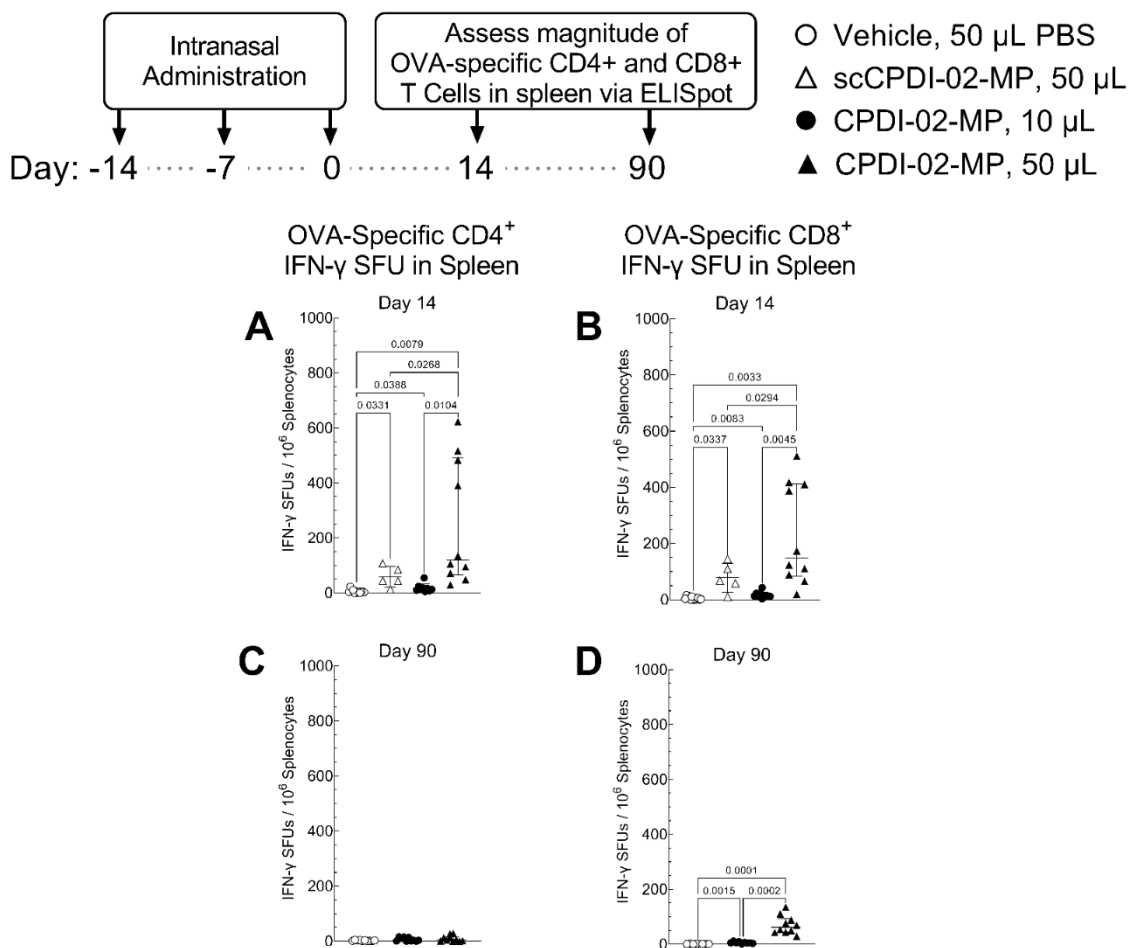


Fig.5.6. Effect of surface-conjugating CPDI-02 to biodegradable microparticles and intranasal administration volume on the magnitude of IFN- γ secretion of systemic OVA-specific CD4⁺ and CD8⁺ T cells in the spleen generated in naïve female C57BL/6 mice after respiratory immunization with encapsulated LPS-free OVA. Vehicle alone (PBS, 50 μ L) or vehicle containing an equivalent dose of LPS-free OVA [50 μ g] encapsulated in PLGA 50:50 microparticles (~1 μ m diam.) with 0.39 wt% surface-conjugated inactive, scrambled scCPDI-02 (scCPDI-02, 50 μ L; Day 14 results only) or 0.40 wt% CPDI-02 (CPDI-02, 10 or 50 μ L) through 2 kDa PEG linkers (Table 4.1) was intranasally administered to naïve female C57BL/6 mice (~8 weeks old; n=5 mice for Day 14 scCPDI-02-SM MP treatment group, and 10 mice for all other treatment groups) on

Days -14, -7, and 0. On Day 14 or Day 90, splenocytes were isolated, purified, and plated in triplicate on pre-coated IFN- γ ELISpot plates in serum-free CTL-Test Media. Cells were co-incubated with 10 μ g/mL of either ISQAVHAAHAEINEAGR [CD4-specific OVA epitope; **(A)** and **(C)**] or SIINFEKL [CD8-specific OVA epitope; **(B)** and **(D)**]. Incubations were for 24 hrs [Day 14 experiments; **(A)** and **(B)**] or 48 hours [Day 90 experiments; **(C)** and **(D)**] at 37°C and 5% CO₂. IFN- γ SFUs for each sample were counted using ImmunoSpot S6 MACRO Plate Analyzer (CTL), averaged, and normalized to SFUs/10⁶ splenocytes. Results were compared by Kruskal-Wallis nonparametric one-way ANOVA with uncorrected Dunn's post-test. Outliers identified by the ROUT method (Q = 1%) were omitted.

CHAPTER 6

**The effect of CPDI-02 adjuvant incorporation strategy on
humoral and cellular immune responses generated by
biodegradable microparticles encapsulating mucosal protein
vaccine**

6.1 Introduction

In Chapters 4 & 5 of this dissertation, we demonstrated that modifying the surface of biodegradable microparticles with CPDI-02 enhances the generation of immunogen-specific humoral and cellular responses to encapsulated protein vaccine (OVA). Surface modification, however, is only one strategy to incorporating adjuvant into biodegradable particle-based mucosal vaccines.

One common adjuvant incorporation strategy into biodegradable particles—aside from surface-modifying particles with adjuvant—is the co-encapsulation of adjuvant and immunogen within the same particle.^{85,130,131} Literature sources that have developed and immunologically characterized this strategy have demonstrated that co-encapsulation of both antigen and adjuvant within the same particle can have a synergistic effect in inducing immune responses—both humoral and cellular—by targeting both the antigen and adjuvant to the endosomal compartment of antigen presenting cells.¹³²⁻¹³⁴

Another conventional, but less commonly reported, approach towards adjuvant incorporation is encapsulating adjuvant and immunogen in separate biodegradable particles, and co-administering both within the same host. Previous research by Ilyinskii et al investigated a version of this strategy, in which antigen (OVA) and adjuvant (R848, a TLR7/8 agonist) were encapsulated in separate biodegradable nanoparticles, and then co-administered together via intramuscular (IM) injection. Compared to the co-administration of free antigen and free adjuvant, co-administration of separate particles encapsulating antigen and adjuvant generated higher titers of OVA-specific IgG in the serum and magnitudes of OVA-specific CD8⁺ T cells in popliteal lymph nodes of mice, amongst other enhanced immune responses.⁸⁴ The utility of this incorporation strategy is promising, but undoubtedly requires further investigation in the context intranasal administration/mucosal vaccination.

Despite the demonstrated efficacy of each of the described adjuvant incorporation strategies, to the best of our knowledge, these three strategies have all not been directly compared to one another within the same animal model. Further, when each of these strategies have been assessed individually, it is infrequent that *both* humoral and cellular immune responses to each strategy are characterized. Thus, in the present study, we seek to directly compare both cellular and humoral immune responses generated by three conventional strategies by which adjuvant is incorporated into biodegradable particles encapsulating mucosal protein vaccine—(i) separately encapsulating both adjuvant and protein vaccine into particles and co-administering (Encapsulated, Co-Administered; “ECA”); (ii) co-encapsulation of adjuvant and protein vaccine into the same particle (Co-Encapsulation, “CE”); and (iii) conjugation of adjuvant to the surface of particles encapsulating protein vaccine (Surface Modification, “SM”) (**Fig.6.1**).

In order to ensure a “fair” comparison between CPDI-02 incorporation strategies, we aim to develop formulations that are as equal as possible in terms of polymer type, particle size, zeta potential, particle formation methodology, and immunogen/adjuvant dosing. By minimizing the differences between biophysical properties of the biodegradable microparticle formulations, any observed differences in humoral and cellular immune responses will likely thus be a direct result of the CPDI-02 incorporation strategy alone.

6.2 Results

6.2.1 Development and characterization of biodegradable microparticles incorporating CPDI-02 and mucosal protein vaccine (OVA)

6.2.1.1 CPDI-02-ECA and scCPDI-02-ECA MPs

As indicated in **Fig.6.1A**, the CPDI-02-ECA MP strategy comprises two separate biodegradable microparticles—one encapsulating only LPS-free OVA

“OVA Only MPs”) and one encapsulating either CPDI-02 (“CPDI-02 Only MPs”) or scCPDI-02 (“scCPDI-02 Only MPs”)—that are co-administered in the same dose. For encapsulating OVA into the OVA Only MPs, we loaded LPS-free OVA at 10 wt% theoretical loading using $W_1/O/W_2$ encapsulation (**Chapter 3, Section 3.3.1**) with a target particle diameter of 1 μm . OVA was consistently encapsulated around ~8 wt% with low burst release (2.9%) (**Table 6.1**) and a diameter of approximately 0.99 μm .

To encapsulate either CPDI-02 or scCPDI-02 into MPs (“CPDI-02 Only MPs” or “scCPDI-02 Only MPs,” respectively, we loaded CPDI-02 or scCPDI-02 at 5 wt% theoretical loading using O_1/O_2 encapsulation (**Chapter 3, Section 3.3.4**) with a target particle diameter of 1 μm . Both CPDI-02 and scCPDI-02 were consistently loaded at around ~2-3 wt%, with particle diameters of 0.97 μm and 1.02 μm , respectively (**Table 6.1**).

6.2.1.2 CPDI-02-CE and scCPDI-02-CE MPs

As indicated in **Fig.6.1B**, the CPDI-02-CE MP strategy involves the co-encapsulation of both LPS-free OVA and either CPDI-02 or scCPDI-02 within the same biodegradable microparticle. We loaded LPS-free OVA at 10 wt% theoretical loading and CPDI-02 or scCPDI-02 at 5 wt% theoretical loading using $W_1/O/W_2$ encapsulation, with a target particle diameter of 1 μm (**Chapter 3, Section 3.3.3**). For both CPDI-02-CE and scCPDI-02-CE MPs, OVA was encapsulated around ~7-8 wt% with low burst release (2.7% and 3.3%, respectively). CPDI-02/scCPDI-02 were both encapsulated around ~2 wt%. Particle diameters for CPDI-02-CE and scCPDI-02-CE MPs were 1.08 μm and 1.05 μm , respectively (**Table 6.1**)

6.2.1.3 CPDI-02-SM and scCPDI-02-SM MPs

To encapsulate LPS-free ovalbumin (OVA) in biodegradable microparticles (MP) surface-conjugated with CPDI-02 or inactive, scrambled CPDI-02 (scCPDI-02), we activated the surface of MP with maleimide (MAL) groups through 2 kDa PEG linkers by physically incorporating diblock copolymers of PLLA(10K)-PEG(2K)-MAL into PLGA 50:50 MP by interfacial activity assisted surface functionalization (IAASF) during $W_1/O/W_2$ encapsulation of LPS-free OVA at 10 wt% theoretical loading^{105,106} (**Section 3.3.2; Fig 4.1A**). We then conjugated sulfhydryl (cysteine)-activated CPDI-02 or scCPDI-02 to MAL-activated PEG on the MP surface through protease-labile N-terminal Cys-Gly-Arg-Arg linkers (**Fig 4.1B**). OVA was consistently encapsulated at ~5 to 6 wt% with minimal burst release (0.4 to 0.8%). MP surface was conjugated with ~0.4 wt% CGRR-CPDI-02 (“CPDI-02-SM MP”) or CGRR-scCPDI-02 (“scCPDI-02-SM MP”). CPDI-02-SM and scCPDI-02-SM MP particle diameters were found to be 1.12 μm and 1.21 μm , respectively (**Table 6.1**).

6.2.1.4 Dosing of OVA and CPDI-02 or scCPDI-02 in developed ECA, CE, and SM microparticle formulations

To facilitate “fair” immunologic assessments between differing CPDI-02 adjuvant incorporation strategies into biodegradable microparticles, it is critical that immunizations with each incorporation strategy are to contain an equivalent dose of encapsulated LPS-free OVA (50 μg , as in Chapters 4 & 5). Due to the nature of the CPDI-02-CE and CPDI-02-SM incorporation strategies (where OVA is contained within the same particle as either CPDI-02 or scCPDI-02; **Fig.6.1B&C**), defining the amount of administered OVA for each incorporation strategy will dictate the amount of administered CPDI-02 or scCPDI-02. Specifically, a 50 μg

LPS-free OVA equivalent for these incorporation strategies will contain: 13.8µg CPDI-02 in the CPDI-02-CE MPs; 11.3µg scCPDI-02 in the scCPDI-02-CE MPs; 3.2µg CPDI-02 in the CPDI-02-SM MPs; and 3.8µg of scCPDI-02 in the scCPDI-02-SM MPs (**Table 6.1**). Being unable to adjust the amount of CPDI-02 or scCPDI-02 is an inherent disadvantage for the CE and SM incorporation strategies, and a noted limitation of studies presented within Chapter 6. Due to the nature of the CPDI-02-ECA incorporation strategy (where OVA and CPDI-02/scCPDI-02 are encapsulated individually in separate microparticles; **Fig.6.1A**), however, the amount of administered CPDI-02 or scCPDI-02 can be adjusted relative to the amount of administered OVA. Thus, for the CPDI-02-ECA and scCPDI-02-ECA incorporation strategies, the amount of administered CPDI-02 or scCPDI-02 was conservatively normalized to the amount of CPDI-02 within CPDI-02-SM MPs (for a 50µg OVA dose equivalent, this is 3.2µg of CPDI-02 or scCPDI-02), given that the SM formulations contain less adjuvant than their CE counterparts.

6.2.2 CPDI-02-ECA MP strategy generates greater magnitudes of OVA-specific IgA ASCs in the lungs of naïve mice compared to CPDI-02-CE and CPDI-02-SM MP strategies

For an early indication of humoral immune responses, we sought to determine the effect that CPDI-02 incorporation strategy into biodegradable microparticles encapsulating OVA has on the generation of OVA-specific ASCs in the lungs. Naive female C57BL/6 mice (n=10 total mice from two independent studies for CPDI-02-based treatment groups; n=5 mice for vehicle alone and scCPDI-02-based treatment groups) were intranasally administered on Days -14, -7, and 0 with vehicle alone (PBS, 50 µL), or vehicle containing an equivalent dose of LPS-free OVA [50µg] encapsulated

in one of the following CPDI-02 or scCPDI-02 incorporation strategies: (1) scCPDI-02-ECA MPs; (2) CPDI-02-ECA MPs; (3) scCPDI-02-CE MPs; (4) CPDI-02-CE MPs; (5) scCPDI-02-SM MPs; or (6) CPDI-02-SM MPs (**Fig. 6.2**). Dosing of CPDI-02 in the CPDI-02-ECA MP strategy was conservatively normalized to the amount of CPDI-02 in the CPDI-02-SM MP strategy. Magnitudes of OVA-specific IgA, IgM, and IgG ASCs were measured on Day 6 post-treatment. Relative to scCPDI-02-ECA MPs (white circles, **Fig.6.2**), CPDI-02-ECA MPs (black circles, **Fig.6.2**) generated 2,609-fold more OVA-specific IgA ASCs (**Fig.6.2A**), 861-fold more OVA-specific IgM ASCs (**Fig.6.2B**), and 588-fold more OVA-specific IgG ASCs (**Fig.6.2C**). Relative to scCPDI-02-CE MPs (white triangles, **Fig.6.2**), CPDI-02-CE MPs (black triangles, **Fig.6.2**) generated 20-fold more OVA-specific IgA ASCs (**Fig.6.2A**), 54-fold more (but non-significant) OVA-specific IgM ASCs (**Fig.6.2B**), and significantly more OVA-specific IgG ASCs (no detectable spots for scCPDI-02-CE IgG ASCs) (**Fig.6.2C**). Relative to scCPDI-02-SM MPs (white squares, **Fig.6.2**), CPDI-02-SM MPs (black squares, **Fig.6.2**) generated 253-fold more OVA-specific IgA ASCs (**Fig.6.2A**), 184-fold more OVA-specific IgM ASCs (**Fig.6.2B**), and significantly more OVA-specific IgG ASCs (no detectable spots for scCPDI-02-SM IgG ASCs) (**Fig.6.2C**).

When comparing differing CPDI-02-based incorporation strategies, CPDI-02-ECA MPs generated 61-fold more OVA-specific IgA ASCs than the CPDI-02-CE treatment group and 4.6-fold more OVA-specific IgA ASCs than the CPDI-02-SM treatment group (**Fig.6.2A**). Further, the CPDI-02-SM MPs generated 13-fold more OVA-specific IgA ASCs than the CPDI-02-CE treatment group (**Fig.6.2A**). Differences between CPDI-02-based incorporation strategies were non-significant for magnitudes of OVA-specific IgM and IgG ASCs.

6.2.3 CPDI-02-ECA MP strategy generates greater magnitudes of short-term mucosal antibodies against encapsulated protein immunogen in the nasal cavity and lungs of young, naïve mice compared to the CPDI-02-CE MP strategy

Given that CPDI-02-based incorporation strategies into MPs generated higher magnitudes of OVA-specific ASCs relative to their scCPDI-02 counterparts, we expected that CPDI-02-based incorporation strategies would also increase subsequent titers of OVA-specific mucosal antibodies. It is also expected that the different CPDI-02 incorporation strategies will generate differing magnitudes of OVA-specific mucosal IgA antibody titers, given that differences were seen in magnitudes of OVA-specific IgA ASCs in the lungs between those treatment groups. Naive female C57BL/6 mice (n=10 total mice from two independent studies for CPDI-02-based treatment groups; n=5 mice for vehicle alone and scCPDI-02-based treatment groups) were intranasally administered on Days -14, -7, and 0 with vehicle containing an equivalent dose of LPS-free OVA [50µg] encapsulated in one of the following CPDI-02 or scCPDI-02 incorporation strategies: (1) scCPDI-02-ECA MPs; (2) CPDI-02-ECA MPs; (3) scCPDI-02-CE MPs; (4) CPDI-02-CE MPs; (5) scCPDI-02-SM MPs; or (6) CPDI-02-SM MPs (**Fig. 6.3**). Dosing of CPDI-02 in the CPDI-02-ECA MP strategy was conservatively normalized to the amount of CPDI-02 in the CPDI-02-SM MP strategy. OVA-specific IgA titers in nasal lavage fluid (NLF) and titers of OVA-specific IgA and Total IgG in bronchoalveolar lavage fluid (BALF) were determined 14 days post-treatment by ELISA and normalized to vehicle alone treatment group.

Relative to scCPDI-02-ECA MPs (white circles, **Fig.6.3**), CPDI-02-ECA MPs (black circles, **Fig.6.3**) generated $10^{3.2}$ -fold higher IgA titers in the NLF (**Fig.6.3A**), $10^{4.6}$ -fold higher IgA titers in the BALF (**Fig.6.3B**), and $10^{4.0}$ -fold higher Total IgG titers in the BALF (**Fig.6.3C**). Relative to scCPDI-02-CE MPs (white triangles, **Fig.6.3**), CPDI-02-

CE MPs (black triangles, **Fig.6.3**) generated $10^{2.3}$ -fold higher IgA titers in the NLF (**Fig.6.3A**), $10^{3.2}$ -fold higher IgA titers in the BALF (**Fig.6.3B**), and $10^{4.0}$ -fold higher Total IgG titers in the BALF (**Fig.6.3C**). Relative to scCPDI-02-SM MPs (white squares, **Fig.6.3**), CPDI-02-SM MPs (black squares, **Fig.6.3**) generated $10^{3.4}$ -fold higher IgA titers in the NLF (**Fig.6.3A**), $10^{4.8}$ -fold higher IgA titers in the BALF (**Fig.6.3B**), and $10^{4.9}$ -fold higher Total IgG titers in the BALF (**Fig.6.3C**).

Compared to the CPDI-02-CE MPs, CPDI-02-ECA MPs generated $10^{1.4}$ -fold higher IgA titers in the NLF (**Fig.6.3A**), $10^{1.7}$ -fold higher IgA titers in the BALF (**Fig.6.3B**), and $10^{1.1}$ -fold higher Total IgG titers in the BALF (**Fig.6.3C**). Antibody titer differences between the CPDI-02-ECA and CPDI-02-SM strategies were non-significant, as were the differences between the CPDI-02-CE and CPDI-02-SM strategies in both NLF and BALF.

6.2.4 CPDI-02-ECA MP strategy generates greater magnitudes of OVA-specific IgG ASCs in the spleens of naïve mice compared to CPDI-02-CE and CPDI-02-SM MP strategies

To provide an early indication of the effect that the CPDI-02 incorporation strategy into biodegradable microparticles encapsulating OVA might have on generated systemic humoral immunity, magnitudes of OVA-specific ASCs from the spleens of immunized mice were compared on Day 6 via ELISpot. As in **Sections 6.2.2** and **6.2.3**, treatment groups (n=10 total mice from two independent studies for CPDI-02-based treatment groups; n=5 mice for vehicle alone and scCPDI-02-based treatment groups) were vehicle alone (PBS, 50 μ L), or vehicle containing an equivalent dose of LPS-free OVA [50 μ g] encapsulated in one of the following CPDI-02 or scCPDI-02 incorporation strategies: (1) scCPDI-02-ECA MPs; (2) CPDI-02-ECA MPs; (3) scCPDI-02-CE MPs;

(4) CPDI-02-CE MPs; (5) scCPDI-02-SM MPs; or (6) CPDI-02-SM MPs (**Fig. 6.4**). Dosing of CPDI-02 in the CPDI-02-ECA MP strategy was conservatively normalized to the amount of CPDI-02 in the CPDI-02-SM MP strategy.

Relative to scCPDI-02-ECA MPs (white circles, **Fig.6.4**), CPDI-02-ECA MPs (black circles, **Fig.6.4**) generated 18-fold higher OVA-specific IgA ASCs (**Fig.6.4A**), 10-fold higher OVA-specific IgM ASCs (**Fig.6.4B**), and 71-fold higher OVA-specific IgG ASCs (**Fig.6.4C**). Relative to scCPDI-02-CE MPs (white triangles, **Fig.6.4**), CPDI-02-CE MPs (black triangles, **Fig.6.4**) generated 5.6-fold higher OVA-specific IgA ASCs (**Fig.6.4A**), similar levels of OVA-specific IgM ASCs (**Fig.6.4B**), and 4-fold higher OVA-specific IgG ASCs (**Fig.6.4C**). Relative to scCPDI-02-SM MPs (white squares, **Fig.6.4**), CPDI-02-SM MPs (black squares, **Fig.6.4**) generated 4.7-fold higher OVA-specific IgA ASCs (**Fig.6.4A**), 2-fold higher OVA-specific IgM ASCs (**Fig.6.4B**), and 24-fold higher OVA-specific IgG ASCs (**Fig.6.4C**).

Compared to the CPDI-02-CE MPs and CPDI-02-SM MPs, CPDI-02-ECA MPs generated 5.4-fold and 2.8-fold higher OVA-specific IgG ASCs, respectively, in the spleen (**Fig.6.4C**). Further, compared to the CPDI-02-CE MPs and CPDI-02-SM MPs, CPDI-02-ECA MPs generated a 2.3-fold (albeit non-significant, $P=0.11$) and significant 4.4-fold increase in OVA-specific IgA ASCs, respectively, in the spleen (**Fig.6.4A**). No other significant differences were seen between the CPDI-02-based incorporation strategies for each of the studied OVA-specific ASC isotypes. Thus, the adjuvant incorporation strategy for CPDI-02-based biodegradable microparticles affects the generation of systemic immunogen-specific IgG and IgA ASCs in the spleen.

6.2.5 CPDI-02-ECA MP strategy generates higher short-term systemic OVA-specific antibody titers in the serum of young, naïve mice compared to CPDI-02-CE and CPDI-02-SM MP strategies

Given that CPDI-02-ECA MPs generated higher magnitudes of OVA-specific IgG ASCs than both the CPDI-02-CE MP and CPDI-02 SM MP treatment groups in the spleens of mice 6 days post-treatment (**Fig.6.4**), we expected CPDI-02-ECA would also increase subsequent titers of OVA-specific systemic antibodies. To first determine if CPDI-02 incorporation strategy into biodegradable microparticles affects the generation of short-term systemic antibodies against encapsulated protein immunogen in mice, we again intranasally administered vehicle alone (PBS, 50 μ L), or vehicle containing an equivalent dose of LPS-free OVA [50 μ g] encapsulated in one of the following CPDI-02 or scCPDI-02 incorporation strategies: (1) scCPDI-02-ECA MPs; (2) CPDI-02-ECA MPs; (3) scCPDI-02-CE MPs; (4) CPDI-02-CE MPs; (5) scCPDI-02-SM MPs; or (6) CPDI-02-SM MPs (**Fig. 6.5**). Dosing of CPDI-02 in the CPDI-02-ECA MP strategy was conservatively normalized to the amount of CPDI-02 in the CPDI-02-SM MP strategy. OVA-specific IgG1, IgG2b, IgG2c, and IgG3 titers in the serum were determined 14 days post-treatment by ELISA and normalized to the vehicle alone treatment group.

Compared to scCPDI-02-ECA MPs (white circles, **Fig.6.5**), CPDI-02-ECA MPs (black circles, **Fig.6.5**) generated $10^{2.1}$ -fold higher OVA-specific IgG1 titers (**Fig.6.5A**), $10^{1.4}$ -fold higher OVA-specific IgG2b titers (**Fig.6.5B**), 10^1 -fold higher OVA-specific IgG2c titers (**Fig.6.5C**), and $10^{1.6}$ -fold higher OVA-specific IgG3 titers (**Fig.6.5D**). Compared to scCPDI-02-CE MPs (white triangles, **Fig.6.5**), CPDI-02-CE MPs (black triangles, **Fig.6.5**) generated significantly higher OVA-specific IgG1 titers (**Fig.6.5A**), significantly higher OVA-specific IgG2b titers (**Fig.6.5B**), similar OVA-specific IgG2c titers (**Fig.6.5C**), and significantly higher OVA-specific IgG3 titers (**Fig.6.5D**); specific

fold-increases are unspecified due to undetectable titers in many scCPDI-02-CE samples for all IgG subclasses. Compared to scCPDI-02-SM MPs (white squares, **Fig.6.5**), CPDI-02-SM MPs (black squares, **Fig.6.5**) generated $10^{3.1}$ -fold higher OVA-specific IgG1 titers (**Fig.6.5A**), $10^{1.4}$ -fold higher OVA-specific IgG2b titers (**Fig.6.5B**), $10^{0.8}$ -fold higher (but non-significant) OVA-specific IgG2c titers (**Fig.6.5C**), and $10^{0.7}$ -fold higher OVA-specific IgG3 titers (**Fig.6.5D**).

Compared to the CPDI-02-CE MPs and CPDI-02-SM MPs, CPDI-02-ECA MPs generated: (1) $10^{1.1}$ -fold and 10^1 -fold higher OVA-specific IgG1 titers, respectively (**Fig.6.5A**); (2) $10^{1.5}$ -fold and $10^{0.9}$ -fold higher OVA-specific IgG2b titers, respectively (**Fig.6.5B**); (3) $10^{2.7}$ -fold and $10^{1.1}$ -fold higher OVA-specific IgG2c titers, respectively (**Fig.6.5C**); and (4) $10^{1.3}$ -fold and $10^{0.9}$ -fold higher OVA-specific IgG3 titers, respectively (**Fig.6.5D**). Further, compared to CPDI-02-CE MPs, CPDI-02-SM MPs generated similar magnitudes of OVA specific IgG1 (**Fig.6.5A**) and IgG2b (**Fig.6.5B**) titers, but generated $10^{1.6}$ -fold higher OVA-specific IgG2c titers (**Fig.6.5C**) and $10^{1.3}$ -fold higher OVA-specific IgG3 titers (**Fig.6.5D**). Thus, relative to the CPDI-02-CE and CPDI-02-SM incorporation strategies, the CPDI-02-ECA incorporation strategy is the most effective at generating short-term, immunogen-specific systemic antibodies in the serum of naïve mice.

6.2.6 The effect of CPDI-02 incorporation strategy into biodegradable microparticles encapsulating OVA on the magnitudes of OVA-specific CD4+ and CD8+ T cells in the lungs of young, naïve mice

Because the CPDI-02 incorporation strategy into biodegradable microparticles encapsulating mucosal protein vaccine affected the generation of immunogen-specific mucosal *humoral* immune responses (**Sections 6.2.2 and 6.2.3**), we next sought to

assess whether the CPDI-02 incorporation strategy similarly affected immunogen-specific mucosal *cellular* immune responses. As previously, mice (n=10 total mice from two independent studies for CPDI-02-based treatment groups; n=5 mice for vehicle alone and scCPDI-02-based treatment groups) were treated with vehicle alone (PBS, 50 μ L), or vehicle containing an equivalent dose of LPS-free OVA [50 μ g] encapsulated in one of the following CPDI-02 or scCPDI-02 incorporation strategies: (1) scCPDI-02-ECA MPs; (2) CPDI-02-ECA MPs; (3) scCPDI-02-CE MPs; (4) CPDI-02-CE MPs; (5) scCPDI-02-SM MPs; or (6) CPDI-02-SM MPs (**Fig. 6.6**). At Day 14, we then measured magnitudes of lung-derived, IFN- γ secreting T cells via ELISpot which were specific for either OVA₃₂₃₋₃₃₉ ("ISQAVHAAHAEINEAGR;" binds to I-A(d) MHC class II molecule and is specific for CD4⁺ T cells^{96,97}) or OVA₂₅₇₋₂₆₄ ("SIINFEKL;" binds to MHC class I molecule and is specific to CD8⁺ T cells^{98,99}).

Compared to scCPDI-02-ECA MPs (white circles, **Fig.6.6**), CPDI-02-ECA MPs (black circles, **Fig.6.6**) generated 78-fold higher ISQAVHAAHAEINEAGR-specific IFN- γ SFUs/ 10^6 lung lymphocytes (**Fig.6.6A**) and 15-fold higher SIINFEKL-specific IFN- γ SFUs/ 10^6 lung lymphocytes (**Fig.6.6B**). Compared to scCPDI-02-CE MPs (white triangles, **Fig.6.6**), CPDI-02-CE MPs (black triangles, **Fig.6.6**) generated 57-fold higher ISQAVHAAHAEINEAGR-specific IFN- γ SFUs/ 10^6 lung lymphocytes (**Fig.6.6A**) and 40-fold higher SIINFEKL-specific IFN- γ SFUs/ 10^6 lung lymphocytes (**Fig.6.6B**). Compared to scCPDI-02-SM MPs (white squares, **Fig.6.6**), CPDI-02-SM MPs (black squares, **Fig.6.6**) generated 111-fold higher ISQAVHAAHAEINEAGR-specific IFN- γ SFUs/ 10^6 lung lymphocytes (**Fig.6.6A**) and 14-fold higher SIINFEKL-specific IFN- γ SFUs/ 10^6 lung lymphocytes (**Fig.6.6B**).

Overall, the presence of CPDI-02 significantly enhanced generation of OVA-specific IFN- γ -secreting CD4⁺ and CD8⁺ T cells compared to their counterpart scCPDI-02 incorporation strategies. However, no significant differences in the

magnitudes of OVA-specific IFN- γ -secreting CD4⁺ and CD8⁺ T cells were observed between the differing CPDI-02-based incorporation strategies in the lungs.

6.2.7 CPDI-02-ECA MP and CPDI-02-SM MP strategies generate greater magnitudes of OVA-specific CD4⁺ and CD8⁺ T cells in the spleens of young, naïve mice compared to the CPDI-02-CE MP strategy

Although differing the CPDI-02 incorporation strategy into biodegradable microparticles encapsulating mucosal protein vaccine did not affect the generation of immunogen-specific *mucosal* cellular immune responses (**Section 6.2.6**), we next sought to assess whether the CPDI-02 incorporation strategy might affect immunogen-specific *systemic* cellular immune responses. As in **Section 6.2.6**, mice (n=10 total mice from two independent studies for CPDI-02-based treatment groups; n=5 mice for vehicle alone and scCPDI-02-based treatment groups) were treated with vehicle alone (PBS, 50 μ L), or vehicle containing an equivalent dose of LPS-free OVA [50 μ g] encapsulated in one of the following CPDI-02 or scCPDI-02 incorporation strategies: (1) scCPDI-02-ECA MPs; (2) CPDI-02-ECA MPs; (3) scCPDI-02-CE MPs; (4) CPDI-02-CE MPs; (5) scCPDI-02-SM MPs; or (6) CPDI-02-SM MPs (**Fig. 6.7**). At Day 14, we then measured magnitudes of splenic IFN- γ secreting T cells via ELISpot which were specific for either OVA₃₂₃₋₃₃₉ (ISQAVHAAHAEINEAGR) or OVA₂₅₇₋₂₆₄.

Compared to scCPDI-02-ECA MPs (white circles, **Fig.6.7**), CPDI-02-ECA MPs (black circles, **Fig.6.7**) generated 32-fold higher ISQAVHAAHAEINEAGR-specific IFN- γ SFUs/10⁶ splenocytes (**Fig.6.7A**) and 11-fold higher SIINFEKL-specific IFN- γ SFUs/10⁶ splenocytes (**Fig.6.7B**). Compared to scCPDI-02-CE MPs (white triangles, **Fig.6.7**), CPDI-02-CE MPs (black triangles, **Fig.6.7**) generated 4.4-fold higher ISQAVHAAHAEINEAGR-specific IFN- γ SFUs/10⁶ splenocytes (**Fig.6.7A**) and 5.4-fold

higher SIINFEKL-specific IFN- γ SFUs/ 10^6 splenocytes (**Fig.6.7B**). Compared to scCPDI-02-SM MPs (white squares, **Fig.6.7**), CPDI-02-SM MPs (black squares, **Fig.6.7**) generated 8.5-fold higher ISQAVHAAHAEINEAGR-specific IFN- γ SFUs/ 10^6 splenocytes (**Fig.6.7A**) and 14-fold higher SIINFEKL-specific IFN- γ SFUs/ 10^6 splenocytes (**Fig.6.7B**).

Compared to the CPDI-02-CE MP strategy, the CPDI-02-ECA and CPDI-02-SM MP strategies generated 3.1-fold and 4.7-fold higher ISQAVHAAHAEINEAGR-specific IFN- γ SFUs/ 10^6 splenocytes, respectively (**Fig.6.7A**), and 3.5-fold and 2.2-fold higher SIINFEKL-specific IFN- γ SFUs/ 10^6 splenocytes, respectively (**Fig.6.7B**).

Overall, the presence of CPDI-02 significantly enhanced generation of OVA-specific IFN- γ -secreting CD4⁺ and CD8⁺ T cells compared to their counterpart scCPDI-02 incorporation strategies. Further, the CPDI-02-ECA and CPDI-02-SM MP incorporation strategies generated similar magnitudes of OVA-specific CD4⁺ and CD8⁺ T Cells, both of which were significantly higher than the magnitudes generated by the CPDI-02-CE MP strategy.

Conventional Adjuvant Incorporation Strategies for Biodegradable PLGA Microparticles

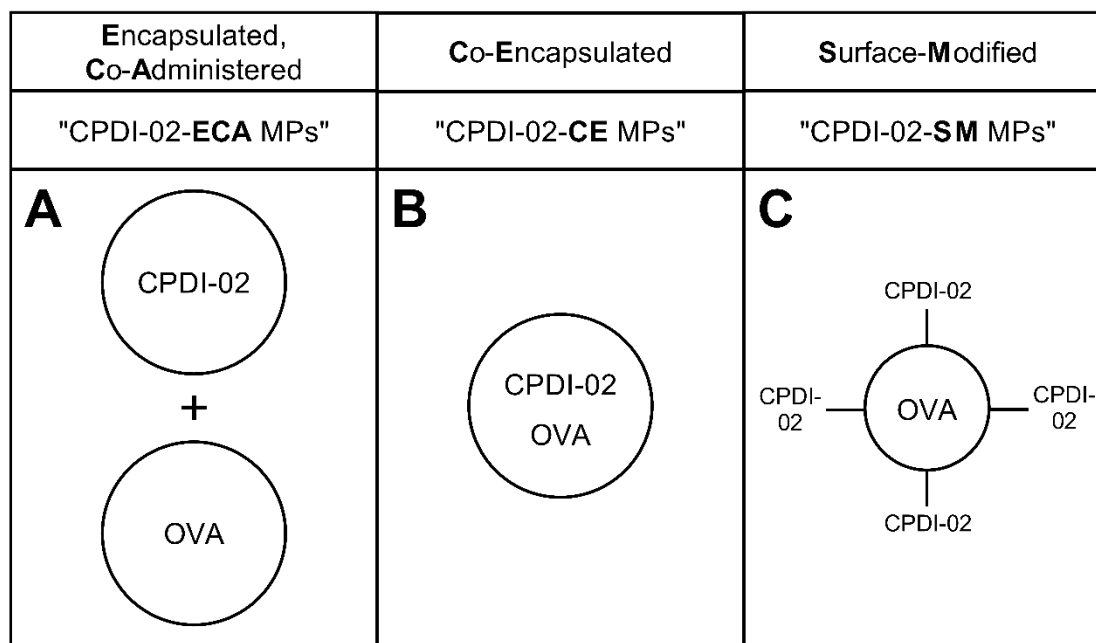


Fig.6.1. Conventional adjuvant incorporation strategies for biodegradable PLGA microparticles. Literature sources have reported several different strategies for incorporating mucosal adjuvants with vaccine in biodegradable particles.⁸⁴⁻⁸⁶ **Fig.6.1A** depicts an incorporation strategy ("CPDI-02-ECA MPs") in which immunogen/protein vaccine (OVA) is encapsulated in a biodegradable particle ("OVA Only MP"), and then co-administered with adjuvant (CPDI-02) that has been encapsulated within a separate biodegradable microparticle ("CPDI-02 Only MP"). **Fig.6.1B** ("CPDI-02-CE MPs") depicts an incorporation strategy in which immunogen/protein vaccine (OVA) is co-encapsulated with adjuvant (CPDI-02) within the same biodegradable microparticle. **Fig.6.1C** ("CPDI-02-SM MPs") depicts an incorporation strategy where adjuvant (CPDI-02) surface modifies a biodegradable microparticle encapsulating immunogen/protein vaccine (OVA). The CPDI-02-SM MP formulation shown in **Fig.6.1C** was utilized throughout Chapters 4 and 5 of this dissertation.

Table 6.1

Formulation	OVA Loading ($\mu\text{g}/\text{mg MP} \pm \text{SD}$)	Burst release ^a (% Loaded OVA)	CPDI-02 or scCPDI-02 Incorporation ^{b,c} ($\mu\text{g}/\text{mg MP} \pm \text{SD}$)	Diameter ^d ($\mu\text{m} \pm \text{SD}$)	Polydispersity Index ^d (PDI \pm SD)	Zeta Potential ^e ($\text{mV} \pm \text{SD}$)
CPDI-02-SM MP	62 \pm 13	0.8 \pm 0.2	4.0 \pm 0.6	1.12 \pm 0.17	0.26 \pm 0.15	-22.5 \pm 3.3
scCPDI-02-SM MP	52 \pm 13	0.4 \pm 0.1	3.9 \pm 0.2	1.21 \pm 0.02	0.36 \pm 0.08	-23.7 \pm 4.3
OVA Only MP (ECA)	82 \pm 5	2.9 \pm 0.3	N/A	0.99 \pm 0.12	0.41 \pm 0.08	-23.3 \pm 2.1
CPDI-02 Only MP (ECA)	N/A	N/A	34.1 \pm 4.0	0.97 \pm 0.14	0.37 \pm 0.15	-17.2 \pm 3.4
scCPDI-02 Only MP (ECA)	N/A	N/A	23.6 \pm 1.1	1.02 \pm 0.05	0.37 \pm 0.07	-17.8 \pm 1.3
CPDI-02-CE MP	70 \pm 10	2.7 \pm 0.4	19.3 \pm 0.8	1.08 \pm 0.02	0.22 \pm 0.08	-18.3 \pm 8.6
scCPDI-02-CE MP	78 \pm 3	3.3 \pm 0.5	17.6 \pm 0.6	1.05 \pm 0.03	0.37 \pm 0.05	-17.5 \pm 2.6

Table 6.1. Representative characteristics of CPDI-02 and scCPDI-02 incorporation strategies into biodegradable PLGA 50:50 microparticles (MP) encapsulating OVA. ^aTotal encapsulated OVA released 24 hr after resuspension in PBS determined by UPLC-AUC quantitation. ^bSurface conjugation of CPDI-02 or scCPDI-02 to CPDI-02-SM/scCPDI-02-SM MP determined by kexin-release / ultra-high performance liquid chromatography (UPLC). ^cCPDI-02 and scCPDI-02 incorporation in ECA and CE strategies determined using NaOH/SDS digestion followed by UPLC-AUC quantitation. ^dDiameter, polydispersity index, and zeta potential determined using ZetaSizer Nano ZS90 (Malvern). Results are representative of at least two independent batches.

Fig.6.2

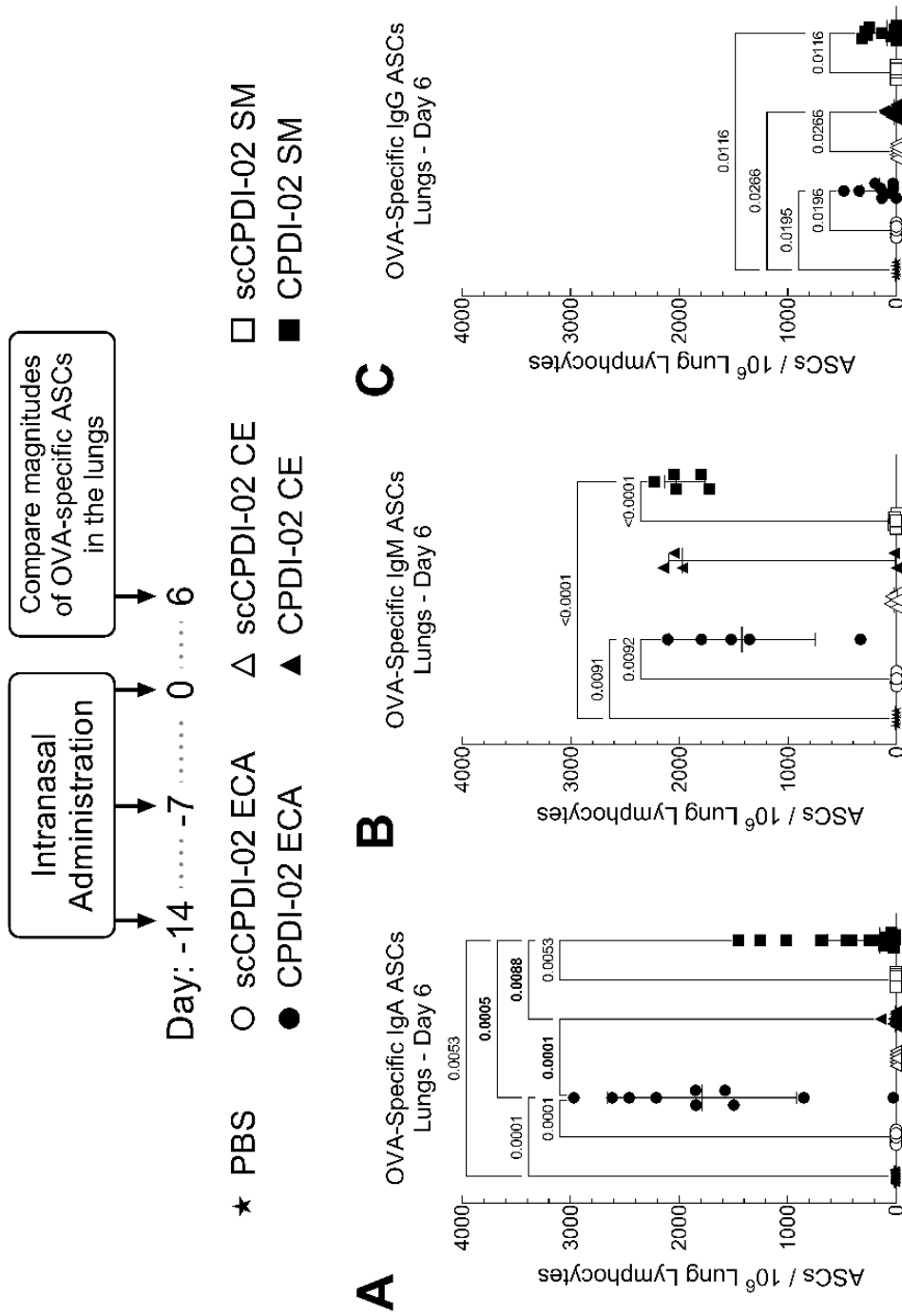


Fig.6.2. Effect of CPDI-02 incorporation strategy into biodegradable microparticles on the magnitudes of short-term mucosal OVA-specific antibody-secreting cells (ASCs) generated in the lungs of naïve female C57BL/6 mice after respiratory immunization with encapsulated LPS-free OVA. Vehicle alone (PBS [50 µL], black stars) or vehicle (PBS [50 µL]) containing an equivalent dose of LPS-free OVA [50µg] encapsulated in PLGA 50:50 microparticles via a differing scCPDI-02/CPDI-02 incorporation strategy (scCPDI-02 ECA [white circles, 3.2µg scCPDI-02], CPDI-02 ECA [black circles, 3.2µg CPDI-02], scCPDI-02 CE [white triangles, 11.3µg scCPDI-02], CPDI-02 CE [black triangles, 13.8µg CPDI-02], scCPDI-02 SM [white squares, 3.8µg scCPDI-02] or CPDI-02 SM [black squares, 3.2µg CPDI-02]; **Table 6.1**) was intranasally administered to naive female C57BL/6 mice (n=10 mice from two independent studies for CPDI-02-based treatment groups; n=5 mice for vehicle alone and scCPDI-02-based treatment groups) on Days -14, -7, and 0. Average OVA-specific (**A**) IgA, (**B**) IgM, and (**C**) IgG antibody secreting cell (ASC) spots / 10⁶ lung lymphocytes ± SD (n=3 replicates per mouse) in the lungs were determined 6 days post-IN administration by ELISpot. Results were compared by Kruskal-Wallis nonparametric one-way ANOVA with uncorrected Dunn's post-test. Outliers identified by the ROUT method (Q = 1%) were omitted. For graphical simplicity, the only P values displayed for each scCPDI-02-based incorporation strategy are the ones corresponding to their respective CPDI-02-based counterpart. Any statistically significant comparisons between CPDI-02-based incorporation strategies are shown in **bold** and underlined.

Fig.6.3

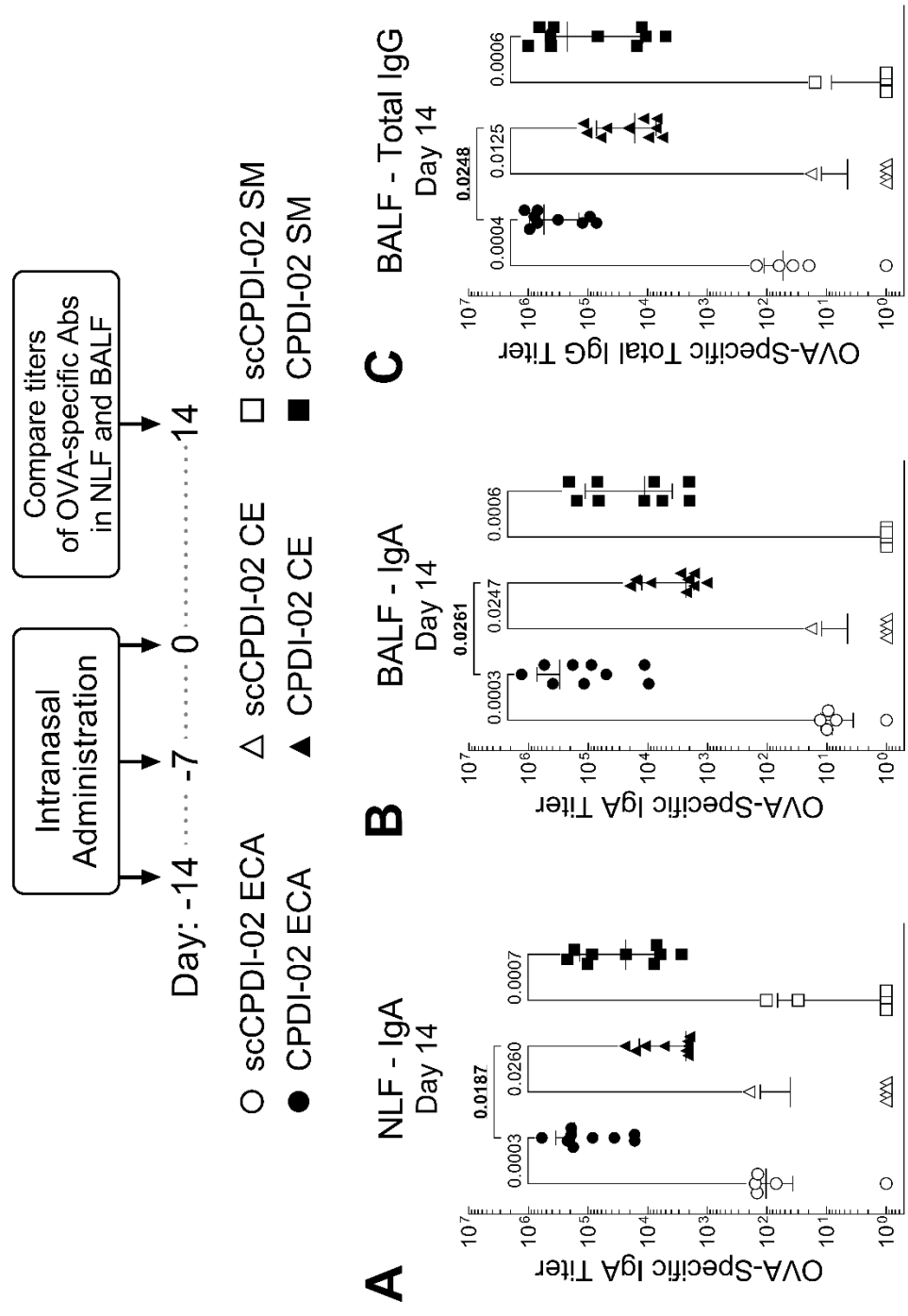


Fig.6.3. Effect of CPDI-02 incorporation strategy into biodegradable microparticles on the short-term OVA-specific antibody titers in the nasal cavities and lungs of naïve female C57BL/6 mice after respiratory immunization with encapsulated LPS-free OVA. Vehicle alone (PBS [50 µL]) or vehicle (PBS [50 µL]) containing an equivalent dose of LPS-free OVA [50µg] encapsulated in PLGA 50:50 microparticles via a differing scCPDI-02/CPDI-02 incorporation strategy (scCPDI-02 ECA [white circles, 3.2µg scCPDI-02], CPDI-02 ECA [black circles, 3.2µg CPDI-02], scCPDI-02 CE [white triangles, 11.3µg scCPDI-02], CPDI-02 CE [black triangles, 13.8µg CPDI-02], scCPDI-02 SM [white squares, 3.8µg scCPDI-02] or CPDI-02 SM [black squares, 3.2µg CPDI-02]; **Table 6.1**) was intranasally administered to naive female C57BL/6 mice (n=10 mice from two independent studies for CPDI-02-based treatment groups; n=5 mice for vehicle alone and scCPDI-02-based treatment groups) on Days -14, -7, and 0. Average OVA-specific titers ± SD of IgA in the nasal lavage fluid (NLF) (**A**) and bronchial lavage fluid (BALF) (**B**) or total IgG in the BALF (**C**) 14 days post-IN administration were determined by ELISA and normalized to vehicle alone (PBS, 50µL) by “positive titer cutoff threshold method.”¹⁰⁰ Resulting titers were compared by Kruskal-Wallis nonparametric one-way ANOVA with uncorrected Dunn’s post-test. Outliers identified by the ROUT method (Q = 1%) were omitted. Non-detectable titers below the positive titer cutoff threshold are shown as 10⁰. For graphical simplicity, the only P values displayed for each scCPDI-02-based incorporation strategy are the ones corresponding to their respective CPDI-02-based counterpart. Any statistically significant comparisons between CPDI-02-based incorporation strategies are shown in **bold** and underlined.

Fig.6.4

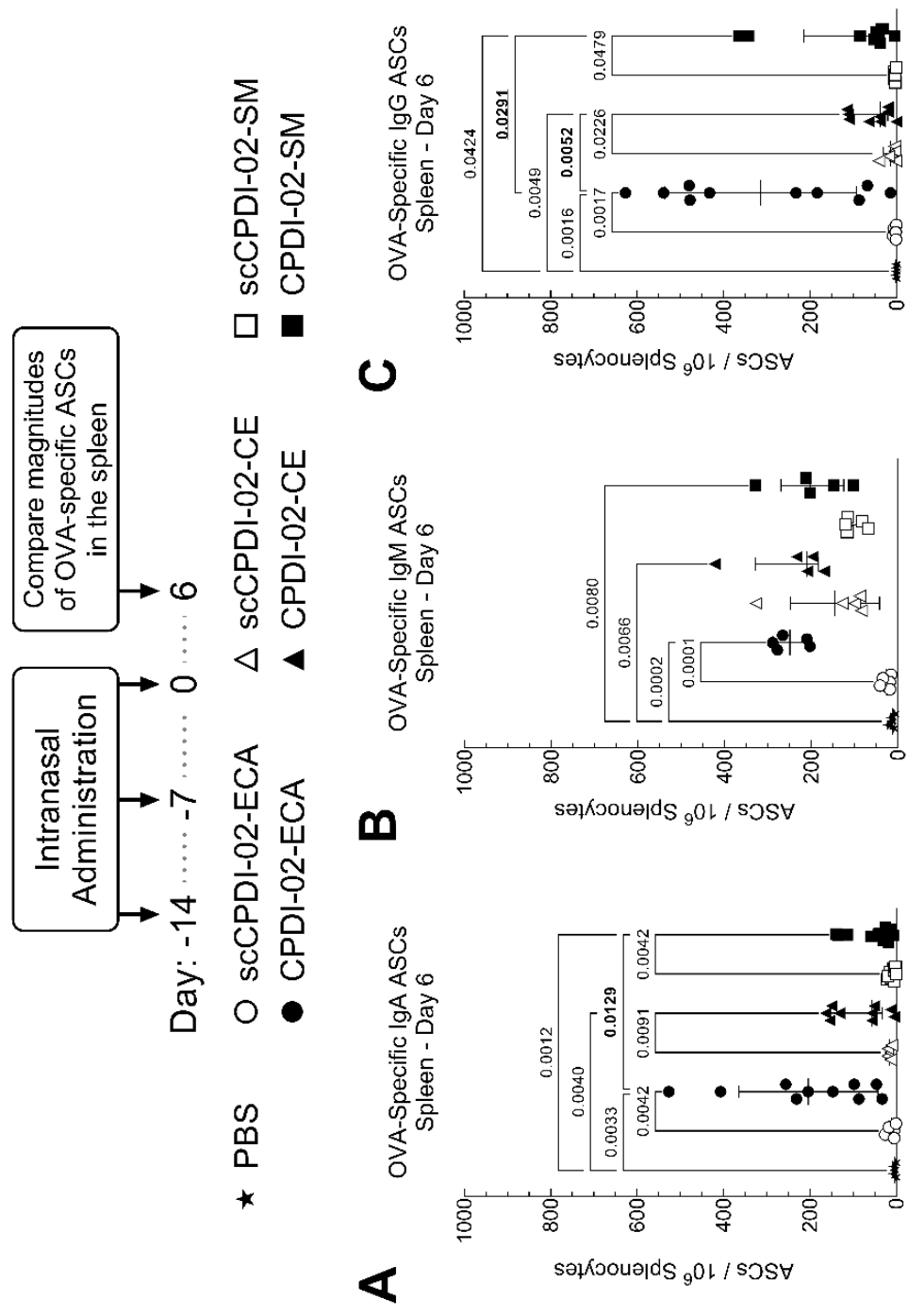


Fig.6.4. Effect of CPDI-02 incorporation strategy into biodegradable microparticles on the magnitudes of short-term systemic OVA-specific antibody-secreting cells (ASCs) generated in the spleens of naïve female C57BL/6 mice after respiratory immunization with encapsulated LPS-free OVA. Vehicle alone (PBS [50 µL], black stars) or vehicle (PBS [50 µL]) containing an equivalent dose of LPS-free OVA [50µg] encapsulated in PLGA 50:50 microparticles via a differing scCPDI-02/CPDI-02 incorporation strategy (scCPDI-02 ECA [white circles, 3.2µg scCPDI-02], CPDI-02 ECA [black circles, 3.2µg CPDI-02], scCPDI-02 CE [white triangles, 11.3µg scCPDI-02], CPDI-02 CE [black triangles, 13.8µg CPDI-02], scCPDI-02 SM [white squares, 3.8µg scCPDI-02] or CPDI-02 SM [black squares, 3.2µg CPDI-02]; **Table 6.1**) was intranasally administered to naïve female C57BL/6 mice (n=10 mice from two independent studies for CPDI-02-based treatment groups; n=5 mice for vehicle alone and scCPDI-02-based treatment groups) on Days -14, -7, and 0. Average OVA-specific (**A**) IgA, (**B**) IgM, and (**C**) IgG antibody secreting cell (ASC) spots / 10⁶ splenocytes ± SD (n=3 replicates per mouse) in the spleen were determined 6 days post-IN administration by ELISpot. Results were compared by Kruskal-Wallis nonparametric one-way ANOVA with uncorrected Dunn's post-test. Outliers identified by the ROUT method (Q = 1%) were omitted. For graphical simplicity, the only P values displayed for each scCPDI-02-based incorporation strategy are the ones corresponding to their respective CPDI-02-based counterpart. Any statistically significant comparisons between CPDI-02-based incorporation strategies are shown in **bold** and underlined.

Fig.6.5

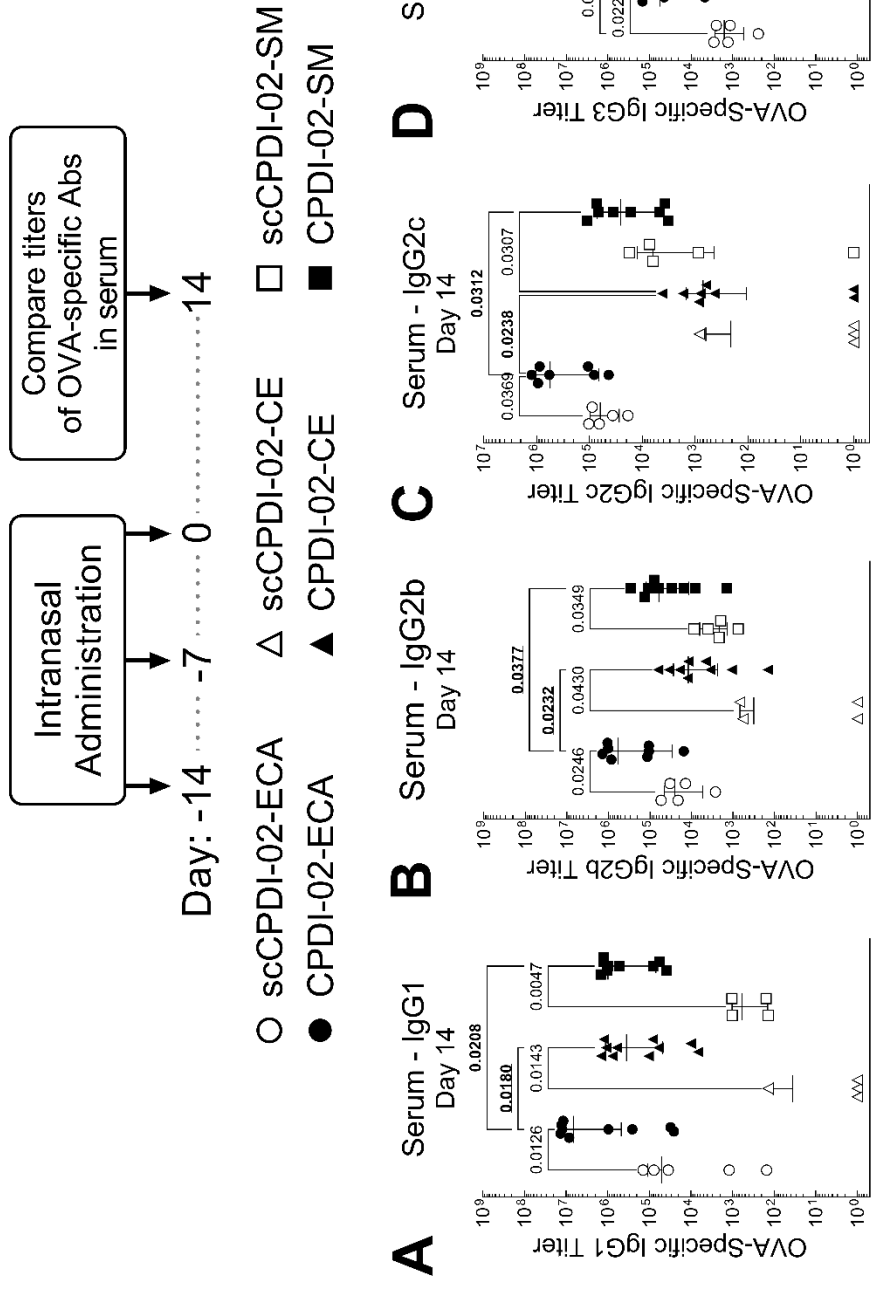


Fig.6.5. Effect of CPDI-02 incorporation strategy into biodegradable microparticles on the short-term OVA-specific antibody titers in the serum of naïve female C57BL/6 mice after respiratory immunization with encapsulated LPS-free OVA. Vehicle alone (PBS [50 µL]) or vehicle (PBS [50 µL]) containing an equivalent dose of LPS-free OVA [50µg] encapsulated in PLGA 50:50 microparticles via a differing scCPDI-02/CPDI-02 incorporation strategy (scCPDI-02 ECA [white circles, 3.2µg scCPDI-02], CPDI-02 ECA [black circles, 3.2µg CPDI-02], scCPDI-02 CE [white triangles, 11.3µg scCPDI-02], CPDI-02 CE [black triangles, 13.8µg CPDI-02], scCPDI-02 SM [white squares, 3.8µg scCPDI-02] or CPDI-02 SM [black squares, 3.2µg CPDI-02]; **Table 6.1**) was intranasally administered to naive female C57BL/6 mice (n=10 mice from two independent studies for CPDI-02-based treatment groups; n=5 mice for vehicle alone and scCPDI-02-based treatment groups) on Days -14, -7, and 0. Average OVA-specific titers ± SD of IgG1 (**A**), IgG2b (**B**), IgG2c (**C**), and IgG3 (**D**) antibodies in the serum were determined 14 days post-immunization by ELISA and normalized to vehicle alone by “positive titer cutoff threshold method.”¹⁰⁰ Resulting titers were compared by Kruskal-Wallis nonparametric one-way ANOVA with uncorrected Dunn’s post-test. Outliers identified by the ROUT method (Q = 1%) were omitted. Non-detectable titers below the positive titer cutoff threshold are shown as 10⁰. For graphical simplicity, the only P values displayed for each scCPDI-02-based incorporation strategy are the ones corresponding to their respective CPDI-02-based counterpart. Any statistically significant comparisons between CPDI-02-based incorporation strategies are shown in **bold** and underlined.

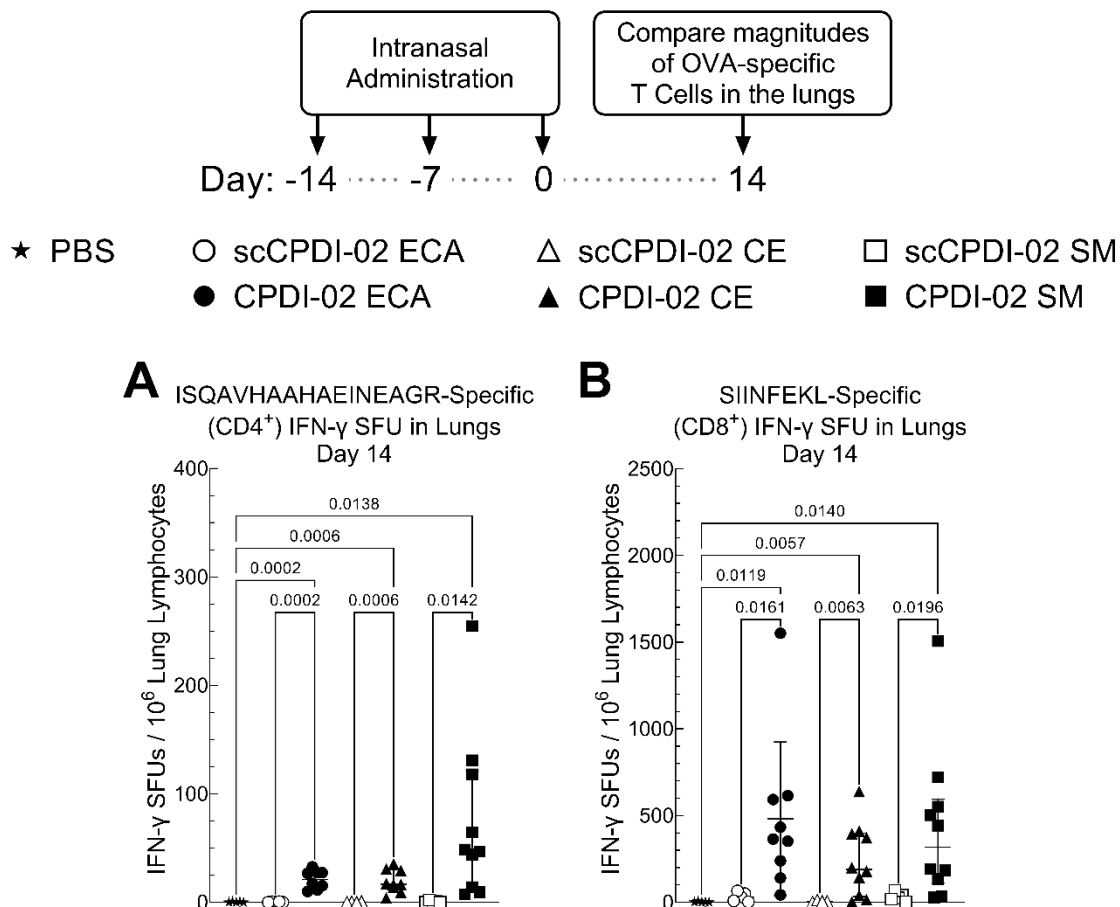


Fig.6.6. Effect of CPDI-02 incorporation strategy into biodegradable microparticles on the magnitude of IFN-γ secretion of mucosal OVA-specific CD4⁺ and CD8⁺ T cells in the lungs generated in naïve female C57BL/6 mice after respiratory immunization with encapsulated LPS-free OVA. Vehicle alone (PBS [50 μL], black stars) or vehicle (PBS [50 μL]) containing an equivalent dose of LPS-free OVA [50μg] encapsulated in PLGA 50:50 microparticles via a differing scCPDI-02/CPDI-02 incorporation strategy (scCPDI-02 ECA [white circles, 3.2μg scCPDI-02], CPDI-02 ECA [black circles, 3.2μg CPDI-02], scCPDI-02 CE [white triangles, 11.3μg scCPDI-02], CPDI-02 CE [black triangles, 13.8μg CPDI-02], scCPDI-02 SM [white squares, 3.8μg scCPDI-02] or CPDI-02 SM [black squares, 3.2μg CPDI-02]; **Table 6.1**) was intranasally administered to naïve female C57BL/6 mice (n=10 mice from two independent studies for

CPDI-02-based treatment groups; n=5 mice for vehicle alone and scCPDI-02-based treatment groups) on Days -14, -7, and 0. On Day 14, lung lymphocytes were isolated, purified, and plated in triplicate on pre-coated IFN- γ ELISpot plates in serum-free CTL-Test Media. Cells were co-incubated with 10 μ g/mL of either ISQAVHAAHAEINEAGR [CD4-specific OVA epitope; **(A)**] or SIINFEKL [CD8-specific OVA epitope; **(B)**] for 24 hrs at 37°C and 5% CO₂. IFN- γ SFUs for each sample were counted using ImmunoSpot S6 MACRO Plate Analyzer (CTL), averaged, and normalized to SFUs/10⁶ lung lymphocytes. Results were compared by Kruskal-Wallis nonparametric one-way ANOVA with uncorrected Dunn's post-test. Outliers identified by the ROUT method (Q = 1%) were omitted. For graphical simplicity, the only P values displayed for each scCPDI-02-based incorporation strategy are the ones corresponding to their respective CPDI-02-based counterpart. Any statistically significant comparisons between CPDI-02-based incorporation strategies are shown in **bold** and underlined.

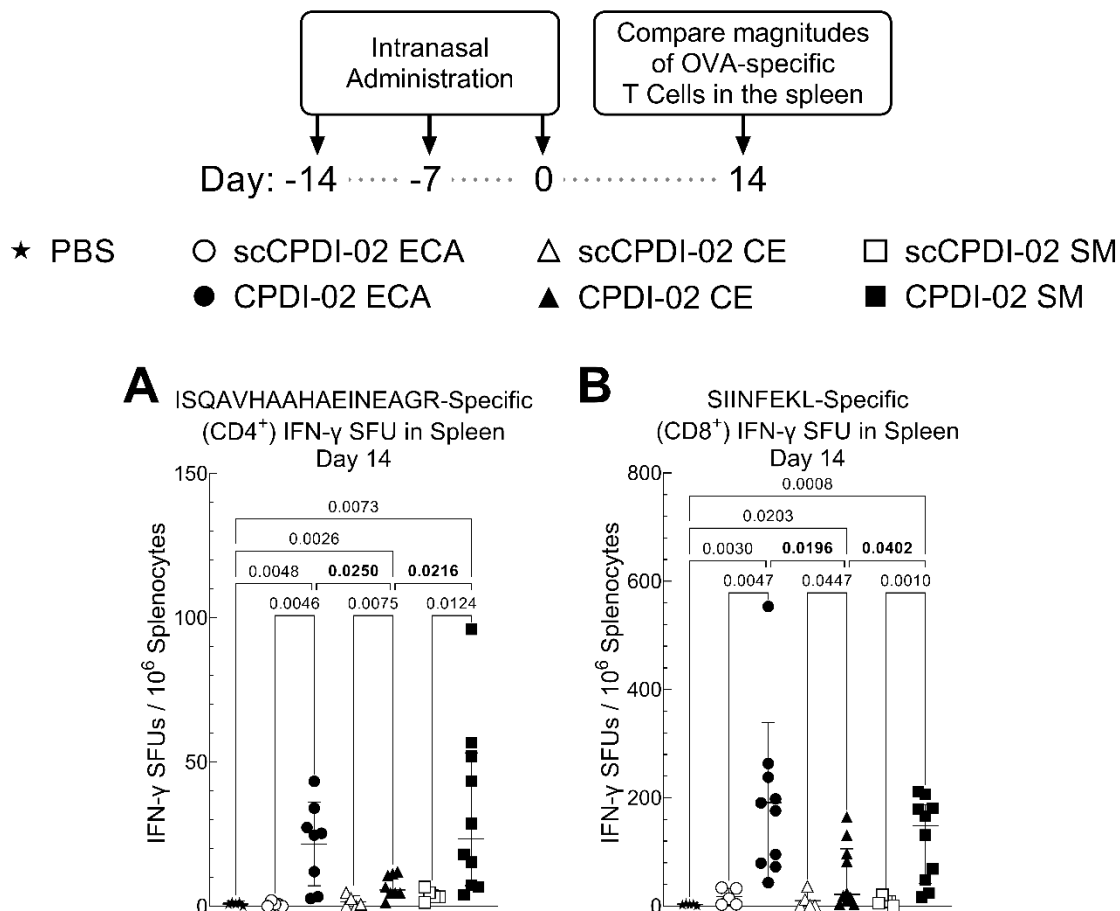


Fig.6.7. Effect of CPDI-02 incorporation strategy into biodegradable microparticles on the magnitude of IFN-γ secretion of systemic OVA-specific CD4⁺ and CD8⁺ T cells in the spleen generated in naïve female C57BL/6 mice after respiratory immunization with encapsulated LPS-free OVA. Vehicle alone (PBS [50 μL], black stars) or vehicle (PBS [50 μL]) containing an equivalent dose of LPS-free OVA [50μg] encapsulated in PLGA 50:50 microparticles via a differing scCPDI-02/CPDI-02 incorporation strategy (scCPDI-02 ECA [white circles, 3.2μg scCPDI-02], CPDI-02 ECA [black circles, 3.2μg CPDI-02], scCPDI-02 CE [white triangles, 11.3μg scCPDI-02], CPDI-02 CE [black triangles, 13.8μg CPDI-02], scCPDI-02 SM [white squares, 3.8μg scCPDI-02] or CPDI-02 SM [black squares, 3.2μg CPDI-02]; **Table 6.1**) was intranasally administered to naïve female C57BL/6 mice (n=10 mice from two independent studies for

CPDI-02-based treatment groups; n=5 mice for vehicle alone and scCPDI-02-based treatment groups) on Days -14, -7, and 0. On Day 14, splenocytes were isolated, purified, and plated in triplicate on pre-coated IFN- γ ELISpot plates in serum-free CTL-Test Media. Cells were co-incubated with 10 μ g/mL of either ISQAVHAAHAEINEAGR [CD4-specific OVA epitope; **(A)**] or SIINFEKL [CD8-specific OVA epitope; **(B)**] for 24 hrs at 37°C and 5% CO₂. IFN- γ SFUs for each sample were counted using ImmunoSpot S6 MACRO Plate Analyzer (CTL), averaged, and normalized to SFUs/10⁶ splenocytes. Results were compared by Kruskal-Wallis nonparametric one-way ANOVA with uncorrected Dunn's post-test. Outliers identified by the ROUT method (Q = 1%) were omitted. For graphical simplicity, the only P values displayed for each scCPDI-02-based incorporation strategy are the ones corresponding to their respective CPDI-02-based counterpart. Any statistically significant comparisons between CPDI-02-based incorporation strategies are shown in **bold** and underlined.

CHAPTER 7

DISCUSSION, CONCLUSIONS, AND FUTURE DIRECTIONS

7.1 Discussion – Chapter 4

In Chapter 4, we hypothesized that conjugation of CPDI-02 to the surface of biodegradable microparticles would affect the generation of mucosal and systemic humoral immune responses by encapsulated protein vaccine after respiratory administration to mice at both short-lived and long-lived timepoints. Our results suggest that this is indeed the case. Compared scCPDI-02-SM MPs and PBS vehicle control, CPDI-02-SM MPs generated: (i) increased numbers of OVA-specific IgA, IgM, and IgG antibody secreting cells (ASCs) in the lungs and spleen, (ii) increased short- and long-lived mucosal IgA and IgG antibody titers, and (iii) increased short- and long-lived OVA-specific serum titers of IgG subclasses.

The systemic humoral immunity findings in Chapter 4 correspond to those by Morgan et al, which showed that IP immunization of female C57BL/6 mice with an OVA-CPDI-02 conjugate induced significantly higher serum titers of OVA-specific IgG1 and IgG2b compared to control treatment groups.¹⁰⁴ The Morgan study indicated that the humoral adjuvanticity of CPDI-02 is likely due “at least in part, to the induction of inflammatory cytokine synthesis that secondarily drives increased T cell function.” Although the route of administration was different in the Morgan study, it is likely that a similar mechanism could be at least partially responsible for humoral responses induced by CPDI-02-SM MPs after intranasal administration. Our later findings in Chapter 5, which showed that CPDI-02-SM MPs delivered to the lungs stimulate the generation of OVA-specific IFN- γ -secreting CD4⁺ T cells (**Fig.5.3**), lend support to this notion. Regardless of the mechanism of action, the combined findings in Chapter 4 indicate that CPDI-02 clearly acts to stimulate immunogen-specific humoral immune responses.

Previous studies on the mucosal adjuvanticity of CPDI-02 only assessed short-term, rather than long-term, timepoints. The results from Chapter 4 at the Day 90 timepoint (**Fig.4.3D-F** and **Fig.4.5E-H**), indicate that the humoral immune responses induced by

CPDI-02 are long-lived. Given that the overall goal of prophylactic vaccination is to generate long-lived protective immunity, these findings demonstrate the utility of CPDI-02 as a suitable adjuvant for mucosal vaccination.

Fig.4.6 assessed the Th1 and Th2 serum antibody profiles of mice intranasally immunized with CPDI-02-SM MPs in a 50 μ L IAV. The increase in the combined ratio ([IgG2b + IgG2c + IgG3] : IgG1) (**Fig.4.6A**) suggests that immune responses generated by CPDI-02-SM MPs in 50 μ L IAV have Th1 bias over time. The Th1 bias shown by CPDI-02-SM MPs in 50 μ L IAV is consistent with the known mechanism of action of CPDI-02, which has previously been shown to induce a Th1-like antibody class switching.⁷⁶ The relatively increased magnitudes of OVA-specific IgG2b and IgG2c titers and decreased magnitude of OVA-specific IgG1 titers seen at Day 90 are likely reflective of Th1-biased antibody class switching, and are the largest contributing factors towards the shift in the overall combined Th1:Th2 ratio (**Fig.4.6A**). The similar average IgG3:IgG1 ratios seen at Day 14 and at Day 90 (0.02 vs 0.04; **Fig.4.6D**) and similar average IgG3 titers at Day 14 and Day 90 ($10^{4.9}$ vs $10^{4.6}$; $P=0.63$) (**Figs.4.5D&H**; statistical comparison not shown graphically) indicate that the IgG3 subclass was likely less involved in the Th1-biased antibody class switching induced by CPDI-02.

Fig.4.7 showed measures of long-term inflammation induced by respiratory administration of scCPDI-02-SM and CPDI-02-SM MPs. Because the difference in inflammation seen between the scCPDI-02-SM in 50 μ L IAV and CPDI-02-SM MPs 50 μ L IAV treatment groups was not statistically different, it is likely that the inflammation is due to the intrinsic properties of the biodegradable microparticles (polymer, potential residual PVA stabilizer, etc) and/or the encapsulated immunogen (OVA), rather than CPDI-02 itself. This is in-line with previous research that suggests CPDI-02 minimizes the amount of inflammation induction compared to the parent C5a molecule, due to its selective activation of macrophages and DCs over inflammation-causing neutrophils.

In addition to the findings regarding the effect of CPDI-02 surface conjugation on humoral immunity, Chapter 4 also provided evidence regarding effect of intranasal administration volume on humoral immune responses. Combining the results from **Fig.4.2** through **Fig.4.5**, the CPDI-02-SM MPs in the 50 μ L IAV treatment group consistently generated greater magnitudes of mucosal and systemic immune responses than the CPDI-02-SM MPs in 10 μ L IAV treatment group (OVA-specific ASCs, and mucosal and systemic OVA-specific antibody titers). Thus, in the context of CPDI-02-SM MPs, larger IAVs are required to generate mucosal and systemic humoral immune responses.

Of note, the 50 μ L IAV treatment group generated greater OVA-specific IgA titers in the NLF compared to the 10 μ L IAV treatment group. Given that a 10 μ L IAV likely localizes entirely within the nasal cavity, these findings are somewhat unexpected. This observed effect, however, is possibly the result of murine nasal anatomy and the related limitations of a small IAV. That is, the volume of the nasal cavities of ~8 week old mice has been previously reported to be ~32 μ L.¹⁰² Thus, a 10 μ L IAV would not be expected to completely fill the nasal cavity, and the CPDI-02-SM MPs delivered in this volume would not be able to coat all nasal mucosal surfaces. As a result, the deposition of particles onto NALT and subsequent induction of immune responses in these regions would be lesser for a 10 μ L IAV. Further studies are necessary to study this particular observation.

7.2 Discussion – Chapter 5

In Chapter 5 of this dissertation, we initially hypothesized that intranasal administration volume would affect the generation of cellular immune responses by OVA encapsulated in CPDI-02-SM-MPs. Our results indicate that IAV indeed has an impact on these types of immune responses. Specifically, relative to vehicle-only and CPDI-02-SM MPs in 10 μ L IAV, CPDI-02-SM MPs in a 50 μ L IAV increased magnitudes of: (1) total OVA-specific CD4+ T cells, as well as CD4+ MPEC, DPEC, EEC, and SLEC at Day 14 in the

lungs; (2) OVA-specific CD4⁺ CD44^{HI}Tet-OVA₃₂₈₋₃₃₇⁺CD127⁺ T cells and CD4⁺ TEM at Day 90 in the lungs; (3) total OVA-specific CD8⁺ T Cells, as well as CD8⁺ MPEC, EEC, and SLEC at Day 14 in the lungs; (4) CD8⁺CD44^{HI}Tet-OVA₂₅₇₋₂₆₄⁺CD127⁺ T cells and CD8⁺ TEM in the lungs at Day 90; (5) ISQAVHAAHAEINEAGR-specific IFN- γ SFUs/10⁶ lung lymphocytes at Day 14; (6) SIINFEKL-specific IFN- γ SFUs/10⁶ lung lymphocytes at Day 14 and Day 90; (7) CD4⁺ DPEC in the spleen at Day 14; (8) CD4⁺CD44^{HI} Tet-OVA₃₂₈₋₃₃₇⁺ CD127⁺ T cells and CD4⁺ TEM at Day 90 in the spleen; (9) total OVA-specific CD8⁺ T cells, as well as OVA-specific CD8⁺ TEM, TEFF, and SLEC at Day 14 in the spleen; (10) CD8⁺CD44^{HI}Tet-OVA₂₅₇₋₂₆₄⁺ CD127⁺ T cells, and CD8⁺ TEM and TCM at Day 90 in the spleen; (11) ISQAVHAAHAEINEAGR-specific IFN- γ SFUs/10⁶ splenocytes at Day 14; and (12) SIINFEKL-specific IFN- γ SFUs/10⁶ splenocytes at Day 14 and Day 90. Overall, CPDI-02-SM MPs in a 50 μ L IAV had much more robust cellular immune responses compared to CPDI-02-SM MPs in a 10 μ L IAV.

In both the lungs and spleen, magnitudes of OVA-specific memory CD8⁺ T cell subsets (**Fig.5.2** and **Fig.5.5**, respectively) directly correlated with magnitudes of OVA-specific IFN- γ secreting CD8⁺ T cell populations measured via ELISpot at both Day 14 and Day 90 for each treatment group. This trend was not as apparent for CD4⁺ T cells in the lungs and spleen, however. In the lungs, differences between 10 μ L IAV and 50 μ L IAV treatment groups were observed when memory subsets of OVA-specific were assessed via FACS at Day 90; there was no difference between those treatment groups in terms of OVA-specific IFN- γ secreting T cell populations measured by ELISpot. In the spleen at Day 14, differences were observed between 10 μ L IAV and 50 μ L IAV treatment groups for OVA-specific IFN- γ secreting T cell populations, whereas only minimal differences were seen via FACS between those treatment groups. For Day 90 it was the reverse—no functional differences were observed via ELISpot between 10 μ L IAV and 50 μ L IAV treatment groups for CD4⁺ T cells in the spleen, whereas notable differences were seen

via FACS between those treatment groups. Given the strong correlation seen with CD8+ T cells, the cause(s) of these discrepancies seen with CD4+ T cells remain somewhat unclear. One possible explanation is that T cells from the specific CD4+ memory subsets that were assessed simply do not elicit high levels of immunogen-specific IFN- γ secretion, and instead rely on the production of other types of cytokines to elicit their downstream immune responses. Further investigation on this front is required.

In addition to confirming that IAV affects the generation of cellular immune responses by CPDI-02-SM MPs encapsulating OVA, Chapter 5 also confirmed and built upon findings from Tallapaka et al, regarding the capability of CPDI-02-surface-modified particles encapsulating immunogen to generate long-lasting cellular immunity.³³ The research in the Tallapaka study only assessed cellular immune responses up to 14 days post-final treatment; the study used the presence of early-appearing T cell memory markers to postulate that surface conjugation of CPDI-02 to MPs induces long-term responses. In the present study, we assessed immune responses at both 14 days post-final treatment *and* at 90 days post-final treatment. This study thus provides confirmatory evidence to this original postulation that conjugation of CPDI-02 to the surface of biodegradable MPs is indeed an effective means at generating long-term cellular immunity. Further, our study provides confirmatory evidence that magnitudes of T cells with early-appearing memory markers does indeed correlate with magnitudes of immunogen-specific T cells at a long-lived timepoint.

7.3 Discussion – Chapter 6

Given the results seen in Chapters 4 and 5, we next sought to determine whether the incorporation strategy of adjuvant (CPDI-02) into biodegradable microparticles encapsulating protein vaccine affects the generation of mucosal and systemic humoral and cellular responses after intranasal administration. In Chapter 6 of this dissertation,

three conventional strategies for incorporating CPDI-02 into PLGA biodegradable microparticles encapsulating OVA vaccine were developed and assessed—(1) encapsulated, co-administered (ECA) MPs, (2) co-encapsulated (CE) MPs, and (3) surface-modified (SM) MPs (**Fig.6.1**).

The first goal of Chapter 6 was to generate biodegradable microparticles for each CPDI-02 incorporation strategy, that were as similar as possible in terms of polymer type, particle size, zeta potential, particle formation methodology, and immunogen/adjuvant dosing. This facilitates equitable comparisons between CPDI-02 incorporation strategies in terms of generated immune responses by each strategy. In **Chapter 3**, we outlined protocols for the formulation of each type of microparticle; each particle type utilized the same types of polymers and sonication techniques in the formulations. All dosing of encapsulated mucosal protein was kept identical (50 μ g equivalent of OVA), and dosing of CPDI-02 was kept as equal as possible (with notable exception of CPDI-02-CE MPs, see **Section 6.2.1.4**). As shown in **Table 6.1**, particle sizes and zeta potentials between CPDI-02 incorporation strategies were very similar; specifically, particles ranged in size from 0.97 to 1.21 μ m, and zeta potentials ranged from -23.7 to -17.2mV. As a whole, the high homogeneity between particle types in terms of biophysical characteristics permit “fair” immunologic comparisons between CPDI-02 incorporation strategies through minimization of any potential formulation-related confounding variables.

After intranasal administration of our developed CPDI-02-based formulations in a murine model, our results indicate that, in general, the ECA incorporation strategy generated: (i) enhanced OVA-specific mucosal humoral immune responses relative to the CE incorporation strategy; (ii) enhanced OVA-specific systemic humoral immune responses relative to the CE and SM incorporation strategies; (iii) similar OVA-specific T cell responses to CE and SM incorporation strategies in the lungs; and (iv) enhanced

OVA-specific systemic T cell responses relative to the CE strategy—but similar to the SM incorporation strategy—in the spleen.

The poorer overall levels of humoral and cellular adjuvanticity seen with the CE strategy is somewhat unexpected. Given that both CPDI-02 and OVA were within the same particle in this strategy, it could be predicted that co-encapsulation would facilitate intimate co-localization of both adjuvant and immunogen upon uptake at induction sites. While this may indeed be true, it is also possible, however, that dissolution of both CPDI-02 and OVA within the same W_1 phase of $W_1/O/W_2$ MP formulation promotes electrostatic interactions between these two species. Indeed, OVA is known to have a slightly negative charge at neutral pH (pH of PBS used in the W_1 phase is 7.2 to 7.4),¹³⁵ whereas CPDI-02 has a slightly positive charge.¹³⁶ Thus, because of this electrostatic attraction between CPDI-02 and OVA, CPDI-02 may be unable to be freely liberated and exert its downstream immunogenic functions as effectively as it does in the SM and ECA strategies. More investigation is necessary to explore the potential causes for relatively weaker generated humoral and cellular immune responses of the CE strategy.

As noted, the SM incorporation strategy for CPDI-02 was also less effective than the ECA strategy in terms of the generation of OVA-specific systemic antibodies. This effect is likely due to the greater levels of sustained release of CPDI-02 inherent with the ECA strategy. Encapsulation of payloads within biodegradable microparticles has been proven to enhance sustained release.¹³⁷ In the context of this study, encapsulating CPDI-02 (like in the ECA strategy) likely enables it to be slowly released, and permits a more sustained systemic activation response. Although having CPDI-02 exposed on the surface of the particle (like in the SM strategy) enables cellular targeting, this means of adjuvant incorporation also enables CPDI-02 to be more easily cleaved and, as a result, more quickly degraded. Quicker degradation would thus stifle the ability of CPDI-02 to be trafficked across mucosal surfaces and stimulate downstream systemic activation.

7.4 Conclusions

In Chapter 4 of this dissertation, it was demonstrated that conjugation of CPDI-02 to the surface of biodegradable PLGA microparticles enhances the generation of short- and long-term mucosal and systemic humoral immune responses to encapsulated protein vaccine after intranasal administration in a murine model. It was also shown that increased delivery to the lungs/lower airways (via a larger intranasal administration volume) of CPDI-02-SM MPs the microparticles enhanced the generation of mucosal and systemic humoral immune responses at short- and long-lived timepoints. This is consistent with other literature sources that cite IAV as a critical parameter for the generation of systemic antibodies by intranasally administered vaccines.⁸²

Previous studies have shown that conjugation of CPDI-02 to the surface of biodegradable PLGA *nanoparticles* (~380nm diameter) encapsulating protein vaccine increases T cell expansion and long-lived memory subsets of epitope-specific CD4+ CD8a+ T cells in the lungs and spleens of mice after intranasal administration at *short-term timepoints*.³³ In Chapter 5 of this dissertation, we expanded on these findings by demonstrating that conjugating CPDI-02 to the surface of biodegradable PLGA *microparticles* (~1µm diameter) encapsulating protein vaccine increases T-cell expansion and memory subsets of epitope-specific CD4+ and CD8a+ T-cells in the lungs and spleens of mice after intranasal administration at short-lived *and long-lived* timepoints. Further, consistent with our findings in Chapter 4, we found that larger intranasal administration volumes of delivery vehicle of the microparticles (50µL vs 10µL) enhances the generation of OVA-specific mucosal and systemic cellular immune responses at both short- and long-lived timepoints.

In Chapter 6 of this dissertation, three conventional strategies for incorporating CPDI-02 into PLGA biodegradable microparticles encapsulating mucosal protein vaccine were developed and assessed—(1) encapsulated, co-administered (ECA) MPs, (2) co-

encapsulated (CE) MPs, and (3) surface-modified (SM) MPs (**Fig.6.1**). Our findings demonstrate that each CPDI-02-based MP incorporation strategy enhances the generation of humoral and cellular immune responses relative to their scrambled, inactivated scCPDI-02 counterparts. Our results further showed that the ECA incorporation strategy generated: (i) enhanced OVA-specific mucosal humoral immune responses relative to the CE incorporation strategy; (ii) enhanced OVA-specific systemic humoral immune responses relative to the CE and SM incorporation strategies; (iii) similar OVA-specific T cell responses to CE and SM incorporation strategies in the lungs; and (iv) enhanced OVA-specific systemic T cell responses relative to the CE strategy—but similar to the SM incorporation strategy—in the spleen. Taken together, our results indicate that the ECA strategy is perhaps the most promising approach towards mucosal immunization—in terms of the ability to generate “optimal” magnitudes of humoral and cellular immune responses—of the three conventional CPDI-02 incorporation strategies that were assessed.

7.5 Future Directions

A major limitation of the studies in Chapter 6 was that mucosal and systemic immune responses were only assessed at a short-term timepoint; timepoints for assays did not extend past 14 days post-final-immunization. While results from Chapter 4 and Chapter 5 indicate that short-term immune responses towards CPDI-02-SM MPs encapsulating OVA strongly correlate with long-term immune responses, it cannot be assumed that this correlation holds for the ECA and CE incorporation strategies. Therefore, it is critical to do comparative long-term (at least 90 days post-final immunization) immunologic assessments for the ECA and CE incorporation strategies.

Microparticle formulations that were developed and assessed in this dissertation utilized LPS-free ovalbumin (OVA) as a model immunogen. In future studies, it must be

determined whether observed trends and differences between differing CPDI-02 incorporation strategies are consistent when disease-specific proteins and epitopes are formulated into the conventional CPDI-02 incorporation strategies. For example, CPDI-02-based nano-/microparticles have previously shown utility in the context of encapsulating a CPDI-02 conjugate of a murine cytomegalovirus (MCMV) cytotoxic T cell (CTL) epitope (pp89).³² MCMV could thus be one such disease target by which to compare CPDI-02 incorporation strategies. Using a disease-specific immunogen in the CPDI-02-based formulations would also permit studies on vaccine protection efficacy in the context of a true pathogen.

In Chapter 6, the dose of CPDI-02 administered in the CPDI-02 ECA strategy was conservatively normalized to the amount of CPDI-02 administered in the CPDI-02-SM strategy based on a 50µg OVA equivalent (both strategies dosed 3.2µg CPDI-02 per mouse). These dosages were both lesser than the dose of CPDI-02 administered in the CPDI-02-CE strategy (13.8µg per mouse for a 50µg OVA equivalent). The CPDI-02-ECA strategy is unique compared to the two other conventional CPDI-02 incorporation strategies in that the amount of administered CPDI-02 is adjustable relative to a defined amount of administered immunogen (OVA). In short, the nature of the ECA strategy inherently enables CPDI-02 dose scaling, and facilitates “fine tuning” increasingly larger doses of CPDI-02, simply by administering greater amounts of the “CPDI-02 Only” MP formulation. It will be the aim of future studies to do a dose response assessment for varying the levels of CPDI-02 using the ECA strategy, while maintaining a constant dose of OVA. Such studies will assess the effects of ramping CPDI-02 dosing on the generation of epitope-specific humoral and cellular immunity.

Finally, given the results of the present studies, it is also of interest to assess the immunologic effects of administering different permutations of the conventional CPDI-02 incorporation strategies. One such example might be co-administering CPDI-02-SM MPs

along with CPDI-02 Only MPs (component from the ECA strategy). Combining the differing incorporation strategies could potentially have an additive or synergistic effect in terms of generated immune responses. Along the same lines, the CPDI-02 Only MPs in particular could be exploited through co-administration with completely different types of nanoscale formulations and vaccine types (liposomes, solid lipid nanoparticles, mRNA vaccines, live-attenuated vaccines, etc.).

Overall, the results and assays shown within this dissertation provide a framework for future studies on CPDI-02-based mucosal vaccines, both in terms of (1) formulation approaches/adjuvant-incorporation strategies and (2) the means by which to comprehensively characterize humoral and cellular immune responses to an intranasally administered vaccine in a murine model.

CHAPTER 8

REFERENCES

1. Hellfritzsich, M. & Scherliess, R. Mucosal Vaccination via the Respiratory Tract. *Pharmaceutics* **11**(2019).
2. Davis, S.S. Nasal vaccines. *Adv Drug Deliv Rev* **51**, 21-42 (2001).
3. McGhee, J.R. & Fujihashi, K. Inside the mucosal immune system. *PLoS Biol* **10**, e1001397 (2012).
4. Musumeci, T., Bonaccorso, A. & Puglisi, G. Epilepsy Disease and Nose-to-Brain Delivery of Polymeric Nanoparticles: An Overview. *Pharmaceutics* **11**(2019).
5. Ozsoy, Y., Gungor, S. & Cevher, E. Nasal delivery of high molecular weight drugs. *Molecules* **14**, 3754-3779 (2009).
6. Skwarczynski, M. & Tóth, I.n. *Micro- and nanotechnology in vaccine development*, (Elsevier/William Andrew, Amsterdam ; Boston, 2017).
7. Ugwoke, M.I., Agu, R.U., Verbeke, N. & Kinget, R. Nasal mucoadhesive drug delivery: background, applications, trends and future perspectives. *Adv Drug Deliv Rev* **57**, 1640-1665 (2005).
8. Perry, M. & Whyte, A. Immunology of the tonsils. *Immunol Today* **19**, 414-421 (1998).
9. Fujimura, Y. Evidence of M cells as portals of entry for antigens in the nasopharyngeal lymphoid tissue of humans. *Virchows Arch* **436**, 560-566 (2000).
10. Arora, P., Sharma, S. & Garg, S. Permeability issues in nasal drug delivery. *Drug Discov Today* **7**, 967-975 (2002).
11. Merkus, F.W., Verhoef, J.C., Schipper, N.G. & Martin, E. Nasal mucociliary clearance as a factor in nasal drug delivery. *Adv Drug Deliv Rev* **29**, 13-38 (1998).
12. Gebert, A. & Pabst, R. M cells at locations outside the gut. *Semin Immunol* **11**, 165-170 (1999).

13. Takano, K., *et al.* HLA-DR- and CD11c-positive dendritic cells penetrate beyond well-developed epithelial tight junctions in human nasal mucosa of allergic rhinitis. *J Histochem Cytochem* **53**, 611-619 (2005).
14. Rescigno, M., *et al.* Dendritic cells express tight junction proteins and penetrate gut epithelial monolayers to sample bacteria. *Nature immunology* **2**, 361-367 (2001).
15. Bernocchi, B., Carpentier, R. & Betbeder, D. Nasal nanovaccines. *International journal of pharmaceutics* **530**, 128-138 (2017).
16. Boraschi, D. & Italiani, P. From Antigen Delivery System to Adjuvanticy: The Board Application of Nanoparticles in Vaccinology. *Vaccines (Basel)* **3**, 930-939 (2015).
17. Rivera, A., Siracusa, M.C., Yap, G.S. & Gause, W.C. Innate cell communication kick-starts pathogen-specific immunity. *Nature immunology* **17**, 356-363 (2016).
18. Csaba, N., Garcia-Fuentes, M. & Alonso, M.J. Nanoparticles for nasal vaccination. *Adv Drug Deliv Rev* **61**, 140-157 (2009).
19. Hart, B.A., *et al.* Liposome-mediated peptide loading of MHC-DR molecules in vivo. *FEBS Lett* **409**, 91-95 (1997).
20. Ben Ahmeida, E.T., Gregoriadis, G., Potter, C.W. & Jennings, R. Immunopotential of local and systemic humoral immune responses by ISCOMs, liposomes and FCA: role in protection against influenza A in mice. *Vaccine* **11**, 1302-1309 (1993).
21. Cunha, S., Amaral, M.H., Lobo, J.M.S. & Silva, A.C. Lipid Nanoparticles for Nasal/Intranasal Drug Delivery. *Crit Rev Ther Drug Carrier Syst* **34**, 257-282 (2017).

22. Muller, R.H., Shegokar, R. & Keck, C.M. 20 years of lipid nanoparticles (SLN and NLC): present state of development and industrial applications. *Curr Drug Discov Technol* **8**, 207-227 (2011).
23. Morein, B. The iscom: an immunostimulating system. *Immunol Lett* **25**, 281-283 (1990).
24. Coulter, A., *et al.* Intranasal vaccination with ISCOMATRIX adjuvanted influenza vaccine. *Vaccine* **21**, 946-949 (2003).
25. Cibulski, S.P., *et al.* Novel ISCOMs from Quillaja brasiliensis saponins induce mucosal and systemic antibody production, T-cell responses and improved antigen uptake. *Vaccine* **34**, 1162-1171 (2016).
26. Leenaars, P.P., Hendriksen, C.F., Koedam, M.A., Claassen, I. & Claassen, E. Comparison of adjuvants for immune potentiating properties and side effects in mice. *Vet Immunol Immunopathol* **48**, 123-138 (1995).
27. Illum, L. Chitosan and its use as a pharmaceutical excipient. *Pharmaceutical research* **15**, 1326-1331 (1998).
28. Garg, U., Chauhan, S., Nagaich, U. & Jain, N. Current Advances in Chitosan Nanoparticles Based Drug Delivery and Targeting. *Adv Pharm Bull* **9**, 195-204 (2019).
29. Perez, C., Castellanos, I.J., Costantino, H.R., Al-Azzam, W. & Griebenow, K. Recent trends in stabilizing protein structure upon encapsulation and release from bioerodible polymers. *J Pharm Pharmacol* **54**, 301-313 (2002).
30. Clark, M.A., Jepson, M.A. & Hirst, B.H. Exploiting M cells for drug and vaccine delivery. *Adv Drug Deliv Rev* **50**, 81-106 (2001).
31. Pavot, V., *et al.* Poly(lactic acid) and poly(lactic-co-glycolic acid) particles as versatile carrier platforms for vaccine delivery. *Nanomedicine (Lond)* **9**, 2703-2718 (2014).

32. Karuturi, B.V.K., *et al.* Encapsulation of an EP67-Conjugated CTL Peptide Vaccine in Nanoscale Biodegradable Particles Increases the Efficacy of Respiratory Immunization and Affects the Magnitude and Memory Subsets of Vaccine-Generated Mucosal and Systemic CD8+ T Cells in a Diameter-Dependent Manner. *Mol Pharm* **14**, 1469-1481 (2017).
33. Tallapaka, S.B., *et al.* Surface conjugation of EP67 to biodegradable nanoparticles increases the generation of long-lived mucosal and systemic memory T-cells by encapsulated protein vaccine after respiratory immunization and subsequent T-cell-mediated protection against respiratory infection. *International journal of pharmaceutics* **565**, 242-257 (2019).
34. Almoustafa, H.A., Alshawsh, M.A. & Chik, Z. Technical aspects of preparing PEG-PLGA nanoparticles as carrier for chemotherapeutic agents by nanoprecipitation method. *International journal of pharmaceutics* **533**, 275-284 (2017).
35. Lagreca, E., *et al.* Recent advances in the formulation of PLGA microparticles for controlled drug delivery. *Prog Biomater* **9**, 153-174 (2020).
36. Ochi, M., Wan, B., Bao, Q. & Burgess, D.J. Influence of PLGA molecular weight distribution on leuprolide release from microspheres. *International journal of pharmaceutics* **599**, 120450 (2021).
37. Makadia, H.K. & Siegel, S.J. Poly Lactic-co-Glycolic Acid (PLGA) as Biodegradable Controlled Drug Delivery Carrier. *Polymers (Basel)* **3**, 1377-1397 (2011).
38. Oyewumi, M.O., Kumar, A. & Cui, Z. Nano-microparticles as immune adjuvants: correlating particle sizes and the resultant immune responses. *Expert Rev Vaccines* **9**, 1095-1107 (2010).

39. Dua, K., Hansbro, P., Haggi, M. & Wadhwa, R. *Targeting chronic inflammatory lung diseases using advanced drug delivery systems*, (Elsevier, Waltham, 2020).
40. Moreno-Sastre, M., Pastor, M., Salomon, C.J., Esquisabel, A. & Pedraz, J.L. Pulmonary drug delivery: a review on nanocarriers for antibacterial chemotherapy. *J Antimicrob Chemother* **70**, 2945-2955 (2015).
41. Huang, Y. & Donovan, M.D. Large molecule and particulate uptake in the nasal cavity: the effect of size on nasal absorption. *Adv Drug Deliv Rev* **29**, 147-155 (1998).
42. Hirota, K., *et al.* Optimum conditions for efficient phagocytosis of rifampicin-loaded PLGA microspheres by alveolar macrophages. *J Control Release* **119**, 69-76 (2007).
43. Carr, R.M., *et al.* Nasal-associated lymphoid tissue is an inductive site for rat tear IgA antibody responses. *Immunol Invest* **25**, 387-396 (1996).
44. Eyles, J.E., Bramwell, V.W., Williamson, E.D. & Alpar, H.O. Microsphere translocation and immunopotential in systemic tissues following intranasal administration. *Vaccine* **19**, 4732-4742 (2001).
45. Marasini, N., Skwarczynski, M. & Toth, I. Intranasal delivery of nanoparticle-based vaccines. *Ther Deliv* **8**, 151-167 (2017).
46. Dawes, G.J., *et al.* Size effect of PLGA spheres on drug loading efficiency and release profiles. *J Mater Sci Mater Med* **20**, 1089-1094 (2009).
47. Klose, D., Siepman, F., Elkharraz, K., Krenzlin, S. & Siepman, J. How porosity and size affect the drug release mechanisms from PLGA-based microparticles. *International journal of pharmaceutics* **314**, 198-206 (2006).
48. Gutierrez, I., Hernandez, R.M., Igartua, M., Gascon, A.R. & Pedraz, J.L. Size dependent immune response after subcutaneous, oral and intranasal administration of BSA loaded nanospheres. *Vaccine* **21**, 67-77 (2002).

49. Nagamoto, T., Hattori, Y., Takayama, K. & Maitani, Y. Novel chitosan particles and chitosan-coated emulsions inducing immune response via intranasal vaccine delivery. *Pharmaceutical research* **21**, 671-674 (2004).
50. Torres, M.P., *et al.* Polyanhydride microparticles enhance dendritic cell antigen presentation and activation. *Acta Biomater* **7**, 2857-2864 (2011).
51. Audran, R., *et al.* Encapsulation of peptides in biodegradable microspheres prolongs their MHC class-I presentation by dendritic cells and macrophages in vitro. *Vaccine* **21**, 1250-1255 (2003).
52. Men, Y., Thomasin, C., Merkle, H.P., Gander, B. & Corradin, G. A single administration of tetanus toxoid in biodegradable microspheres elicits T cell and antibody responses similar or superior to those obtained with aluminum hydroxide. *Vaccine* **13**, 683-689 (1995).
53. Peter, K., Men, Y., Pantaleo, G., Gander, B. & Corradin, G. Induction of a cytotoxic T-cell response to HIV-1 proteins with short synthetic peptides and human compatible adjuvants. *Vaccine* **19**, 4121-4129 (2001).
54. Pizza, M., *et al.* Mucosal vaccines: non toxic derivatives of LT and CT as mucosal adjuvants. *Vaccine* **19**, 2534-2541 (2001).
55. Matsuo, K., *et al.* Cytokine mRNAs in the nasal-associated lymphoid tissue during influenza virus infection and nasal vaccination. *Vaccine* **18**, 1344-1350 (2000).
56. Takaki, H., Ichimiya, S., Matsumoto, M. & Seya, T. Mucosal Immune Response in Nasal-Associated Lymphoid Tissue upon Intranasal Administration by Adjuvants. *J Innate Immun* **10**, 515-521 (2018).
57. Bode, C., Zhao, G., Steinhagen, F., Kinjo, T. & Klinman, D.M. CpG DNA as a vaccine adjuvant. *Expert Rev Vaccines* **10**, 499-511 (2011).

58. Jia, Y., Krishnan, L. & Omri, A. Nasal and pulmonary vaccine delivery using particulate carriers. *Expert Opin Drug Deliv* **12**, 993-1008 (2015).
59. Wang, X. & Meng, D. Innate endogenous adjuvants prime to desirable immune responses via mucosal routes. *Protein Cell* **6**, 170-184 (2015).
60. Staats, H.F., *et al.* Cytokine requirements for induction of systemic and mucosal CTL after nasal immunization. *J Immunol* **167**, 5386-5394 (2001).
61. Eo, S.K., Lee, S., Kumaraguru, U. & Rouse, B.T. Immunopotential of DNA vaccine against herpes simplex virus via co-delivery of plasmid DNA expressing CCR7 ligands. *Vaccine* **19**, 4685-4693 (2001).
62. Lapuente, D., *et al.* IL-1beta as mucosal vaccine adjuvant: the specific induction of tissue-resident memory T cells improves the heterosubtypic immunity against influenza A viruses. *Mucosal Immunol* **11**, 1265-1278 (2018).
63. Kayamuro, H., *et al.* Interleukin-1 family cytokines as mucosal vaccine adjuvants for induction of protective immunity against influenza virus. *J Virol* **84**, 12703-12712 (2010).
64. Morgan, E.L., *et al.* Identification and characterization of the effector region within human C5a responsible for stimulation of IL-6 synthesis. *J Immunol* **148**, 3937-3942 (1992).
65. Ember, J.A., Sanderson, S.D., Taylor, S.M., Kawahara, M. & Hugli, T.E. Biologic activity of synthetic analogues of C5a anaphylatoxin. *J Immunol* **148**, 3165-3173 (1992).
66. Karuturi, B.V., Tallapaka, S.B., Phillips, J.A., Sanderson, S.D. & Vetro, J.A. Preliminary evidence that the novel host-derived immunostimulant EP67 can act as a mucosal adjuvant. *Clin Immunol* **161**, 251-259 (2015).

67. Taylor, S.M., Sherman, S.A., Kirnarsky, L. & Sanderson, S.D. Development of response-selective agonists of human C5a anaphylatoxin: conformational, biological, and therapeutic considerations. *Curr Med Chem* **8**, 675-684 (2001).
68. Tempero, R.M., *et al.* Molecular adjuvant effects of a conformationally biased agonist of human C5a anaphylatoxin. *J Immunol* **158**, 1377-1382 (1997).
69. Ulrich, J.T., Cieplak, W., Paczkowski, N.J., Taylor, S.M. & Sanderson, S.D. Induction of an Antigen-Specific CTL Response by a Conformationally Biased Agonist of Human C5a Anaphylatoxin as a Molecular Adjuvant. *The Journal of Immunology* **164**, 5492-5498 (2000).
70. Sanderson, S.D., *et al.* Immunization to nicotine with a peptide-based vaccine composed of a conformationally biased agonist of C5a as a molecular adjuvant. *Int Immunopharmacol* **3**, 137-146 (2003).
71. Ganger, S. & Schindowski, K. Tailoring Formulations for Intranasal Nose-to-Brain Delivery: A Review on Architecture, Physico-Chemical Characteristics and Mucociliary Clearance of the Nasal Olfactory Mucosa. *Pharmaceutics* **10**(2018).
72. Shen, H., *et al.* Enhanced and prolonged cross-presentation following endosomal escape of exogenous antigens encapsulated in biodegradable nanoparticles. *Immunology* **117**, 78-88 (2006).
73. Silva, A.L., *et al.* Optimization of encapsulation of a synthetic long peptide in PLGA nanoparticles: low-burst release is crucial for efficient CD8(+) T cell activation. *Eur J Pharm Biopharm* **83**, 338-345 (2013).
74. Chadwick, S., Kriegel, C. & Amiji, M. Nanotechnology solutions for mucosal immunization. *Adv Drug Deliv Rev* **62**, 394-407 (2010).
75. Lycke, N. Recent progress in mucosal vaccine development: potential and limitations. *Nature reviews. Immunology* **12**, 592-605 (2012).

76. Morgan, E.L., *et al.* Enhancement of in vivo and in vitro immune functions by a conformationally biased, response-selective agonist of human C5a: implications for a novel adjuvant in vaccine design. *Vaccine* **28**, 463-469 (2009).
77. Alshammari, A.M., *et al.* Targeted Amino Acid Substitution Overcomes Scale-Up Challenges with the Human C5a-Derived Decapeptide Immunostimulant EP67. *ACS Infect Dis* **6**, 1169-1181 (2020).
78. Hegde, G.V., Meyers-Clark, E., Joshi, S.S. & Sanderson, S.D. A conformationally-biased, response-selective agonist of C5a acts as a molecular adjuvant by modulating antigen processing and presentation activities of human dendritic cells. *Int Immunopharmacol* **8**, 819-827 (2008).
79. Lobaina Mato, Y. Nasal route for vaccine and drug delivery: Features and current opportunities. *International journal of pharmaceutics* **572**, 118813 (2019).
80. Southam, D.S., Dolovich, M., O'Byrne, P.M. & Inman, M.D. Distribution of intranasal instillations in mice: effects of volume, time, body position, and anesthesia. *Am J Physiol Lung Cell Mol Physiol* **282**, L833-839 (2002).
81. Eyles, J.E., Spiers, I.D., Williamson, E.D. & Alpar, H.O. Tissue distribution of radioactivity following intranasal administration of radioactive microspheres. *J Pharm Pharmacol* **53**, 601-607 (2001).
82. Eyles, J.E., Williamson, E.D. & Alpar, H.O. Immunological responses to nasal delivery of free and encapsulated tetanus toxoid: studies on the effect of vehicle volume. *International journal of pharmaceutics* **189**, 75-79 (1999).
83. Miller, M.A., *et al.* Visualization of murine intranasal dosing efficiency using luminescent *Francisella tularensis*: effect of instillation volume and form of anesthesia. *PLoS One* **7**, e31359 (2012).
84. Ilyinskii, P.O., *et al.* Adjuvant-carrying synthetic vaccine particles augment the immune response to encapsulated antigen and exhibit strong local immune

- activation without inducing systemic cytokine release. *Vaccine* **32**, 2882-2895 (2014).
85. Mathew, S., Lendlein, A. & Wischke, C. Characterization of protein-adjuvant coencapsulation in microparticles for vaccine delivery. *Eur J Pharm Biopharm* **87**, 403-407 (2014).
86. Fahmy, T.M., Demento, S.L., Caplan, M.J., Mellman, I. & Saltzman, W.M. Design opportunities for actively targeted nanoparticle vaccines. *Nanomedicine (Lond)* **3**, 343-355 (2008).
87. Sanderson, S.D., *et al.* Decapeptide agonists of human C5a: the relationship between conformation and spasmogenic and platelet aggregatory activities. *J Med Chem* **37**, 3171-3180 (1994).
88. Sanchez, A., Villamayor, B., Guo, Y., Mclver, J. & Alonso, M.J. Formulation strategies for the stabilization of tetanus toxoid in poly(lactide-co-glycolide) microspheres. *International journal of pharmaceutics* **185**, 255-266 (1999).
89. Herrmann, J. & Bodmeier, R. Biodegradable, somatostatin acetate containing microspheres prepared by various aqueous and non-aqueous solvent evaporation methods. *Eur J Pharm Biopharm* **45**, 75-82 (1998).
90. Hackley, V.A. & Clogston, J.D. Measuring the hydrodynamic size of nanoparticles in aqueous media using batch-mode dynamic light scattering. *Methods Mol Biol* **697**, 35-52 (2011).
91. Mizuno, K., Nakamura, T., Ohshima, T., Tanaka, S. & Matsuo, H. Characterization of KEX2-encoded endopeptidase from yeast *Saccharomyces cerevisiae*. *Biochem Biophys Res Commun* **159**, 305-311 (1989).
92. Nakayama, K. Furin: a mammalian subtilisin/Kex2p-like endoprotease involved in processing of a wide variety of precursor proteins. *Biochem J* **327 (Pt 3)**, 625-635 (1997).

93. Golde, W.T., Gollobin, P. & Rodriguez, L.L. A rapid, simple, and humane method for submandibular bleeding of mice using a lancet. *Lab Anim (NY)* **34**, 39-43 (2005).
94. McCaskill, M.L., *et al.* Alcohol exposure alters mouse lung inflammation in response to inhaled dust. *Nutrients* **4**, 695-710 (2012).
95. Takahashi, Y., *et al.* Effect of histamine H4 receptor antagonist on allergic rhinitis in mice. *Int Immunopharmacol* **9**, 734-738 (2009).
96. McFarland, B.J., Sant, A.J., Lybrand, T.P. & Beeson, C. Ovalbumin(323-339) peptide binds to the major histocompatibility complex class II I-A(d) protein using two functionally distinct registers. *Biochemistry* **38**, 16663-16670 (1999).
97. Johnsen, G. & Elsayed, S. Antigenic and allergenic determinants of ovalbumin--III. MHC Ia-binding peptide (OA 323-339) interacts with human and rabbit specific antibodies. *Mol Immunol* **27**, 821-827 (1990).
98. Rotzschke, O., *et al.* Exact prediction of a natural T cell epitope. *European journal of immunology* **21**, 2891-2894 (1991).
99. Lipford, G.B., Hoffman, M., Wagner, H. & Heeg, K. Primary in vivo responses to ovalbumin. Probing the predictive value of the Kb binding motif. *J Immunol* **150**, 1212-1222 (1993).
100. Frey, A., Di Canzio, J. & Zurakowski, D. A statistically defined endpoint titer determination method for immunoassays. *Journal of immunological methods* **221**, 35-41 (1998).
101. Zrein, M., De Marcillac, G. & Van Regenmortel, M.H. Quantitation of rheumatoid factors by enzyme immunoassay using biotinylated human IgG. *Journal of immunological methods* **87**, 229-237 (1986).
102. Gross, E.A., Swenberg, J.A., Fields, S. & Popp, J.A. Comparative morphometry of the nasal cavity in rats and mice. *J Anat* **135**, 83-88 (1982).

103. Poole, J.A., *et al.* Protein kinase C epsilon is important in modulating organic-dust-induced airway inflammation. *Exp Lung Res* **38**, 383-395 (2012).
104. Morgan, E.L., Thoman, M.L., Sanderson, S.D. & Phillips, J.A. A novel adjuvant for vaccine development in the aged. *Vaccine* **28**, 8275-8279 (2010).
105. Patil, Y.B., Toti, U.S., Khdair, A., Ma, L. & Panyam, J. Single-step surface functionalization of polymeric nanoparticles for targeted drug delivery. *Biomaterials* **30**, 859-866 (2009).
106. Toti, U.S., Guru, B.R., Grill, A.E. & Panyam, J. Interfacial activity assisted surface functionalization: a novel approach to incorporate maleimide functional groups and cRGD peptide on polymeric nanoparticles for targeted drug delivery. *Molecular pharmaceutics* **7**, 1108-1117 (2010).
107. Lefevre, E.A., Carr, B.V., Prentice, H. & Charleston, B. A quantitative assessment of primary and secondary immune responses in cattle using a B cell ELISPOT assay. *Vet Res* **40**, 3 (2009).
108. McCluskie, M.J., Weeratna, R.D. & Davis, H.L. Intranasal immunization of mice with CpG DNA induces strong systemic and mucosal responses that are influenced by other mucosal adjuvants and antigen distribution. *Mol Med* **6**, 867-877 (2000).
109. Abbas, A.K., Lichtman, A.H. & Pillai, S. *Cellular and Molecular Immunology E-Book*, (Elsevier Health Sciences, 2021).
110. Wu, H.Y. & Russell, M.W. Nasal lymphoid tissue, intranasal immunization, and compartmentalization of the common mucosal immune system. *Immunol Res* **16**, 187-201 (1997).
111. Bronte, V. & Pittet, M.J. The spleen in local and systemic regulation of immunity. *Immunity* **39**, 806-818 (2013).

112. Fornefett, J., *et al.* Comparative analysis of humoral immune responses and pathologies of BALB/c and C57BL/6 wildtype mice experimentally infected with a highly virulent *Rodentibacter pneumotropicus* (*Pasteurella pneumotropica*) strain. *BMC Microbiol* **18**, 45 (2018).
113. Cetre, C., *et al.* Profiles of Th1 and Th2 cytokines after primary and secondary infection by *Schistosoma mansoni* in the semipermissive rat host. *Infect Immun* **67**, 2713-2719 (1999).
114. Mosley, Y.C., Radder, J.E. & HogenEsch, H. Genetic Variation in the Magnitude and Longevity of the IgG Subclass Response to a Diphtheria-Tetanus-Acellular Pertussis (DTaP) Vaccine in Mice. *Vaccines (Basel)* **7**(2019).
115. Plumlee, C.R., *et al.* Early Effector CD8 T Cells Display Plasticity in Populating the Short-Lived Effector and Memory-Precursor Pools Following Bacterial or Viral Infection. *Sci Rep* **5**, 12264 (2015).
116. Kaech, S.M., *et al.* Selective expression of the interleukin 7 receptor identifies effector CD8 T cells that give rise to long-lived memory cells. *Nature immunology* **4**, 1191-1198 (2003).
117. Yuzefpolskiy, Y., Baumann, F.M., Kalia, V. & Sarkar, S. Early CD8 T-cell memory precursors and terminal effectors exhibit equipotent in vivo degranulation. *Cell Mol Immunol* **12**, 400-408 (2015).
118. Beyersdorf, N., Ding, X., Tietze, J.K. & Hanke, T. Characterization of mouse CD4 T cell subsets defined by expression of KLRG1. *European journal of immunology* **37**, 3445-3454 (2007).
119. Ahlers, J.D. & Belyakov, I.M. Memories that last forever: strategies for optimizing vaccine T-cell memory. *Blood* **115**, 1678-1689 (2010).
120. Obar, J.J. & Lefrancois, L. Early events governing memory CD8+ T-cell differentiation. *Int Immunol* **22**, 619-625 (2010).

121. Obar, J.J. & Lefrancois, L. Early signals during CD8 T cell priming regulate the generation of central memory cells. *J Immunol* **185**, 263-272 (2010).
122. Obar, J.J. & Lefrancois, L. Memory CD8+ T cell differentiation. *Ann N Y Acad Sci* **1183**, 251-266 (2010).
123. Huster, K.M., *et al.* Selective expression of IL-7 receptor on memory T cells identifies early CD40L-dependent generation of distinct CD8+ memory T cell subsets. *Proc Natl Acad Sci U S A* **101**, 5610-5615 (2004).
124. Gasper, D.J., Tejera, M.M. & Suresh, M. CD4 T-cell memory generation and maintenance. *Crit Rev Immunol* **34**, 121-146 (2014).
125. Woodland, D.L. & Scott, I. T cell memory in the lung airways. *Proc Am Thorac Soc* **2**, 126-131 (2005).
126. Renkema, K.R., *et al.* KLRG1(+) Memory CD8 T Cells Combine Properties of Short-Lived Effectors and Long-Lived Memory. *J Immunol* **205**, 1059-1069 (2020).
127. Kaech, S.M., Wherry, E.J. & Ahmed, R. Effector and memory T-cell differentiation: implications for vaccine development. *Nature reviews. Immunology* **2**, 251-262 (2002).
128. Jameson, S.C. & Masopust, D. Understanding Subset Diversity in T Cell Memory. *Immunity* **48**, 214-226 (2018).
129. Panagioti, E., Klenerman, P., Lee, L.N., van der Burg, S.H. & Arens, R. Features of Effective T Cell-Inducing Vaccines against Chronic Viral Infections. *Front Immunol* **9**, 276 (2018).
130. Beaudette, T.T., *et al.* In vivo studies on the effect of co-encapsulation of CpG DNA and antigen in acid-degradable microparticle vaccines. *Mol Pharm* **6**, 1160-1169 (2009).

131. Dolen, Y., *et al.* Co-delivery of PLGA encapsulated invariant NKT cell agonist with antigenic protein induce strong T cell-mediated antitumor immune responses. *Oncoimmunology* **5**, e1068493 (2016).
132. Krieg, A.M. Antiinfective applications of toll-like receptor 9 agonists. *Proc Am Thorac Soc* **4**, 289-294 (2007).
133. Kasturi, S.P., *et al.* Programming the magnitude and persistence of antibody responses with innate immunity. *Nature* **470**, 543-547 (2011).
134. Wagner, H. The immunogenicity of CpG-antigen conjugates. *Adv Drug Deliv Rev* **61**, 243-247 (2009).
135. Ianeselli, L., *et al.* Protein-protein interactions in ovalbumin solutions studied by small-angle scattering: effect of ionic strength and the chemical nature of cations. *J Phys Chem B* **114**, 3776-3783 (2010).
136. Cavaco, C.K., *et al.* A novel C5a-derived immunobiotic peptide reduces *Streptococcus agalactiae* colonization through targeted bacterial killing. *Antimicrob Agents Chemother* **57**, 5492-5499 (2013).
137. Han, F.Y., Thurecht, K.J., Whittaker, A.K. & Smith, M.T. Bioerodable PLGA-Based Microparticles for Producing Sustained-Release Drug Formulations and Strategies for Improving Drug Loading. *Front Pharmacol* **7**, 185 (2016).